2016

Thiol-Acrylate Polymerization Kinetics and Applications in Microfluidics

Michael Perrin Tullier
Louisiana State University and Agricultural and Mechanical College

THIOL-ACRYLATE POLYMERIZATION KINETICS AND APPLICATIONS IN MICROFLUIDICS

A Dissertation

Submitted to the Graduate Faculty of the
Louisiana State University and
Agricultural and Mechanical College
in partial fulfillment of the
requirements for the degree of
Doctor of Philosophy

in

The Department of Chemistry

by
Michael Perrin Tullier
B.S., Louisiana State University, 2012
May 2017

ACKNOWLEDGEMENTS

Firstly, I would like to express my sincere thanks to my advisor, Dr. John A Pojman, without whom this would not be possible. Ever since taking me into his lab as an undergraduate looking for work, he has given me the freedom to pursue my own ideas and has been a beacon of positivity during times of stress and frustration. Thank you for your acceptance of my skeptical nature and for all of your advice and guidance.

I would also like to thank the other members of my committee, Dr. David Spivak and Dr. Donghui Zhang who have challenged me both in research and in the classroom. Your interest in my work and different schools of thought pushed me to think about things from new perspectives and helped me develop as a researcher.

I am also truly grateful to the members of the Pojman research team, past and present, for their advice and friendship. Thank you for all of your help, stimulating conversations, and welcome distractions over the past six years.

I would like to thank the members of my family for their support throughout this process. I would especially like to thank my parents, Patrick and Renée Tullier, and my grandparents for their love and positive example. The education you have provided me has allowed me to succeed both academically and personally.

Finally, I owe a great deal of thanks to my wife Julie for her patience and understanding, especially over the last few months, and to my son Matthew for usually sleeping through most of the night.

TABLE OF CONTENTS

LIST OF ABBREVIATIONS

AA	Activated Acrylate
ATR	Attenuated Total Reflectance
BDDA	Butanediol Diacrylate
BSA	Bovine Serum Albumin
BuOH	Butanol
CFU	Colony Forming Unit
DAPI	4′,6-Diamidino-2-Phenylindole
DEA	Diethylamine
DEOA	Diethanolamine
E. coli	*Escherichia coli*
EA	Excess Acrylate
EEOA	Ethyl Ethanolamine
ELISA	Enzyme Linked Immunosorbent Assay
ET	Excess Thiol
ETMPTMP	Ethoxylated Trimethylolpropane Tris(3-Mercaptopropionate)
FAM	Carboxyfluorescein
FITC	Fluorescein Isothiocyanate
FTIR	Fourier Transform Infrared
GDMP	Glycol Di(3-Mercaptopropionate)
LA	Lauryl Acrylate
LIGA	*Lithographie Galvanoformung Abformung*

LOC	Lab On A Chip
LPS	Lipopolysaccharide
MEHQ	Monomethyl Ether Hydroquinone
NOA81	Norland Optical Adhesive 81
PBS	Phosphate Buffer Saline
PCR	Polymerase Chain Reaction
PDLC	Polymer Dispersed Liquid Crystal
PDMS	Poly(Dimethylsiloxane)
PEGDA	Poly(Ethylene Glycol) Diacrylate
PEGMEA	Poly(Ethylene Glycol) Methyl Ether Acrylate
PETA	Pentaerythritol Triacrylate
PETMP	Pentaerythritol Tetra(3-Mercaptopropionate)
PETTA	Pentaerythritol Tetraacrylate
PMB	Polymyxin B
PMMA	Poly(Methyl Methacrylate)
POC	Point of Care
PS	Poly(Styrene)
PTFE	Poly(Tetrafluoroethylene)
PUMA	Polyurethane Methacrylate
TAMR	Thiol-Acrylate Microfluidic Resin
TAP	Tris-Acetate-Phosphate
TBC	Tert-Butyl Catechol
TEA	Triethylamine

TEMPO	2,2,6,6-Tetramethylpiperidine 1-Oxyl
TMPETA	Trimethylolpropane Ethoxylate Triacrylate
TMPPTA	Trimethylolpropane Propoxylate Triacrylate
TMPTA	Trimethylolpropane Triacrylate
TMPTMP	Trimethylolpropane Tris(3-Mercaptopropionate)
TPE	Thermoset Polyester
TPP	Triphenylphosphine
TRITC	Tetramethylrhodamine Isothiocyanate
UV	Ultraviolet
μ-TAS	Micro Total Analysis System

ABSTRACT

The reaction kinetics and some applications in the field of microfluidics for thiol-acrylate Michael addition polymerizations using multifunctional monomers have been researched and are presented here. The polymerization rate constants for base-catalyzed systems were found to increase with increasing thiol and acrylate functionality, which was attributed to the intramolecular interactions between functional groups. The nucleophile-initiated thiol-acrylate Michael addition polymerization kinetics were monitored via FTIR, and it was determined that the increase in the rate of reaction in these multifunctional systems was significantly less dramatic than the increase observed in monofunctional systems. While no radical polymerization was observed during most typical thiol-acrylate Michael addition reactions, spontaneous radical polymerization can occur in certain systems where the Michael addition rate is low, such as towards the end of nucleophile-initiated reactions, base-catalyzed reactions with low base concentrations, and reactions performed using monomers with low functionality.

Several material properties of a thiol-acrylate microfluidic resin (TAMR) were investigated including the cure kinetics, hydrophilicity, solvent absorption, and elastic modulus. The material was shown to cure at 50 °C in 3 hours or at room temperature in 10 hours. The water contact angle of these materials was shown to vary based on the hydrophilicity of the resin curing surface, but it is generally lower than other microfluidic materials, such as poly(dimethylsiloxane) (PDMS). The swelling of TAMR in a variety of solvents was quantified and determined to be superior to PDMS in organic solvents. The elastic modulus of TAMR was shown to vary with cure time and resin formulation with a maximum of ~10.5 MPa for the systems studied. A simple surface modification of

the TAMR was performed using a thiol-acrylate Michael addition reaction between thiol groups on the resin surface and a modifying acrylate. Two microfluidic applications of TAMR have been presented. The first is a fluorescence-based bacterial detection device which uses the selective binding of bacteria to an antibody bound to the TAMR surface to confirm the presence of the pathogen. The second device uses a thiol-acrylate hydrogel in combination with TAMR to produce a gradient-generating microfluidic device for studying algal chemotaxis.

CHAPTER 1. INTRODUCTION

1.1 Thiol-Ene Chemistry

First appearing in a 1905 report by Posner[1], thiol-ene chemistry is not a recent development, but it has only been in the past twenty years that the majority of applications for these versatile reactions have been reported. In general, a thiol-ene reaction involves the formation of a carbon-sulfur bond between a thiol group (R-SH) and a carbon-carbon double bond (alk*ene*). Although Posner is generally credited with the discovery of thiol-ene reactions, the addition of sulfur to ene groups had been taking place since the 1830s in the vulcanization of rubber, which was first patented by Goodyear in 1844.[2] Early examples of thiol-ene polymerizations by Marvel et al. appeared in the late 1940s and early 1950s,[3-4] but significant progress was not made until the 1970s with several works by Morgan et al.[5-6] on the photo-initiated curing of thiol-ene systems. After another period of little progress, thiol-ene chemistry made a comeback in the 1990s, mainly due to the efforts of Jacobine et al.[7-9] Finally, after a large volume of work from Hoyle, Bowman, and others[10-18] in the early 2000s, the scientific community realized the potential of this chemistry.

There are two main types of thiol-ene reactions, the first of which is a radical process illustrated in Scheme 1.1. Depending on the structures of the thiol and ene, this reaction can be used to produce polymers or perform click type coupling reactions. The reaction can be initiated using a thermal or photo-radical initiator, but irradiation with ultraviolet (UV) light is sufficient to form a thiyl radical from a thiol group. The thiyl radical formed in the initiation step goes on to add across the double bond of an ene group to form the most stable radical. This newly formed radical will abstract the proton

from a thiol group to from a new thiyl radical (chain transfer step) that can start propagation again. Termination of the propagating radical can occur through several radical coupling pathways.

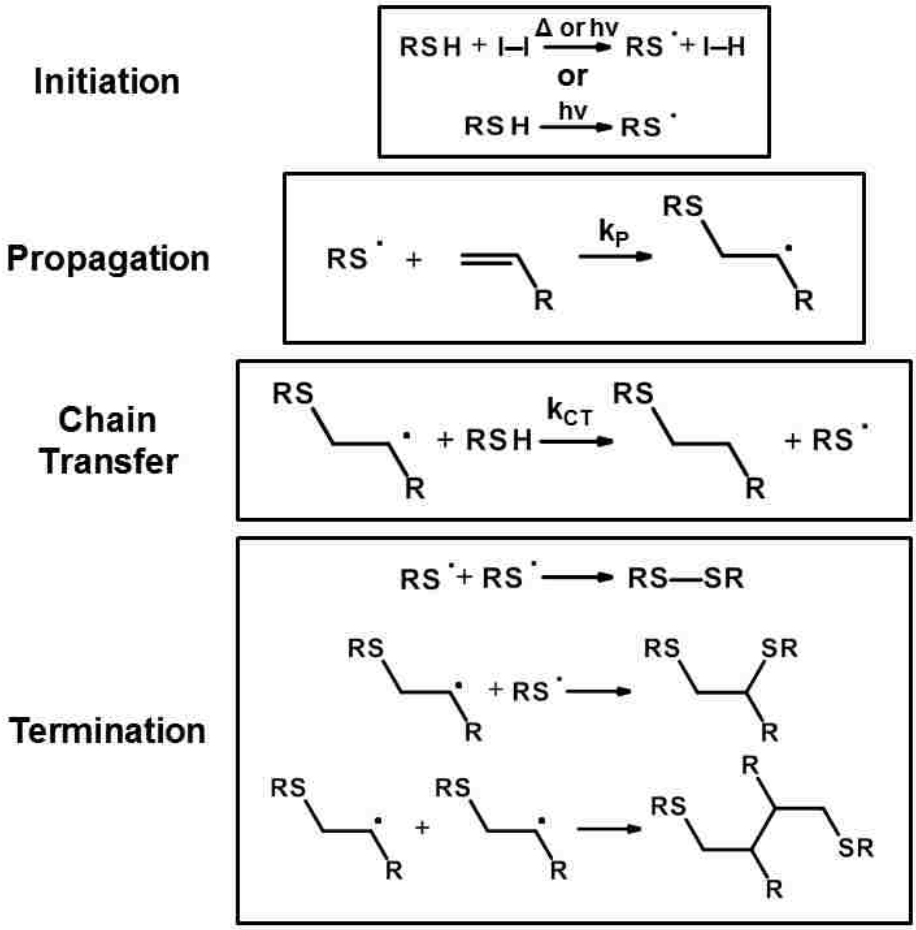

Scheme 1.1 General thiol-ene radical polymerization mechanism where I-I indicates a radical initiator

The remainder of this document will focus on polymer synthesis using thiol-ene reactions, but the applications of thiol-ene click coupling are a major area of study as well.[14, 19-20]

Scheme 1.1 demonstrates that thiol-ene radical polymerizations will proceed via a step-growth mechanism, as first predicted by Kharasch et al.,[21] since both functional groups must come together to form the new bond and the reaction of monofunctional

monomers only gives a small molecule. However, while polymer formation occurs in a stepwise fashion, the mechanism has characteristics of a chain-growth system since an initiating radical will propagate and chain transfer continuously until a termination event occurs. Also, these reactions do not exhibit the traditional second-order overall kinetics associated with step-growth polymerizations. Depending on the structure of the ene and thiol groups, the polymerization kinetics may be independent of the ene or thiol concentration.[15, 22] If the propagation step proceeds significantly more rapidly than the chain transfer step (see Scheme 1.1), then the rate limiting step will only depend on the thiol group concentration. If the chain transfer step and propagation step occur at roughly the same rate, then the reaction will be half order in both ene and thiol.

The difference in the rates of the propagation and chain transfer steps depends on the stability of the carbon-centered radical formed after the addition of a thiol group to an ene, the electron density of the ene, and the availability of the thiol hydrogen. More stabilized radicals have a decreased rate of chain transfer and thus have higher propagation to chain transfer ratio (k_p/k_{CT}). The same is true for thiols where the thiol hydrogen is only mildly acidic and thus cannot be abstracted easily. Enes with increased electron densities give higher k_p values. The combination of all of these factors ultimately determines the k_p/k_{CT} and thus the kinetics by which these reactions proceed. Given the same thiol, acrylates and allyl ethers have k_p/k_{CT} >10 and show thiol-dependent kinetics while vinyl ethers and norbornenes have k_p/k_{CT} ~1 and depend on both thiol and ene concentrations. The overall rate of polymerization follows the trend where norbornene > vinyl ether > acrylate > allyl ether.[22] More acidic thiols, such

as mercaptopropionates and thioglycolates have increased reactivity compared to alkyl thiols and more rapid chain transfer steps.[12, 23]

An interesting situation arises if the ene used in the polymerization is able to homopolymerize via a radical mechanism (Scheme 1.2). Acrylates are frequently cured on their own using a radical-chain-growth mechanism, and when combined with thiols, the thiol-ene step growth mechanism and the hompolymerization of the acrylate compete. Using an alkyl thiol, the ratio of the acrylate homopolymerization rate constant to the chain transfer to thiol rate constant was found to be 1.5.[24]

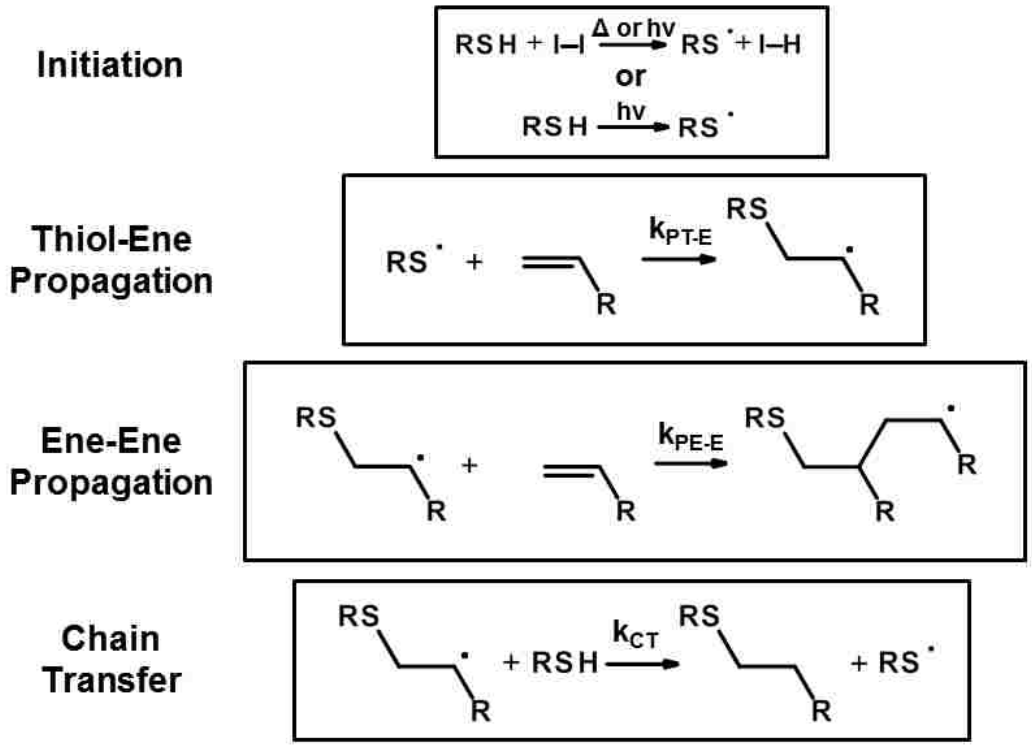

Scheme 1.2 Thiol-ene radical polymerization with ene homopolymerization

The combination of these two mechanisms leads to changes in properties with changing thiol/acrylate ratios. As thiol content is increased, the glass transition temperature and storage modulus decrease because of the decrease in crosslink density associated with a shift towards the step-growth mechanism.[24-25] Enes that

homopolymerize can be added to typical thiol-ene systems to give a variety of network structures and material properties based on the competing reaction mechanisms.[26-27]

Compared to typical radical polymerizations of alkenes, thiol-ene reactions have a number of important advantages. Perhaps the most interesting feature of radical polymerizations involving thiols is that they are not affected by oxygen inhibition.[12, 23, 25, 28] Scheme 1.3 illustrates how the addition of a thiol circumvents the typical pathway of oxygen inhibition in the radical polymerization of enes. Without the presence of thiols, molecular oxygen will react with a carbon-centered propagating radical to form a peroxy radical, which is much less reactive than the carbon radical.[29-30] However, if thiol groups are present, the peroxy radical can abstract a thiol hydrogen to give a thiyl radical, which can continue propagation.

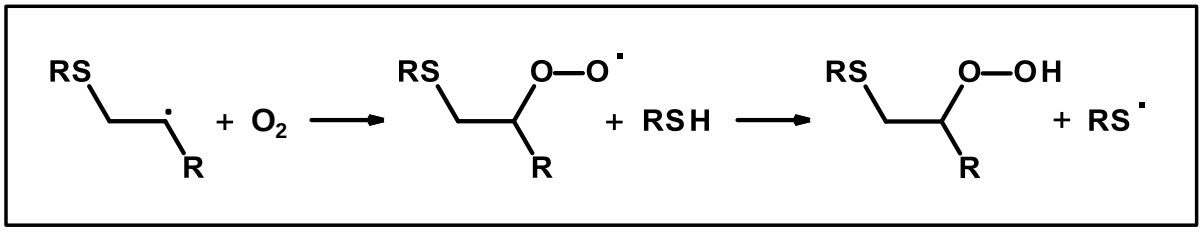

Scheme 1.3 Oxygen inhibition in thiol-ene systems

Thiol-ene radical polymerizations can be initiated using typical radical initiators, but they are not required since the sulfur-hydrogen bond of thiols can be cleaved using UV light.[12, 19, 23-24, 31-33] Using 254 nm light, the reaction can be initiated without the need for photoinitiators which improves aging properties and maximum cure depths, although the process is not as efficient as with an initiator.[12, 31] The gelation of thiol-ene materials occurs at higher conversion than with other radical ene polymerizations due to the step-growth network formation process. This prevents the network from accumulating stresses, leads to low shrinkage, gives nearly homogenous materials, and

promotes higher conversion of functional groups.[12, 19, 23, 27] Two notable disadvantages of thiol-ene chemistry are the inability to store thiols and enes together and the odor associated with thiols. When mixed, thiol-ene systems have very poor shelf lives before spontaneous polymerization occurs. This could be due to several possible circumstances including a base-catalyzed addition reaction if the ene is electron deficient, the decomposition of peroxide or hydroperoxide impurities to generate radicals, the ineffectiveness of some types of radical inhibitors found in enes due to the lack of oxygen inhibition, or a ground-state charge transfer complex forming between thiol end ene which generates radicals.[12, 34-38]

Early applications of thiol-ene chemistry focused on the coatings industry where research by Morgan and others attempted to highlight the benefits of this new technology, especially its insensitivity to oxygen.[12, 39-40] Although their efforts to get thiol-ene polymerizations adopted on a large scale were unsuccessful, the ability to cure these systems in thin layers without excluding oxygen is an area of renewed interest today.[31, 41-43] Thiol-ene systems have been used as adhesives for a number of years, most notable by Norland Products, who sell them commercially.[44-46] This chemistry has also been used to produce optical materials with high glass transition temperatures and refractive indexes.[12, 47-50] Another exciting application of thiol-ene chemistry is in the production of polymer dispersed liquid crystal (PDLC) systems.[12, 51-55] One application of these materials is in “smart” windows that can switch between transparent and opaque when an electric field is applied. Some other applications of thiol-ene chemistry include energy absorbing materials,[56-58] frontal polymerization systems,[59-60] and hydrogels.[61-64]

1.2 Thiol-Michael Additions

The second main type of thiol-ene reaction is the thiol-Michael addition reaction, which proceeds via an anionic mechanism. In general, a Michael addition is the addition of a nucleophile to an electron deficient carbon-carbon double bond and was named after Arthur Michael who originally described them in 1887.[65] Classic Michael additions involve carbanion based nucleophiles like enolates, but other nucleophiles can undergo the reaction as well, although they are frequently called “Michael-type” additions.[66] Unlike the carbon centered anions in classic Michael additions, some nucleophiles do not have to be charged to add to the olefin, such as amines or phosphines, but thiols must be deprotonated in order to react. There is a discrepancy in the literature as to when the first thiol-Michael addition was reported. A 2013 review by Nair et al. cites a 1964 article by Allen et al. on the addition of alkyl thiols to a variety of calcones,[67-68] while a 2010 review by Hoyle et al. cites a 1947 article by Hurd and Gershbein on the reactions of several mercaptans with acrylic derivatives.[19, 69-70] One possible explanation for this inconsistency is that only the 1964 paper actually describes the reaction as a Michael addition. Regardless of their reasoning, the 1940s papers clearly demonstrate the base-catalyzed addition of a thiol to carbon-carbon double bonds.

Scheme 1.4 illustrates the general mechanism for the base-catalyzed thiol-Michael addition reaction. In the initiation step, the thiol is deprotonated by a base to form a thiolate anion. This is followed by the propagation step where the thiolate adds to an electrophilic ene to form a stabilized carbanion. Next, the carbanion will deprotonate the base catalyst, which was protonated in the initiation step, to regenerate

it. An alternative mechanism proposed by Chan et al. involves initiation of the polymerization reaction by a nucleophile as shown in Scheme 1.5.[18] The first step involves the nucleophile adding to the carbon-carbon double bond in much the same way that the thiol does in the propagation step. The strongly basic carbanion produced by the addition of the nucleophile deprotonates a thiol to give the reactive thiolate that adds to another ene to start the cycle over again. Commonly used initiating nucleophiles include primary or secondary alkyl amines, bicyclic amidines, and phosphines. One disadvantage of the nucleophile-initiated mechanism is that some of the ene groups are used up in the initiation process, and these addition products will exist as an impurity in the polymer, but the concentration of nucleophile used is typically extremely small.

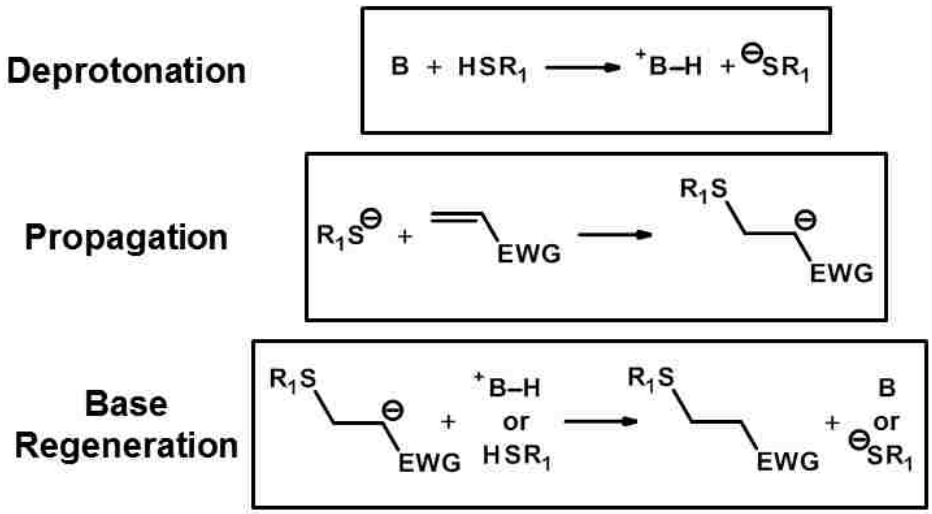

Scheme 1.4 General base-catalyzed thiol-Michael addition mechanism

As with the radical thiol-ene mechanism, the thiol-Michael polymerizations proceed via a step-growth mechanism; however, since the chain transfer step is a proton transfer to a strong carbanion base, the rate-limiting step is exclusively the propagation step. The nucleophile-initiated reaction has chain polymerization properties

similar to the radical thiol-ene mechanism since the anion can undergo propagation and chain transfer continuously.

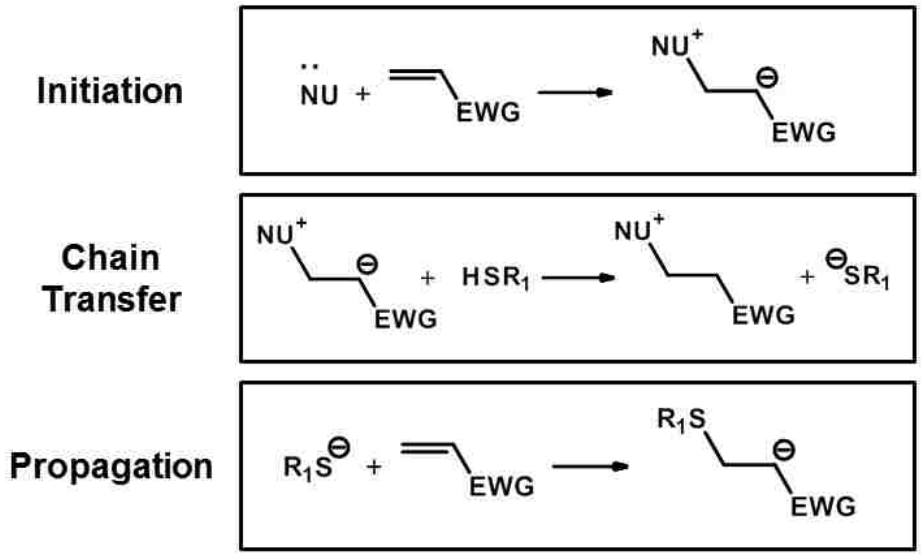

Scheme 1.5 General nucleophile-initiated thiol-Michael addition mechanism

Nucleophile initiated thiol-Michael additions typically have much higher reaction rates than base-catalyzed reactions since the equilibrium between thiolate and base lies further to the right when the primary base responsible for the thiol deprotonation is a carbanion. Additionally, the most available acidic proton for the carbanion to abstract after the propagation step is the thiol proton instead of the protonated amine catalyst. Scheme 1.6 illustrates some of the differences between the nucleophile-initiated and base-catalyzed reaction pathways. It is important to note that the propagation reaction and therefore the rate-limiting step in the polymerization are the same regardless of which pathway is used. The reactivity of enes in thiol-Michael polymerization reactions increases with decreasing electron density of the carbon-carbon double bond. Some commonly used enes in thiol-Michael additions are, in order of decreasing reactivity, maleimides, vinyl sulfones, acrylates, crotonates and methacrylates.[67] Thiol reactivity is

largely dependent on the pK_a of the thiol with thioglycolates reacting faster than mercaptopropionates, which in turn react more quickly than alkyl thiols.[18]

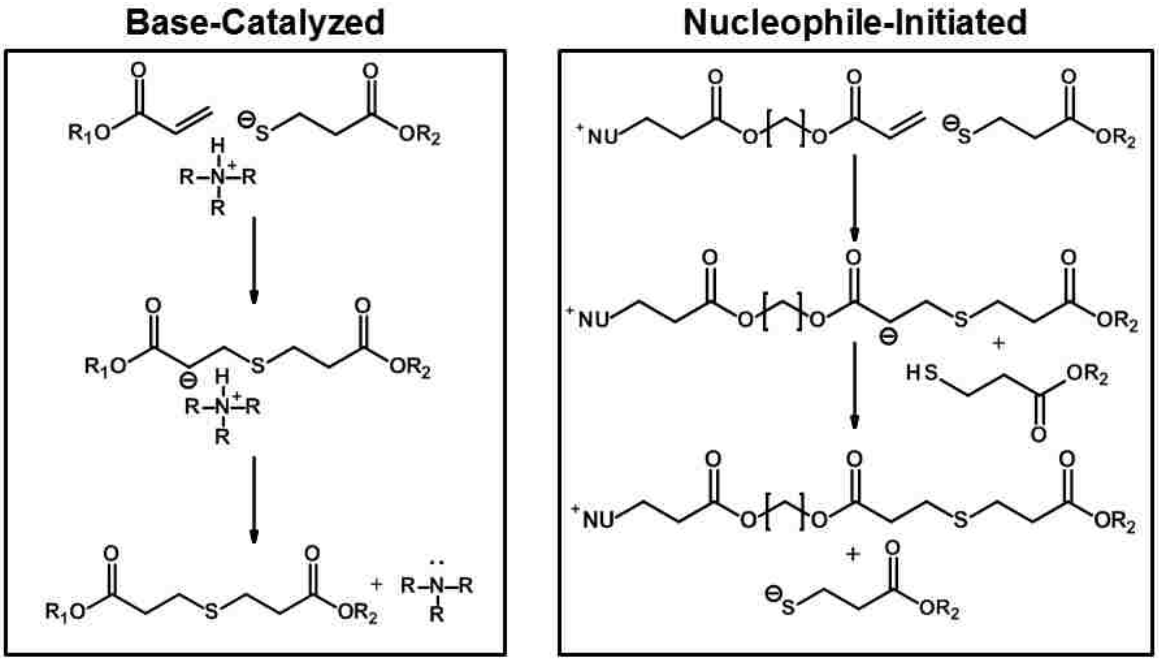

Scheme 1.6 Mechanistic differences between the two thiol-Michael addition reactions

Some of the benefits of thiol-Michael addition polymerizations include room temperature curing, a wide variety of commercially available monomers, solvent optional reactions, low hazard monomers and initiators, high conversions, and mild radical-free conditions.[66] Thiol-Michael addition polymerization reactions have been used to produce antimicrobial materials,[71] microparticles,[72] crosslinked biomaterials for tissue repair,[73-75] microfluidic resins,[76-77] hydrogels,[78-80] block copolymers,[81-82] grafted polymers,[83-84] star polymers,[85-87] dendritic polymers,[88-89] polymer-biomolecule conjugates,[90-92] biodegradable polymers,[93] and many other interesting products.[20, 66-67]

CHAPTER 2. THE KINETICS OF THIOL-ACRYLATE POLYMERIZATION REACTIONS USING MULTIFUNCTIONAL MONOMERS

2.1 Chapter Summary

Kinetic studies were performed on thiol-acrylate Michael addition polymerizations using a variety of multifunctional monomers and two different reaction mechanisms. The effect of secondary acrylate functionality in multifunctional acrylates was found to be consistent with observations made for monofunctional monomers. Increasing the thiol or acrylate functionality was found to increase the rate constant for polymerization in base-catalyzed systems. The primary reason for this is likely to be intramolecular effects increasing the reactivity of the functional groups, but the increase in thiol reactivity could also be caused by an entropic effect of having multiple groups held together in close proximity. The initial polymerization rates of trifunctional monomers were determined in the nucleophile-initiated thiol-acrylate Michael addition polymerization reaction. As in monofunctional systems, the change in mechanism gave faster polymerization rates, but the increase was not nearly as dramatic. The increase in viscosity associated with the gelation of multifunctional systems likely hinders the diffusion of the active species and causes the decrease in rate. The absence of radical polymerization processes during thiol-acrylate Michael addition polymerizations was confirmed, but radical polymerizations appear to initiate when the rate of the Michael addition is low. Any significant radical polymerization will dramatically affect the network structure, properties, and functional group conversion in the material, so this finding is especially important for making thiol-acrylate materials.

2.2 Introduction

The thiol-acrylate Michael addition reaction is a useful tool for click-type functionalization and making polymer materials; however, surprisingly little is known about the reaction kinetics, especially outside of model systems. Probably the most significant reports on this topic were published by Chan et al. in 2010,[18] in which the differences between the base-catalyzed and nucleophile-initiated mechanisms were explored, and by Kilambi et al. in 2007 and 2008,[94-95] where the effect of monomer side groups on the reaction kinetics was investigated. While these reports made significant contributions towards understanding of factors that affect the rate of thiol-acrylate Michael addition reactions, these studies were conducted using model systems where monofunctional monomers were used almost exclusively. This only addresses the behavior of these reactions when used as a functionalization technique and does not confirm if the same trends will be observed when making thiol-acrylate polymeric materials which require the use of multifunctional monomers.

The genesis of this project was the general observation that thiol-acrylate polymer systems using one acrylate, pentaerythritol triacrylate (PETA), gelled more quickly than those using trimethylolpropane triacrylate (TMPTA), even though the same thiol and amine concentrations were used. Even more interesting was that the two monomers only differed by one functional group at one position, a hydroxyl group on PETA, and a methyl group on TMPTA (see Scheme 2.1). One possible explanation was that the increased viscosity of PETA, due to hydrogen bonding, caused the mixture to physically gel sooner than TMPTA. The other possibility was that for whatever reason, PETA was reacting faster than TMPTA under the same conditions. In order to

answer that question and others, the kinetics of thiol-acrylate polymerization were investigated for a variety of thiol and acrylate monomers.

2.3 Materials and Methods

2.3.1 Materials

Pentaerythritol triacrylate (PETA) and trimethylolpropane triacrylate (TMPTA) were purchased from Alfa Aesar. Triethylamine ≥99% (TEA) was purchased from Sigma Aldrich and Alfa Aesar. Trimethylolpropane tris(3-mercaptopropionate) (TMPTMP) was purchased from Evans Chemetics, Sigma Aldrich, and TCI America. 2-ethylhexyl 3-mercaptopropionate ≥97% (EHM) was acquired from TCI America. Glycol di(3-mercaptopropionate) (GDMP) and Ethoxylated trimethylolpropane tris(3-mercaptopropionate) 700 (ETMPTMP 700) were generously donated by Evans Chemetics. SR454, SR499, and SR502 were purchased from Sartomer, and tris (2-hydroxy ethyl) isocyanurate triacrylate (TITA) was generously donated by Sartomer. Ebecryl 53 (EB53) was acquired from Cytec. Trimethylolpropane ethoxylate triacrylate average M_n ~912 (TMPETA 912), 1,4-butanediol diacrylate 90% (BDDA), pentaerythritol tetraacrylate (PETTA), pentaerythritol tetrakis(3-mercaptopropionate) >95% (PETMP), hexylamine 99% (HAm), dipropylamine 99% (DPA), triphenylphosphine ≥95% (TPP), 4-tert-butylcatechol ≥98% (TBC), 4-methoxyphenol 99% (MEHQ), and 2,2,6,6-tetramethylpiperidine 1-oxyl 98% (TEMPO) were purchased from Sigma Aldrich. See Scheme 2.1 for reagent structures.

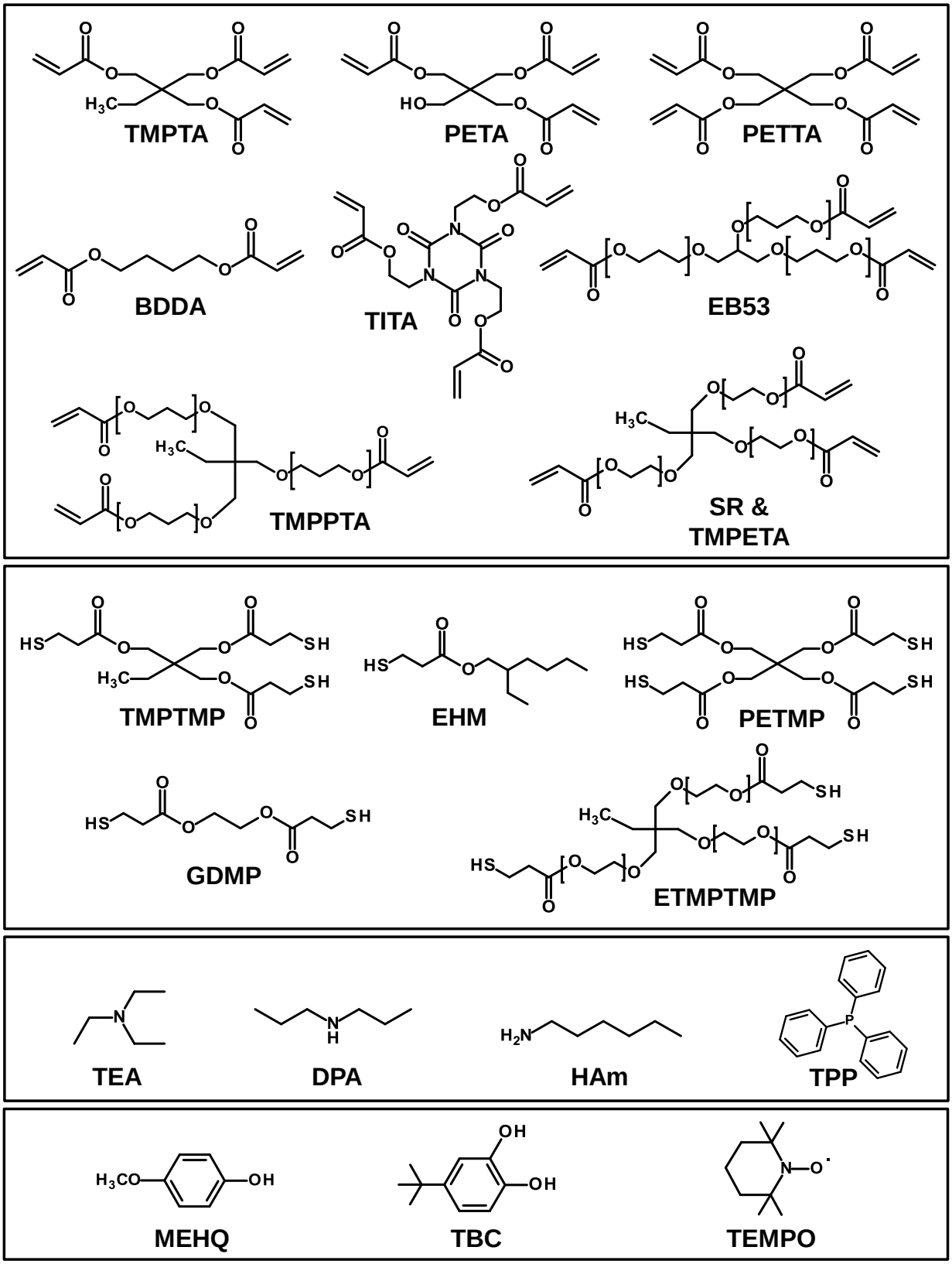

Scheme 2.1 Reagent structures

2.3.2 Experimental Methods

Acquiring FTIR Spectra

A Bruker Tensor 27 Fourier transform infrared (FTIR) spectrometer equipped with a Pike Miracle single-bounce diamond attenuated total reflectance (ATR) cell was used to track the conversion of thiol and acrylate groups over time. The thiol and acrylate were added sequentially to a glass vial with the denser monomer on the bottom. This was done to prevent mixing the two components prematurely since if an amine is added to a mixed sample, local gelation can occur and prevent a homogenous mixture from forming. Once the two monomers were added, the FTIR spectrometer was prepared. The instrument was fitted with a liquid sample cell to contain the monomer mixture around the ATR crystal, and a blank was performed on the empty cell. Once the instrument was set up, the necessary volume of amine was pipetted into the monomers. In the case of triphenylphosphine (TPP), which is a solid, it was dissolved in acetone at 10% then pipetted into the monomers. The vial was capped, inverted several times, and shaken to ensure thorough mixing. An aliquot of the mixture was removed from the vial and placed into the FTIR sample cell as quickly as possible. The FTIR was set to acquire spectra at a regular interval for a set duration, for example every 60 seconds for two hours. Data was acquired between 650 and 4000 cm^{-1} with a resolution of 4 cm^{-1}. Sixteen scans were taken for each spectrum, and all of the reactions were performed at room temperature.

FTIR Data Processing

Once the FTIR data was acquired, the data was processed using Bruker's FTIR software package, Opus. A 9-point smooth was performed on the spectra and baseline

correction was done using 10 iterations of the concave rubber band correction with 64 baseline points. As part of the acquisition process, the software was set to perform a CO_2 peak correction, so one was not done during the post-acquisition processing. After the smooth and baseline correction, the area under the peaks of interest was determined using the built in integration program. The thiol group concentration was monitored using the S-H stretching peak centered at 2573 cm^{-1}. The acrylate group concentration was tracked using the C=C stretching vibration doublet centered at 1625 cm^{-1}, and the C=C-H out of plane bending vibration at 810 cm^{-1} was used as a supplemental peak (see Figure 2.1). The bounds for each peak were determined visually, and method B was used in the Opus integration protocol. Using a macro generously provided by Bruker, the spectra were sequentially integrated and the results printed to a text file for further analysis.

Calculations and Data Fitting

After processing the data and performing the integrations using OPUS, the resulting text files were imported into Microsoft's Excel. Conversion of both thiol and acrylate groups was determined according to the formula

$$\text{Percent Conversion} = \frac{M_0 - M_t}{M_0} \times 100 \qquad \text{Eq. 2.1}$$

where M_0 is the initial monomer peak area and M_t is the peak area at time t. The first spectrum acquired was set as time zero, and it is assumed that no conversion of functional groups occurred before this time. However, this assumption is not strictly true, since some small amount of time passes from when the components are mixed to when the first spectrum is acquired, but this is unavoidable and has a minimal impact on the data analysis. In order to find monomer group concentrations, the concentration at

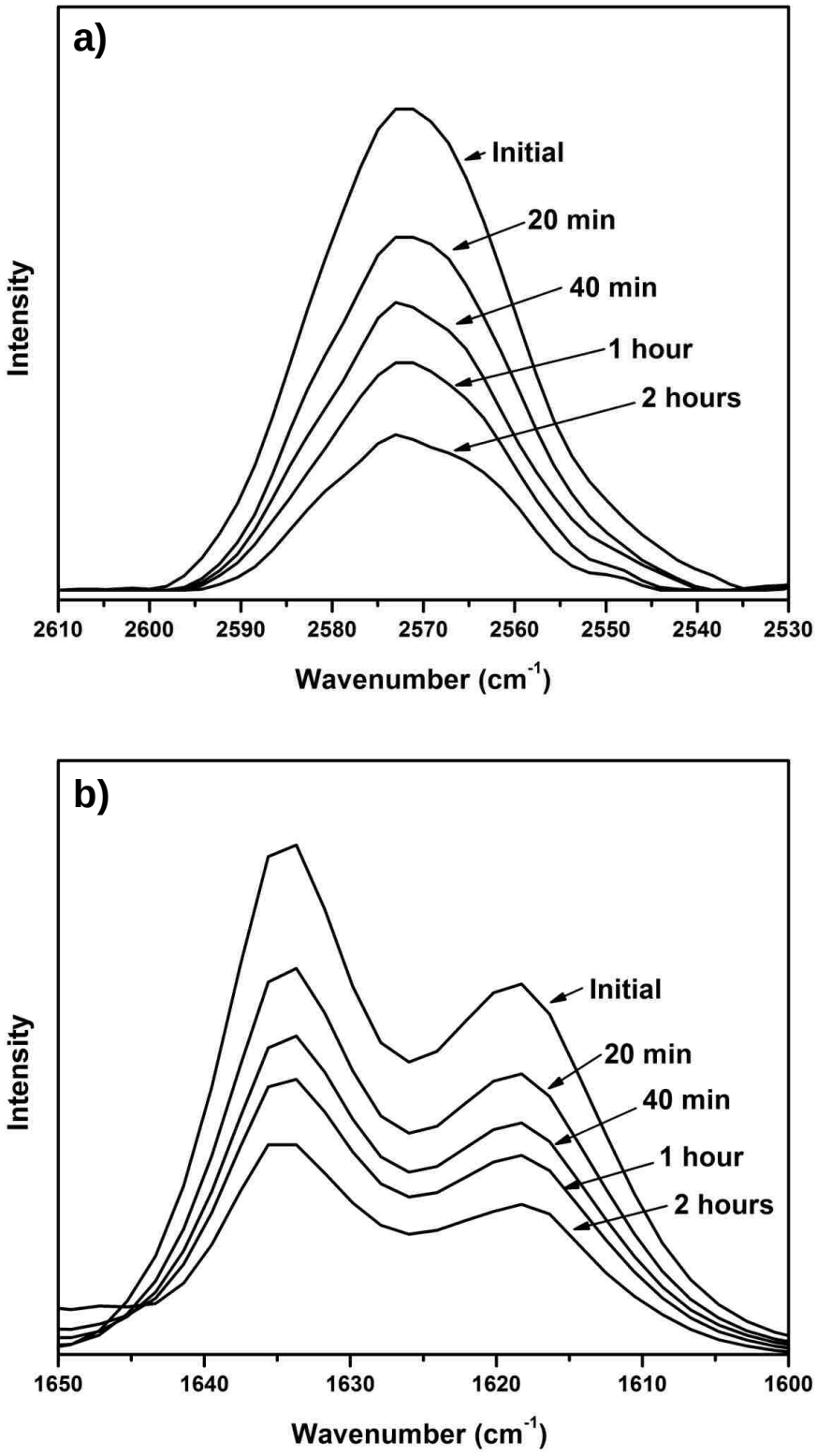

Figure 2.1 Example FTIR peaks for a) the thiol S-H bond stretching and b) the acrylate C=C bond stretching

time zero was set to the theoretical initial concentrations (moles functional groups/kg), and then the percent conversion was used to determine the amount of monomer that reacted over a given time interval.

2.4 Kinetic Fitting

2.4.1 Base-Catalyzed Reactions

Base-catalyzed thiol-acrylate polymerizations are known to proceed via an anionic step-growth mechanism,[18] and thus the basic rate equation is that of a step-growth polymerization,[66, 96-97]

$$\text{Rate} = k[\text{RSH}][\text{RCH} = \text{CH}_2] \qquad \text{Eq. 2.2}$$

where k is the rate constant, [RSH] is the thiol group concentration, and [RCH=CH_2] is the acrylate group concentration. However, since the thiol group is not the reactive species, as shown in Scheme 1.4, it must be replaced by the thiolate anion concentration to give

$$\text{Rate} = k[\text{S}^-][\text{RCH} = \text{CH}_2] \qquad \text{Eq. 2.3}$$

where [S^-] is the thiolate anion concentration. While this equation is now representative of the reaction behavior seen in thiol-Michael addition reactions, the thiolate anion concentration cannot be measured easily, which makes determining the rate constant more difficult. However, a substitution can be made for [S^-] by using the equilibrium equation between thiol groups and the base catalyst

$$K_{eq} = \frac{[\text{S}^-][\text{HB}^+]}{[\text{SH}][\text{B}]} \qquad \text{Eq. 2.4}$$

where [B] is the concentration of the base catalyst and [HB^+] is the concentration of the protonated catalyst after reacting with a thiol group. Since these reactions are

performed neat and the thiol-acrylate mixture is only moderately polar, the thiolate and protonated base will exist as a close ion pair instead of two individual compounds.[97-98] Considering this, Equation 2.4 can be rewritten to combine the thiolate and protonated base into one species [S^-HB^+]. This species is equivalent mechanistically to the [S^-] concentration that appeared in the rate law described earlier. Solving the modified Equation 2.4 for the active thiol species concentration and substituting that into Equation 2.3 yields Equation 2.5.

$$\text{Rate} = kK_{eq}[B][SH][RCH=CH_2] \qquad \text{Eq. 2.5}$$

This equation can be simplified into Equation 2.6 by combining the terms that stay constant during the reaction, which include the equilibrium constant and the catalyst concentration, into one term that is designated k_{app}.

$$\text{Rate} = k_{app}[SH][RCH=CH_2] \qquad \text{Eq. 2.6}$$

In order to find k_{app} using reaction data, the concentrations of thiol and acrylate groups over time need to be fit to an equation modeling their behavior.[99] In the simplest case, where thiol and acrylate group concentrations are equal, the reaction behavior can be written as a differential equation with only one concentration (Eq. 2.7) where [M] is the concentration of either monomer at time t.

$$-\frac{d[M]}{dt} = k_{app}[M]^2 \qquad \text{Eq. 2.7}$$

Equation 2.7 can be solved by integrating between time zero and time t and $[M]_0$, the initial monomer concentration, and [M]. After separation of variables, the integral can be written as Equation 2.8.

$$\int_{[M]_0}^{[M]_t} -\frac{1}{[M]^2} d[M] = \int_0^t k_{app} dt \qquad \text{Eq. 2.8}$$

Solving the integral yields Equation 2.8, which can be used to find k_{app} by plotting the inverse of monomer concentration versus time and performing a linear fit to determine the slope.

$$\frac{1}{[M]_t} = k_{app}t + \frac{1}{[M]_0} \qquad \text{Eq. 2.9}$$

Alternatively, Equation 2.9 can be rearranged into Equation 2.10, which can be fit using a non-linear approach.

$$[M]_t = \frac{[M]_0}{1+[M]_0 k_{app}t} \qquad \text{Eq. 2.10}$$

If the thiol and acrylate group concentrations are not equivalent at the start of the reaction, the simplified form used in Equation 2.7 is invalid; therefore, Equation 2.11 must be used

$$-\frac{d[A]}{dt} = k_{app}[A][B] \qquad \text{Eq. 2.11}$$

where the thiol and acrylate concentrations have been replaced by [A] and [B] and B is the monomer in excess. In order to simplify the differential equation, a new term, Δ, is introduced, which is the difference between [B] and [A]. Replacing the [B] in Equation 2.11 by (Δ + [A]) and integrating gives Equation 2.12.

$$\int_{[A]_0}^{[A]_t} -\frac{1}{[A](\Delta+[A])} d[A] = \int_0^t k_{app} dt \qquad \text{Eq. 2.12}$$

This evaluates to Equation 2.13,

$$\frac{1}{\Delta} \ln \frac{[A]+\Delta}{[A]}\Big|_{[A]_0}^{[A]_t} = k_{app}t\Big|_0^t \qquad \text{Eq. 2.13}$$

and after applying the limits of integration, the Δ inside the natural log terms is substituted for ([B] – [A]) at the appropriate times, zero or t, to give Equation 2.14.

$$\ln\frac{[B]_t}{[A]_t} = k_{app}\Delta t + \ln\frac{[B]_0}{[A]_0} \qquad \text{Eq. 2.14}$$

This equation can be used to find k_{app} by plotting the natural log of $[B]_t/[A]_t$ versus time and dividing by Δ. Solving for $[A]_t$ and replacing $[B]_t$ with $(\Delta + [A]_t)$ yields Equation 2.15, which can be used to find k_{app} with a nonlinear least squares fitting routine.

$$[A]_t = \frac{\Delta[A]_0}{[B]_0 e^{k_{app}\Delta t} - [A]_0} \qquad \text{Eq. 2.15}$$

All linear fitting was performed using Excel's built in "LINEST" function. Nonlinear fits were performed using Excel's Solver function, which takes an initial value for a variable and alters it until a set of conditions are fulfilled, such as minimizing the residual sum of squares between a set of data and a fitting model by modulating the key variable in the fitting equation. In this case, the acquired data was compared to points obtained from substituting the known values into a fitting equation (described below). The differences between the data points and the fit output points were taken, squared, and totaled. Solver was used to alter the unknown fit parameter until the sum of squares was minimized using the GRG Nonlinear solving method. Both the linear and nonlinear fits were used to find k_{app} using both the thiol and acrylate group concentrations for each system. The k_{app} values obtained from using each monomer concentration profile were averaged for the linear and nonlinear fits. These two values were then averaged to give the final k_{app} value reported for each experiment.

The base concentration used in each experiment was generally kept at a constant mole percent relative to thiol groups (except where otherwise noted), but this leads to different concentrations in mol/kg of amine, which was used for the data fitting process. Therefore, for monomers with different molecular weights, the amine

concentrations actually vary. To correct for this, the k_{app}/[B] will be compared for each system. The initial rate and final monomer conversion were also used to compare the thiol-acrylate systems. The initial rate was determined by plotting the monomer concentration versus time until 30% conversion was reached, or a minimum of 6 data points, and taking the slope of the resulting curve. The final conversion after the experiment run time, 2 hours, was determined by averaging the last 5 conversion points for each functional group. A minimum of three separate FTIR experiments were performed for each monomer system, the results were averages, and the standard deviation was reported as error.

2.4.2 Nucleophile-Initiated Reactions

The rate law and fitting process described above only works for thiol-acrylate polymerizations that proceed via the base-catalyzed mechanism. Polymerizations following the nucleophile-initiated mechanism have a different rate law, but it is unknown at this point. Mechanistic factors that complicate the formation of an accurate rate law in nucleophile-initiated thiol-Michael additions include: the consumption of ene through initiation and propagation, the behavior of amines as both nucleophiles and bases at different points in the reaction, and the sequential nature of the nucleophile addition to give polymerization. While the development of a rate law for this process would be a worthy venture, that problem will not be addressed here. Since k_{app} cannot be determined without an accurate rate law, other metrics will be used to compare systems that proceed via this alternate mechanism such as the initial rate and the final conversion of functional groups.

The initial rate was determined by plotting the monomer concentration versus time until 30% conversion was reached, or a minimum of 6 data points, and taking the slope of the resulting curve. The final conversion after the experiment run time, 2 hours, was determined by averaging the last 5 conversion points for each functional group.

2.4.3 Monomer Purity

The monomers used in this study were all commercially available and used as received without any further purification. Unfortunately, multifunctional thiol and acrylate compounds are not available in highly pure forms, and the purity of these compounds is generally not well reported. Pentaerythritol triacrylate (PETA), for example, is sold as technical grade with a definite molecular weight and structure listed, but it actually is a complex mixture of reaction products.[100] The primary impurities in PETA are the diacrylate and tetraacrylate associated with under and over esterifying pentaerythritol with acrylic acid. Other minor impurities include Michael addition products between the pentaerythritol alcohol and the acrylic acid double bond, the esters produced using that product, and dimers. Trimethylolpropane tris(3-mercaptopropionate) (TMPTMP), which is a trifunctional thiol, is produced by esterifying trimethylolpropane with mercaptopropionic acid. The major impurity in TMPTMP is mercaptopropionic acid, which was present at a concentration of 7% in one commercially-obtained sample. All of the other thiols and acrylates used in the following studies are likely to have similar impurities to the ones discussed above.

Therefore, due to the uncertain purity of the reaction components, the rate constant values obtained in this study are almost certainly not the true values for the pure monomer systems; however, the value of these results lies within the insight they

provide into the reaction behavior of these compounds in real world applications. Comparing the obtained rate constants, and other parameters, across a variety of different thiols and acrylates with large structural and functionality differences should allow some general trends to be observed.

2.5 PETA v TMPTA: The Effect of Monomer Side Groups

The k_{app}/[B] was determined for both PETA and TMPTA when reacted with TMPTMP in a theoretical 1-1 functional group ratio using 0.33 mol% TEA relative to thiol groups. As shown in Table 2.1, PETA is in fact reacting more quickly with TMPTMP than TMPTA is under the same conditions. The k_{pp}/[TEA] value obtained for PETA is nearly twice that of TMPTA, as is the initial rate of the reaction. This leads to an average overall conversion of 68 ± 2% in 2 hours with PETA as compared to 53 ± 1% with TMPTA.

Table 2.1 TMPTA v PETA Kinetics

Acrylate	K_{app}/[TEA] (kg^2 mol^{-2} min^{-1})	Initial Rate (mol kg^{-1} min^{-1})	Final Conversion (%)
TMPTA[a]	0.157 ± 0.004	0.028 ± 0.001	53 ± 1
PETA[a]	0.30 ± 0.03	0.052 ± 0.003	68 ± 2

a) All reactions performed with TMPTMP

Based on this data, the primary reason PETA gels more quickly than TMPTA is the faster polymerization rate, which is most likely due to the presence of the hydroxyl group in PETA. It has been demonstrated in monofunctional systems that side groups on acrylate monomers can have a large impact on the acrylate reactivity due to intramolecular effects that make the double bond more susceptible to nucleophilic attack.[95, 101] In the case of PETA, the hydroxyl group is altering the electronics of the acrylate double bonds to make them more susceptible to attack by the thiolate anion.

The hydroxyl group on PETA could also increase the rate of the thiol-Michael addition by increasing the polarity of the system, which has been shown to increase the rate of Michael addition reactions.[95] In the case of base-catalyzed systems, the increased polarity stabilizes the thiolate anion and allows for increased separation between it and the protonated base, which increases its reactivity towards the acrylate double bond. In order to determine if that concentration of hydroxyl groups could significantly alter the polarity of the mixture and increase the reaction rate constant, butanol (BuOH) was added to TMPTA in a ratio of 3-1 acrylate groups to alcohols to mimic the concentration in PETA. As shown in Table 2.2, there was a slight increase in the k_{app}/[TEA] for the TMPTA with BuOH, but it was within experimental error. Interestingly, the initial rate and final conversion in the alcohol system both decreased, which means that any increase in rate constant afforded by the increased polarity of the alcohol was overshadowed by the effect that decreasing the thiol and acrylate group concentration had on the overall polymerization reaction.

Table 2.2 TMPTA Kinetics with Added Alcohol

Acrylate	K_{app}/[TEA] ($kg^2\ mol^{-2}\ min^{-1}$)	Initial Rate ($mol\ kg^{-1}\ min^{-1}$)	Final Conversion (%)
TMPTA[a]	0.157 ± 0.004	0.028 ± 0.001	53 ± 1
TMPTA + BuOH[a,b]	0.17 ± 0.03	0.022 ± 0.004	50 ± 5

a) All reactions performed with TMPTMP b) 3-1 Acrylate to -OH by moles

Based on this data, it is evident that the increased reactivity observed in PETA is linked to the intramolecular effect the hydroxyl group has on the acrylate groups and not on the increase in system polarity that it brings compared to TMPTA. These findings are in agreement with those reported by Kilambi et al. who demonstrated that the incorporation of a functional group into the acrylate molecule has a much greater effect on the rate constant than simply adding in that functional group via a solvent.[94-95]

2.6 The Effect of Acrylate Structure on the Polymerization Kinetics

In order to determine if acrylate structural variations other than functional group changes affected the base-catalyzed Michael addition polymerization rate of triacrylates with TMPTMP, the kinetics for a series of other acrylates were determined. Table 2.3 lists the kinetic parameters for seven additional triacrylates in addition to PETA and TMPTA all polymerized with TMPTMP at room temperature using 0.33 mol% TEA relative to thiol groups. Entries 3-6 are all triacrylates based on TMPTA with a poly(ethylene glycol) (PEG) segment between the core and each acrylate group (see Scheme 2.1 for structures). There is no statistical difference in the k_{app}/[TEA] with increasing PEG segment length for the first 3 monomers, but TMPETA 912 has a higher k_{app}/[TEA] than the other ethoxylated monomers and even TMPTA. The only difference between TMPETA 912 and SR502 is the length of the PEG segment, so an increase in rate constant was not expected, especially since it had not increased between SR454 and SR502. Michael addition rate constants have previously been shown to decrease as spacer length increased in a diacrylate system, which was attributed to a reduction in the intramolecular effects that each acrylate group had on the electronics of the other as the distance between them grew.[95] In that study, the spacer was changed from two carbons to six, so one possible reason why a reduction in rate constant was not observed in this system is due to the intramolecular contributions from the PEG spacers themselves. The relatively high reactivity of TMPETA 912 could be partially due to the increased polarity of the system from the PEG spacers, but that is unlikely given that there was no increase in k_{app}/[TEA] between TMPTA and the other ethoxylated monomers. One additional difference between the SR series monomers and TMPETA

912 is their different sources. It is possible that an impurity that is absent in the SR series monomers but is present TMPETA 912 is the cause of the increased reactivity.

Table 2.3 Kinetics of TMPTA Variants

Entry	Acrylate[a]	Structural Difference	k_{app}/[TEA] (kg^2 mol^{-2} min^{-1})
1	TMPTA	-	0.157 ± 0.004
2	PETA	-OH for $-CH_3$	0.30 ± 0.03
3	SR454	Ethoxylated (1 per arm)	0.143 ± 0.004
4	SR499	Ethoxylated (2 per arm)	0.13 ± 0.01
5	SR502	Ethoxylated (3 per arm)	0.13 ± 0.02
6	TMPETA 912	Ethoxylated (4-5 per arm)	0.20 ± 0.02
7	TITA	Cyanuric Acid Based	0.26 ± 0.03
8	EB53	Glycerol Based and Propoxylated	0.082 ± 0.009
9	TMPPTA	Propoxylated (~2 per arm)	0.044 ± 0.005

a) All reactions performed with TMPTMP

TITA has a k_{app}/[TEA] in between TMPTA and PETA, but the structure is very different. TITA is based on cyanuric acid, and the increase in rate constant relative to TMPTA is likely due to intramolecular interactions with the cyanurate core that reduce the activation energy of the Michael addition, similarly to the carbamate functionalized acrylates studied previously.[101] EB53 and TMPPTA gave the lowest k_{app}/[TEA] which is surprising given their relative structural similarity to the ethoxylated TMPTA monomers. The reason for the low reactivity could be due to the extra carbon present in the propxylate spacer present in EB53 and TMPPTA compared to the ethoxylate spacer in the other monomers. Increasing the number of propxylates from 1 to 2 appeared to significantly increase the rate constant, but since the base alcohol also changed from glycerol to trimethylolpropane the effect cannot be isolated to a single cause. The increase in the number of propxylate groups could decrease the rate constant due the higher number of carbons between the acrylate groups. Alternatively, using glycerol as

the central compound could increase the intramolecular effect that the acrylates have on each other compared to trimethylolpropane since two of the acrylate groups are only separated by two carbons in EB53 while all three are separated by 3 carbons in TMPPTA.

2.7 The Effect of Monomer Functionality on the Polymerization Kinetics

In order to determine the effect of monomer functionality on the kinetics of base-catalyzed thiol-acrylate polymerizations, a series of acrylates and thiols with varying functionalities were studied. Table 2.4 contains the results for several acrylates reacted with TMPTMP and 0.33 mol% TEA relative to thiol groups.

Table 2.4 Effect of Acrylate Functionality on the Polymerization Kinetics

Acrylate[a]	**Functionality**	**k_{app}/[TEA] (kg^2 mol^{-2} min^{-1})**
BDDA	2	0.101 ± 0.003
TMPTA	3	0.157 ± 0.004
PETTA	4	0.23 ± 0.01

a) All reactions performed with TMPTMP

Clearly the acrylate functionality affects the polymerization reaction kinetics as there is a significant increase in the k_{app}/[TEA] with increasing acrylate functionality. As with PETA, the increase in rate constant observed with increasing acrylate functionality is consistent with the theory that secondary functionalities containing electronegative atoms increase the reactivity of their surrounding acrylate groups. This effect has been previously observed when increasing the acrylate functionality from 1 to 2, and further increases in functionality appear to also follow this trend.[95]

The effect of thiol functionality on the polymerization kinetics was also determined by fitting for k_{app}/[TEA] for when reacting several different mercaptopropionates with TMPTA using 0.33 mol% TEA relative to thiol groups. As

shown by Table 2.5, the thiol functionality also has a considerable effect on the reaction behavior.

Table 2.5 Effect of Thiol Functionality on the Polymerization Kinetics

Thiol[a]	**Functionality**	**k_{app}/[TEA] (kg^2 mol^{-2} min^{-1})**
EHM[b]	1	0.031 ± 0.002
GDMP[c]	2	0.071 ± 0.007
TMPTMP	3	0.157 ± 0.004
PETMP	4	0.29 ± 0.01

a) All reactions performed with TMPTA b) Acquired using 3.33 mol% TEA c) Rate constant determined over first 15 minutes of reaction

With each increase in thiol functionality, the k_{app}/[TEA] value essentially doubled, which when compared to the effect of acrylate functionality, suggests that the rate constant is more strongly influenced by whatever effect increasing thiol functionality has on the reaction. Similar to the effect of increasing acrylate functionality, one possible explanation for the increase in rate constant is the electronic effect of the esters present in the mercaptopropionate groups lowering the pK_a of the thiol, which is known to increase Michael addition reactivity in base-catalyzed systems.[102] Altering the acidity of the thiol group will shift the K_{eq} towards products, and since it is incorporated into the k_{app} term, this will increase the rate constant. In order to test this theory, the kinetics were determined for an ethoxylated trithiol (ETMPTMP 700) under the same reaction conditions. If the increase in rate constant with increasing thiol functionality is due to an effect similar to what was observed in the acrylates, the k_{app}/[TEA] for the ethoxylated monomer should remain comparable to the non-ethoxylated TMPTMP. When the reaction was performed using the typical TEA concentration of 0.33 mol% relative to thiol groups, the reaction proceeded very slowly then was overshadowed by a radical polymerization (see Section 2.9 for more information on radical reactions). This was the

first indication that the reaction rate constant for the ETMPTMP 700 was not the same as TMPTMP, since reactions using TMPTMP with that amine concentration progress at reasonable rates. In order to effectively determine the k_{app}/[TEA] for the ETMPTMP 700, the [TEA] was raised to 3.33 mol% relative to thiol groups. The reaction proceeded successfully at this amine concentration, and the k_{app}/[TEA] was determined to be 0.086 ± 0.006 kg^2 mol^{-2} min^{-1}. This falls significantly closer to the rate constant observed for dithiol than to TMPTMP, which is opposite of the trend seen in the acrylates. This suggests that there may be another reason for the increase in rate constant observed with increasing thiol functionality.

One thing that adding the ethylene glycol repeating units to TMPTMP does affect is the distance between the thiol groups in the molecule. It is possible that having multiple thiol groups close together in a multifunctional monomer could facilitate the deprotonation and subsequent addition to an acrylate of one thiol group after the addition of the first. When an enolate is formed after the addition of a thiolate, it can either abstract a proton from a thiol group or a protonated amine, but for multifunctional thiols, the likelihood of direct thiol deprotonation by an enolate could increase since the local concentration of thiol groups increases with functionality. Unfortunately, in order to formulate a better hypothesis, experiments using every functionality combination of thiol and acrylate need to be performed, as well as kinetic runs using other trithiols where the thiol groups are physically separated from one another.

2.8 The Nucleophile-Initiated Mechanism

When using monofunctional thiols and acrylates, Chan et al. demonstrated a 3 order of magnitude increase in the rate of reaction when switching from TEA to

hexylamine (HAm) which corresponds to a change in the reaction mechanism for base-catalyzed to nucleophile initiated.[18] In order to determine if this same effect occurs in multifunctional monomer systems, thiol-acrylate reactions were performed using primary, secondary, and tertiary amines as well as a phosphine. Table 2.6 contains the initial rates of polymerization for TMPTA and PETA with TMPTMP using 0.33 mol% of each amine relative to thiol groups and 0.165 mol% of TPP.

Table 2.6 Initial Polymerization Rates (mol kg^{-1} min^{-1}) in Both Mechanisms

Acrylate[a]	**TEA (3°)**	**DPA (2°)**	**HAm (1°)**	**TPP[b]**
TMPTA	0.028 ± 0.001	0.234 ± 0.004	0.17 ± 0.02	0.104 ± 0.008
PETA	0.052 ± 0.003	0.18 ± 0.02	0.11 ± 0.05	0.13 ± 0.03

a) All reactions performed with TMPTMP b) Performed using 0.165% TPP

When the amine was changed from TEA to DPA, the reaction mechanism switched from base-catalyzed to nucleophile-initiated, and the initial rate increased by ~8.4x in TMPTA and only ~3.5x in PETA. Considering the reported rate increase was ~286x when switching between those two amines in a monofunctional system, the modest increase observed in this multifunctional system was somewhat surprising. In addition to the relatively small increase in rate, the monomer that exhibited the higher reaction rate switched from PETA in the base-catalyzed mechanism to TMPTA in the nucleophile initiated mechanism. Changing the amine from DPA to Ham should also increase the polymerization rate, but the observed rates of reaction decreased slightly for both PETA and TMPTA. In addition to amines, phosphines are potent nucleophiles that will initiate thiol-Michael polymerization and have much faster polymerization rate than tertiary amines. When TPP was used to initiate the reaction, the initial rate was slightly higher in PETA than TMPTA, which was the opposite of the primary and secondary amines. When 0.33 mol% of the TPP was used to initiate the

polymerization, the conversion was extremely rapid, so 0.165 mol% was used to ensure that the monomer mixture could be placed on the FTIR before significant reaction occurred. Considering that half as much TPP was used to obtain the initial rate values, the phosphine-initiated reaction initial rate cannot be directly compared to the amines.

The inversion of reactivity from PETA to TMPTA with the change in the reaction mechanism is likely due, once again, to the hydroxyl group in PETA. Although the two mechanisms are referred to by different names, they operate in a very similar manner since the enolate produced by the addition of the initiating nucleophile to an ene is nothing more than a strong base. Instead of using an amine base such as TEA (pk_a = 10.8), the nucleophile-initiated mechanism generates a much stronger enolate base (pk_a ~ 25) in situ, which shifts the equilibrium between thiolate and base to the right and increases the thiolate concentration and thus the reaction rate.

Another similarity is that both bases are regenerated during the course of the reaction, except that a new enolate is formed with every thiol addition instead of the same protonated base being reactivated after deprotonation. Keeping this in mind, any compound containing even slightly acidic hydrogens can be deprotonated by the enolate to form a weaker base, which will decrease the reaction rate by altering the base-thiolate equilibrium. The identity of the protic species is the most dominant factor in determining what effect its presence has on the reaction since a relatively poor acid, like water ($pk_a \approx 15.7$), will simply slow the reaction while a strong acid can stop the reaction from occurring completely.[102-103] Alcohols, like in PETA, have pk_a values of ~17 and should slow the reaction since they still form a strong base upon deprotonation,

which is likely why PETA does not perform as well in the nucleophile-initiated reactions despite its increased Michael addition reactivity compared to TMPTA.

The one nucleophile-initiated system where PETA performed slightly better than TMPTA was with TPP. One possible explanation for this is that the enhanced nucleophilicity of the phosphine was able to produce enough propagating chains to overcome the inhibitory effects of the alcohol on the reaction. One interesting difference between the amine-initiated and phosphine-initiated systems is that amines can act both as bases and nucleophiles, while phosphines are generally poor bases and will only add to the ene as a nucleophile. This is consistent with observations of an short induction period at the beginning of the phosphine-initiated systems (see Figure 2.2) which is absent when any of the amines are used.[104]

In the amine systems, even if protic species are inhibiting the chain-like nucleophile initiated pathway by protonating the enolate, the amines can still operate as bases and catalyze the reaction. In the phosphine systems, the induction time represents the consumption of the enolates produced when the phosphine adds to an ene, which slows the polymerization down dramatically, but once all of the protic species have been consumed, the reaction proceeds normally. This theory is consistent with the observation that increasing the phosphine content shortens the induction time since the protic impurities are consumed more quickly by the higher enolate concentration.

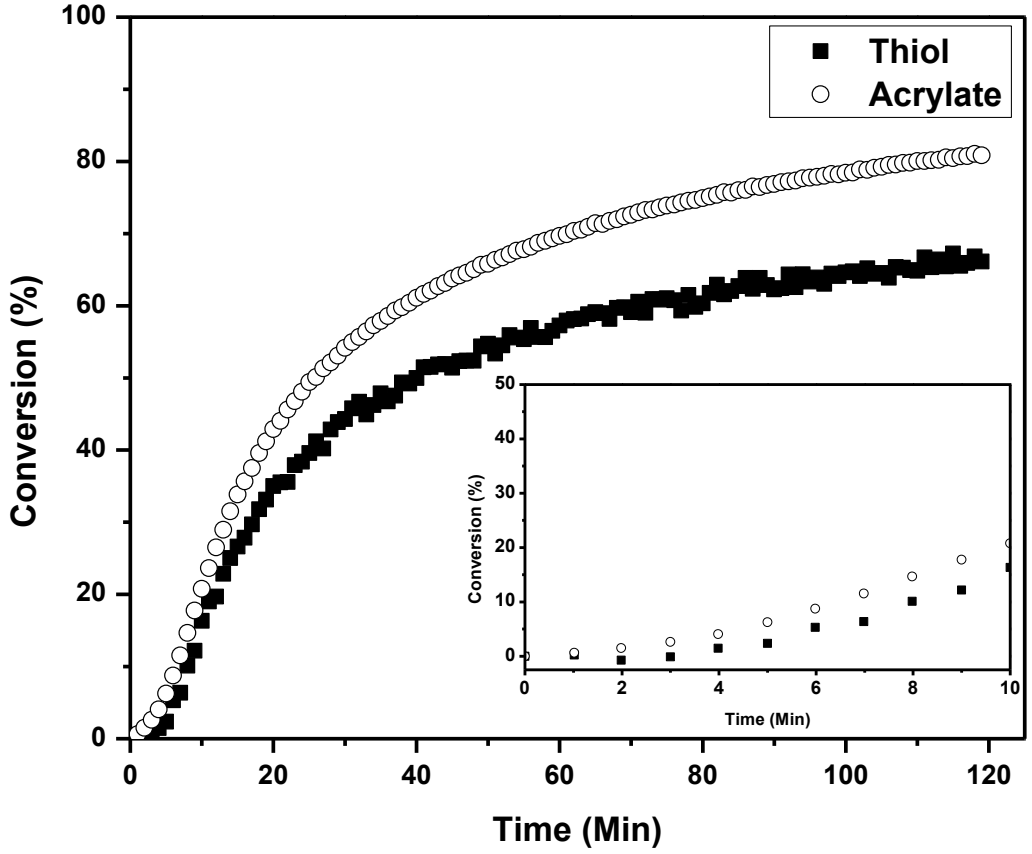

Figure 2.2 Induction time observed for a phosphine-initiated reaction (inset shows the first 10 minutes of polymerization)

The decreased reactivity of PETA in the nucleophile-initiated thiol-Michael addition systems can be attributed to the hydroxyl group, but both TMPTA and PETA had lower polymerization rates than expected. One difference between the well-studied monofunctional systems and these multifunctional monomer systems is that the reaction mixtures gel as the polymerization progresses. Under the base-catalyzed mechanism, the gelation process has little effect on the polymerization rate since the base catalyst is typically a small molecule that can diffuse easily throughout the polymer network to continuously deprotonate thiol. In the nucleophile-initiated mechanism however, the nucleophile imitates a propagating chain but is covalently bound into the network, so after just one polymerization step, the base responsible for deprotonating a thiol to

continue the reaction is now, at minimum, a dimer of the thiol and acrylate monomers. This much larger molecule will diffuse more slowly through the reaction mixture which could shift the equilibrium constant and slow the reaction. Another possible explanation is that even though enolates are extremely strong bases, in multifunctional acrylates, the steric hindrance around that carbanion is likely increased due to the presence of the other acrylate groups in monomer and the added multifunctional thiol molecule. High steric hindrance could offset some of the rate increase gained by producing a strong base and dampen the overall effect of switching mechanisms.

2.9 The Effect of Background Radical Reactions

One of the disadvantages of thiol-ene systems is their poor shelf life since mixtures of thiols and enes will spontaneously polymerize with time. Figure 2.3 shows the conversion profile for a 1-1 mixture of PETA and TT1 with no added amine. Even during the two-hour duration of the experiment, over 80% of the acrylate groups reacted. The difference in the thiol and acrylate conversions indicates that a radical thiol-ene reaction is occurring since the rate of acrylate radical homopolymerization is significantly faster than chain transfer to thiol. The induction period is also indicative of a radical polymerization since the inhibitor in the acrylate must be consumed before significant reaction can occur. The extent of the radical reaction over this short timescale was surprising, and it was important to determine if this background process was affecting the measured rates and rate constants for the thiol-Michael reactions. To determine whether or not significant radical polymerization was occurring during the thiol-Michael addition polymerization studies, the k_{app}/[TEA] was determined for a system with and without a radical inhibitor present. First, a series of preliminary kinetics

runs were performed to determine the ratio of TMPTA and TMPTMP that would give exactly 1-1 conversion.

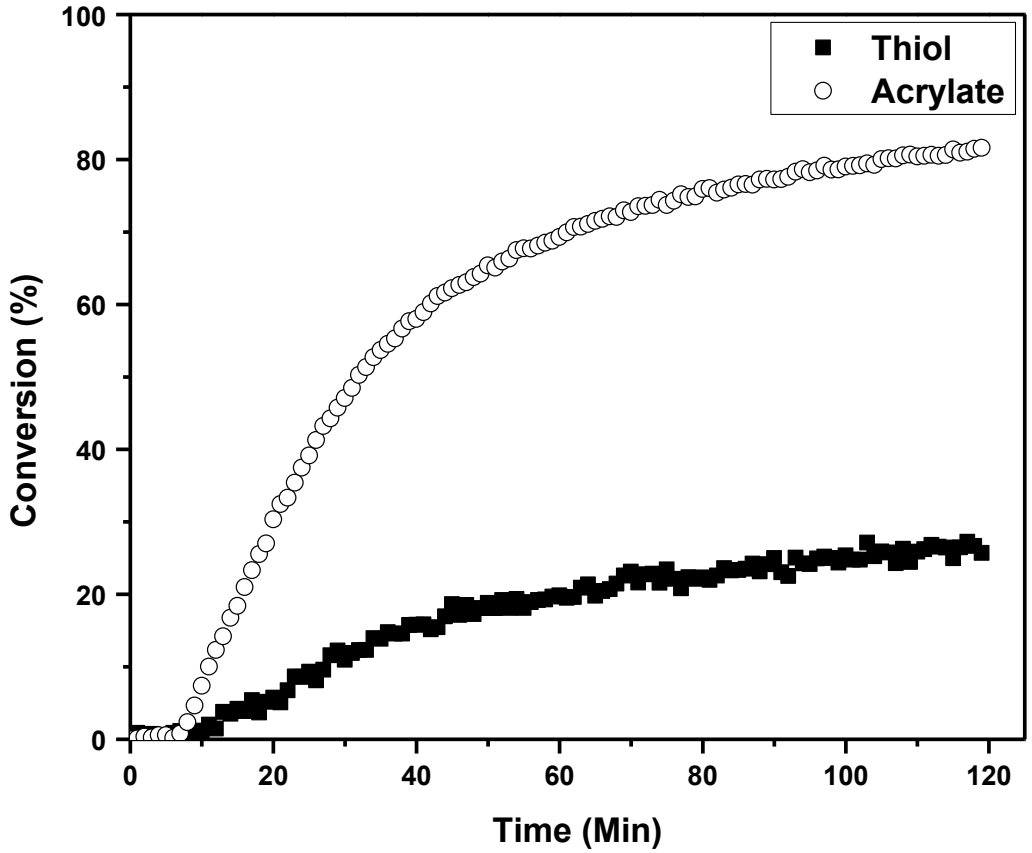

Figure 2.3 Radical polymerization in a PETA-TMPTMP mixture

It was determined that 10% excess acrylate (EA) groups were needed to compensate for the monomer impurities and give 1-1 conversion. If there is radical polymerization occurring during the Michael addition, deviations from the exact 1-1 conversion ratio would become evident when a radical inhibitor was added. The next step was to find an inhibitor and concentration that would stop any significant radical polymerization from occurring over the 2-hour timescale of the experiment. The ability of several radical inhibitors to stabilize thiol-ene mixtures has been investigated,[105] and based on those results, tert-butylcatchol (TBC) was chosen to stabilize the thiol-acrylate

mixtures. In addition to the 100 ppm of monomethyl ether hydroquinone (MEHQ) that was already present in the TMPTA, an additional 10 ppt of TBC was added to the TMPTA prior to mixing with the TMPTMP. In order to confirm that the added TBC was suppressing the radical polymerization, FTIR runs were performed with and without the TBC on mixtures of TMPTA and TMPTMP with 10% EA and no amine, and example conversion v time plots are displayed in Figure 2.4. Upon the addition of the TBC, no significant functional group conversion was observed over the two hour experiment window. Next, the k_{app}/[TEA] for the thiol-Michael addition between TMPTA and TMPTMP was determined with and without TBC using 0.33 mol% TEA relative to thiol groups.

If there is significant radical polymerization occurring during the Michael addition, there should be an effect on the rate constant as well as a change in the conversion difference between thiol and acrylate. As shown by Table 2.7, the k_{app}/[TEA], initial rate, and final conversion were slightly higher for the radically inhibited samples compared to the uninhibited ones, but the difference does not exceed experimental uncertainty. This, along with the nearly equivalent conversion profiles for thiol and acrylate, suggest that there is essentially no radical polymerization occurring when the thiol-Michael addition reaction is being promoted with a base catalyst. To confirm this and determine the effectiveness of another radical inhibitor, the same procedure was repeated using 2,2,6,6-tetramethylpiperidine 1-oxyl (TEMPO), which is a commonly used free radical trap. As with the TBC, there was essentially no conversion observed over two hours when no amine was added to the monomer mixture. The kinetic data acquired after 0.33 mol% TEA was added is also presented in Table 2.7.

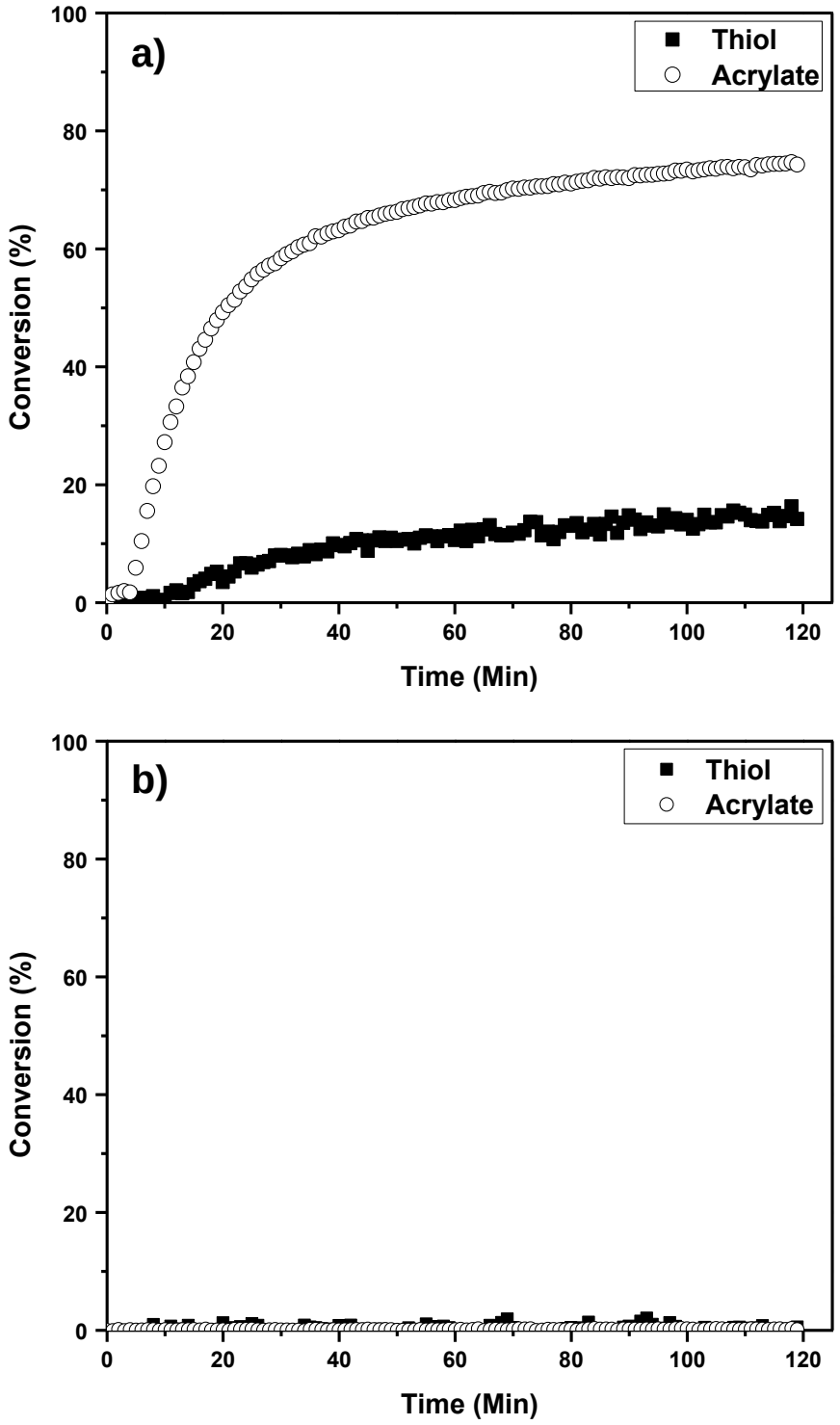

Figure 2.4 Radical polymerization of TMPTA-TMPTMP mixtures with a) no TBC and b) with 10 ppt TBC added

Table 2.7. Effect of radical inhibitors on thiol-Michael addition kinetics

Inhibitor	K_{app}/[TEA][a]	Initial Rate[b]	Average Final Conversion[c]	Average Δ Final Conversion[c,d]
None	0.145 ± 0.005	0.0278 ± 0.0008	51.5 ± 0.7	-0.8 ± 0.5
100 ppm MEHQ + 10 ppt TBC	0.152 ± 0.007	0.030 ± 0.001	53 ± 1	0.6 ± 0.5
100 ppm MEHQ + 10 ppt TEMPO	0.162 ± 0.002	0.0303 ± 0.0004	54.4 ± 0.4	-0.1 ± 1.8

a) $kg^2\ mol^{-2}\ min^{-1}$ b)$mol\ kg^{-1}\ min^{-1}$ c) % d) Thiol conversion - acrylate conversion

Compared to the uninhibited samples, adding TEMPO gave a slight increase in the average k_{app}/[TEA], initial rate, and final conversion, but the conversion profiles of thiol and acrylate remained consistent with each other. While there is no evidence of radical polymerization occurring during the Michael addition, it is possible that the inhibitors, especially TEMPO, are somehow affecting the reaction and increasing the rate constant; however, this effect is relatively minor and was not investigated further.

Several situations where radical polymerization was observed during the thiol-Michael addition reaction were towards the end of many of the nucleophile-initiated kinetic runs as well as during the TMPTA glycol di(3-mercaptopropionate) (GDMP) trials (see Figure 2.5). One thing that these scenarios have in common is that the polymerization rate at these instances is quite low. The GDMP systems react slowly from the onset, but the nucleophile-initiated mechanism have a period of rapid reaction followed by a slow rise due to a shift towards the base-catalyzed mechanism once all of the propagating anionic chains have been transferred to less reactive bases.

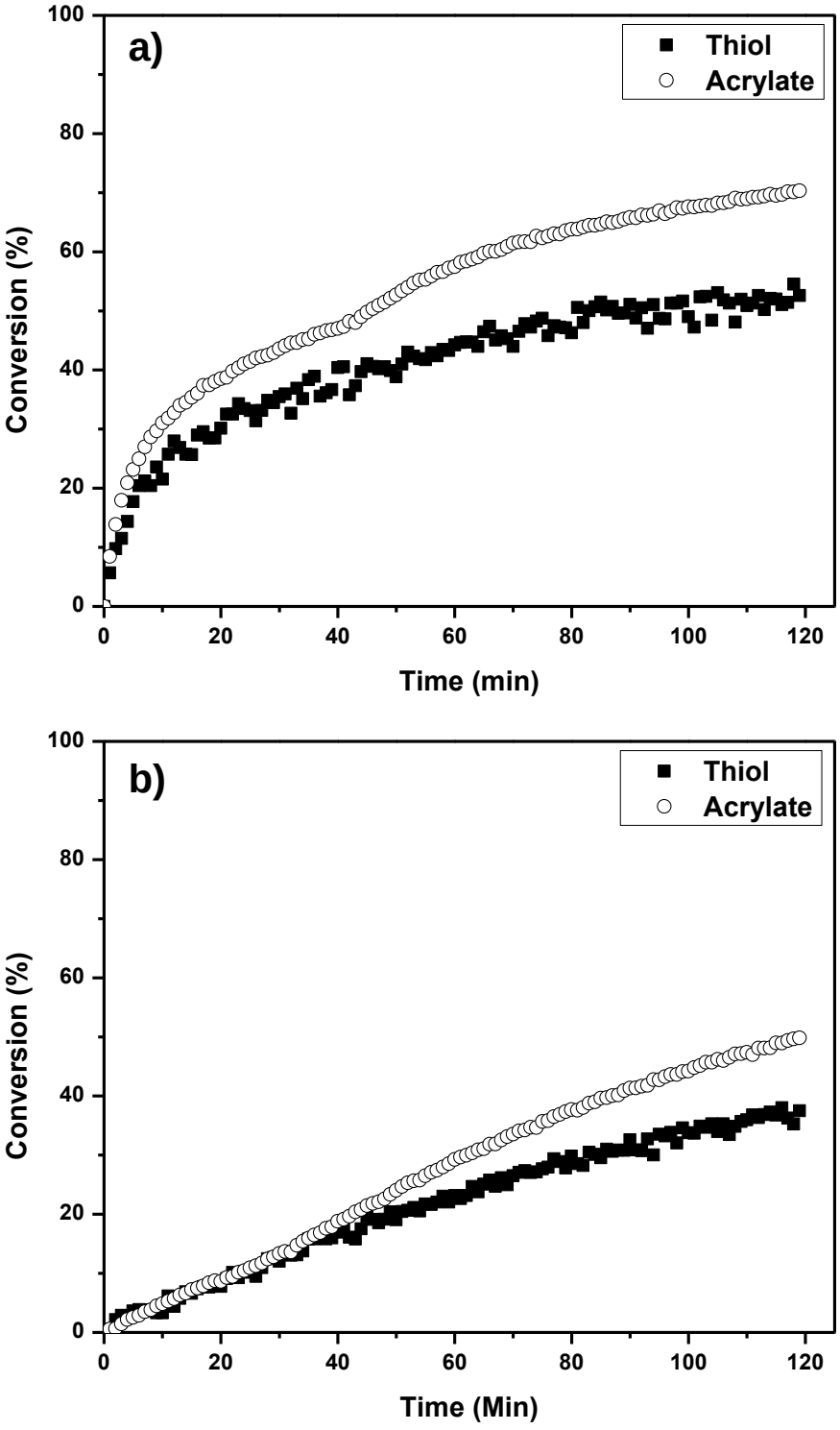

Figure 2.5 Radical polymerization during the thiol-Michael addition of a) TMPTA-TMPTMP with 0.33% Ham and b) TMPTA-GDMP with 0.33% TEA

In order to determine if there was a connection between the low thiol-Michael addition rate and the onset of polymerization, TMPTA and TMPTMP were polymerized in the presence of half the usual amount of TEA (0.165 mol% relative to thiol groups). As illustrated in Figure 2.6, after a short period of slow Michael addition polymerization the split in the conversion profiles and sharp increase in acrylate conversion indicates that a radial polymerization process occurred.

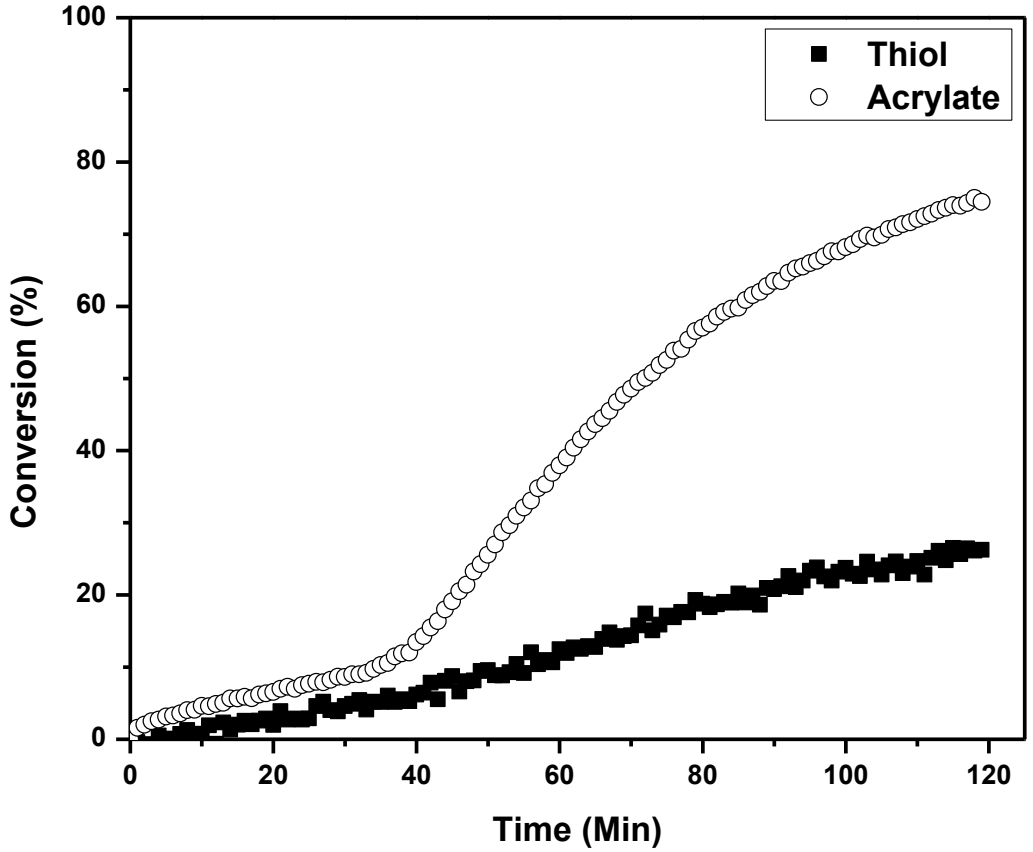

Figure 2.6 Radical polymerization during the thiol-Michael addition of TMPTA and TMPTMP with 0.165 mol% TEA

Since no radical polymerization events were ever observed in TMPTA-TMPTMP systems using 0.33 mol% TEA, the cause of this phenomenon is likely linked to the slow Michael addition rate cause by the low amine concentration. The exact cause of this effect is unknown and was not investigated further in this study, but an abrupt shift in

the polymerization mechanism from anionic to radical is certainly interesting. When making any material using a thiol-acrylate Michael addition polymerization, this process could completely alter the targeted properties of the cured polymer while not showing any obvious signs of change. If unexpected radical polymerization were to occur in a thiol-acrylate sample, the resulting polymer network would be a mixture of acrylate homopolymer and thiol-acrylate Michael addition product, so choosing the right catalyst in an appropriate concentration is crucial to perform the reaction safely but avoid a low reaction rate that could lead to radical polymerization.

2.10 Conclusions

The reaction kinetics and some applications in the field of microfluidics have been researched and presented for thiol-acrylate Michael addition polymerizations using multifunctional monomers. It was determined that a triacrylate containing a hydroxyl group reacts more quickly than the same triacrylate with a methyl group at that position under the same reaction conditions. This was attributed to intramolecular effects altering the double bond character of the acrylate groups, which makes them more susceptible to nucleophilic attack from a thiolate anion. The rate constants for a series of other triacrylates were determined and reported for a base-catalyzed thiol-Michael addition reaction with a trithiol. Increasing the distance between acrylate groups using an ethylene glycol repeating unit had little effect on the rate constant, but when a propylene glycol spacer was incorporated, the reaction slowed considerable, which is likely due to the extra carbon interrupting the electronic interactions between the acrylate groups.

The effect of both acrylate and thiol functionality on the base-catalyzed thiol-Michael addition polymerization rate constant was investigated. When using the same trithiol, the reaction rate constant increased with increasing acrylate functionality. When the thiol functionality was varied while using the same triacrylate, the rate constant increased with increasing functionality except when an ethoxylated trithiol was used. In the acrylates, raising the functionality increases the intramolecular effects between acrylate groups and makes them more reactive. The thiols could also benefit from this same effect, which could alter the pk_a of the thiol group, which in turn would shift the thiolate-base equilibrium and change the observed rate constant. If that is the case, adding an ethylene glycol spacer to the trithiol should not lower the rate constant dramatically, which is the opposite of what was observed. While this phenomenon needs further investigation, it is possible that spreading out the thiol groups further apart in space has some negative effect on polymerization.

The effect of switching from the base-catalyzed to nucleophile-initiated reaction schemes in trifunctional thiol-acrylate systems was also investigated. While there was a reasonable increase in the initial reaction rate, the change was substantially smaller than the observed effect in monofunctional systems. Furthermore, changing the initiator from a secondary to a primary amine had the opposite effect on the reaction rate compared to what is known to occur in monofunctional systems. This was attributed to gelation of the network, which restricts the mobility of the large active chains, or increased steric hindrance around the enolate formed using multifunctional thiols and acrylates. The change in mechanism also affected the order of reactivity for triacrylates with and without the hydroxyl group. While the alcohol does increase the reactivity of

the acrylate double bonds through intramolecular effects, in the nucleophile-initiated mechanism it acts as a chain transfer agent that slows the rate by donating its proton to a stronger enolate base, which lowers the thiolate anion concentration in the reaction. This effect can be overcome when better nucleophiles, such as phosphines, are used to increase the enolate concentration in the reaction.

The presence and effect of radical polymerization reactions during the thiol-acrylate Michael addition polymerizations was investigated. It was determined that there is no significant radical polymerization occurring during the base-catalyzed thiol-acrylate Michael addition polymerizations since the reaction kinetics and conversion were minimally affected by the addition of radical inhibitors. Significant radical polymerization was observed in reactions where the rate of thiol-acrylate Michael additions was low, such as at the end of nucleophile-initiated reactions and base-catalyzed polymerizations with low amine concentrations. This observation is extremely important for thiol-acrylate materials made using the Michael addition polymerization since the presence of an acrylate homopolymer network alters many of the properties of the final material and leaves a large amount of unreacted thiol even though the polymerization appears to proceed normally. The mechanism through which this process is occurring has not been elucidated and more detailed studies will need to be performed to formulate a reasonable hypothesis.

Overall, this research serves as an overview of some interesting effects seen in the thiol-acrylate Michael addition polymerization of multifunctional monomers. Using this work as a starting point, more focused experiments should be designed to better characterize the behaviors and challenge the theories presented here.

CHAPTER 3. THE APPLICATIONS OF THIOL-ACRYLATE MICROFLUIDIC RESIN

3.1 Chapter Summary

In this chapter, thiol-acrylate chemistry has been utilized to produce a material for use in the field of microfluidics. First, the field of microfluidics will be introduced, and some of the challenges associated with using traditional materials for constructing devices will be addressed. Following will be a brief overview of the thiol-acrylate microfluidic resin (TAMR) as developed by Bounds et al. including some of its advantages.[76] Next, the general TAMR production and curing procedures will be discussed. New contributions to this research project will begin with an investigation into several important characteristics of TAMR as they relate to microfluidics including: the hydrophilicity, the modulus, the absorption of solvents, and the bonding mechanism between TAMR pieces. After, the development of a TAMR device used to detect pathogens via fluorescence will be discussed. This study took advantage of some of the advantages of TAMR to produce a device that could detect *E. coli* by two different methods using a simple procedure. The work presented here is an important proof of concept that demonstrates the utility of TAMR and feasibility as a material for the fabrication of microfluidic devices. Finally, another device was constructed using both TAMR and a thiol-acrylate based hydrogel for the study of algal chemotaxis. A thiol-acrylate hydrogel was developed that was able to bond to a piece of TAMR imprinted with microfluidic channels. Chemical gradients were established across the center channel of the device, which was maintained under flow-free conditions.

3.2 Introduction

Microfluidics is a relatively new and increasingly exciting field of research with seemingly limitless applications in the areas of biology, chemistry, and engineering. As the name implies, microfluidic systems utilize micrometer scale channels imprinted into a material to guide the flow of liquids. Several advantages of using channels on this scale are: the low volumes of sample and reagents required, high separation efficiency, increased detection sensitivity, short analysis times, reduced cost of manufacturing, smaller overall size, increased portability, and ability to combine several analysis steps into one device.[106-110] Operating channels at these scales also causes several fluid behaviors to differ from typical examples including flow, diffusion, and capillary action.[111-112] The flow regime in microfluidic channels can transition from turbulent flow at larger channel diameters, where there is constant and unpredictable mixing of the fluid, to laminar flow at smaller channel diameters, where fluid flow is uniform and predictable. This allows users to more accurately control and predict the behavior of components in microfluidic flow streams. Although the fundamentals of how species diffuse through a matrix is not affected by the channel size, the decreased length scale compared to everyday examples increases the impact diffusion has on microfluidic systems. Diffusion in one dimension can be modeled simply as:

$$d^2 = 2Dt \qquad \text{Eq. 3.1}$$

where D is the diffusion coefficient and d is the distance traveled in time t.[111, 113] A relatively small molecule with a diffusion coefficient of 5 x 10^{-5} cm^2/s would take 10,000 seconds to diffuse 1 cm, but when the distance is reduced to 100 μm it would only take 1 second. Capillary action also becomes an important consideration when operating

microfluidic devices, as the distance water will travel through a capillary is inversely proportional to the radius of the tube.

The first reported microfluidic device was developed as a miniaturized gas chromatograph in the late 1970s.[114] Also in that decade, researchers at IBM forced ink through μm-sized orifices and developed the ink jet printing nozzle,[115] but the field of microfluidics did not truly start to develop until the late 1980s, when multiple research groups began producing devices to manipulate liquid samples. These devices were used to improve detection limits for already existing technologies, such as capillary electrophoresis[116] and liquid chromatography,[117] and to manipulate biomolecules for DNA sequencing[118] or enzyme assays.[119] The benefits of using narrow and short microfluidic channels over traditional methods was explored, and the idea of a device capable of performing a series of complex preparatory and analysis tasks in a small package was proposed and named a miniaturized total chemical analysis system (μ-TAS).[108] Early examples of this concept include a device that couples DNA polymerase chain reaction (PCR) amplification to capillary electrophoresis[120] and another that lyses cells, performs a PCR amplification, then sizes the products.[121] Although the μ-TAS term has largely been replaced by lab on a chip (LOC), these early examples laid the foundation for a field that has exploded in popularity over the last two decades.

One of the primary differences between microfluidic devices developed in the 1990s and current technologies is the material with which the devices are constructed. The early work in microfluidics was heavily influenced by the advancements in microelectronic fabrication, and thus they used many of the same techniques and materials, such as photolithography and etching of silicon and glass.[106-107, 110] Silicon

can be a difficult material to work with since it is opaque to both visible and ultraviolet (UV) light, typically requires a clean room environment to process, and has a relatively high cost. Glass is optically transparent but can be challenging to etch accurately since it is an amorphous material.[106-107, 122-123] Despite these disadvantages, early researchers used these materials to develop all of the devices discussed in the previous paragraph as well as several amazing fluid manipulation technologies including microvalves[110, 124] and micropumps.[125-126] However, silicon and glass have largely been replaced by plastics due to their overall lower materials cost, manufacturing cost, and variety of different physical and chemical properties.[123]

The techniques used to manufacture microfluidic devices out of silicon or glass involve the removal of material to create the channels by chemical etching,[114-115, 117] laser ablation,[127-130] or plasma etching.[131-133] Polymeric materials can be fabricated into microfluidic devices by a variety of different techniques due to their wide range of properties. The main methods used to fabricate polymeric microfluidic devices can be grouped into two main categories including destructive techniques and replication. Using methods similar to those used to manufacture glass and silicon devices, areas of a polymer can be selectively removed to fabricate microfluidic channels. One way to accomplish this is laser ablation, which was first used to construct a polymeric microfluidic device in 1997.[123, 134] In this technique, the chemical bonds holding the polymer together are broken by the absorption of pulsed UV light from a laser.[135] The decomposition products are ejected out and away from the area to leave an impression in the polymeric material that is typically around 1 μm deep, which means several passes need to be made over an area to form deeper structures.[136] The pulsed nature

of the laser and multiple passes needed usually leave the surface of the finished device with a wavy pattern.[123] The effectiveness of the ablation can vary based on the polymer composition, so a laser with an emission wavelength closest to a maximum on the polymer absorption spectrum will work the best. Laser ablation can be performed with or without a photomask defining the microfluidic features. If a photomask is used, the channel shapes are cut through the mask material, which is typically a metal. If a photomask is not used, the laser beam needs to be focused to the desired width of the channel, and the material is moved under the beam in the desired pattern. Some of the advantages of laser ablation are the large number of polymers it can be applied to and the small features that can produce. Some of the disadvantages include the surface roughness, irregular shapes in deep features due to the laser defocusing, and the change in surface chemistry due to the ablation process.[123]

Another destructive technique for microfluidic feature fabrication is X-ray lithography. This method uses X-rays to break down the polymer structure into soluble components that are washed away to reveal the channel features. A photomask is used that will absorb X-rays to prevent the entire polymer surface from decomposing. This technique is limited to polymers that have high X-ray absorption and is typically used for poly(methyl methacrylate) (PMMA). Since the source is not pulsed, the features obtained are typically smoother than with laser ablation and high aspect ratio channels can be fabricated, but the need for an X-ray source and the complicated masking procedure hinder widespread use.[123]

Microfluidic channel replication is the other main category of polymeric microstructure fabrication techniques. These methods all use a master that has

impressions of the microfluidic features on its surface. The pattern is transferred from the master to the polymer using a variety of different methods, which gives a polymeric device with the channels embedded in it. These methods can be used to mass-produce devices, but since they rely on a master, the fidelity of the final device features relies heavily on the fabrication methods used to make the master. Polymeric device fabrication techniques that use the replication method include hot embossing, micro-thermoforming, injection molding, and soft lithography, and examples of how these techniques work are presented in Scheme 3.1. In order to facilitate removal of the polymeric device from the master, the surface of the master mold needs to be chemically compatible with the polymer and physically smooth. Ideally, the master mold material should be durable enough to survive a multitude of replication cycles.[136]

The first three of the replication methods listed above, hot embossing, micro-thermoforming, and injection molding, require strong masters, and metals are a popular choice due to their durability. Molds can be fabricated directly out of metal using conventional physical techniques[137-138] or electro-discharge machining.[139-140] Alternatively, molds fabricated using additive processes can be electroplated with a metal to produce durable masters. An example of this is the *lithographie* (lithography), *galvanoformung* (electroplating), *abformung* (molding) process, or LIGA.[141-142] When making masters with LIGA, X-rays are used, with a mask of the desired pattern, to remove material from a resist (typically PMMA) sitting on top of a conductive substrate. Once the degraded resist is dissolved away, a metal is electroplated onto the substrate which fills the pattern left by the exposed resist. The rest of the resist is stripped away leaving the substrate with a positive impression of the microfluidic pattern in metal.

Materials other than metal can be used for masters, such as silicon[143] or other polymers,[144-145] but they lack the durability of metal molds.

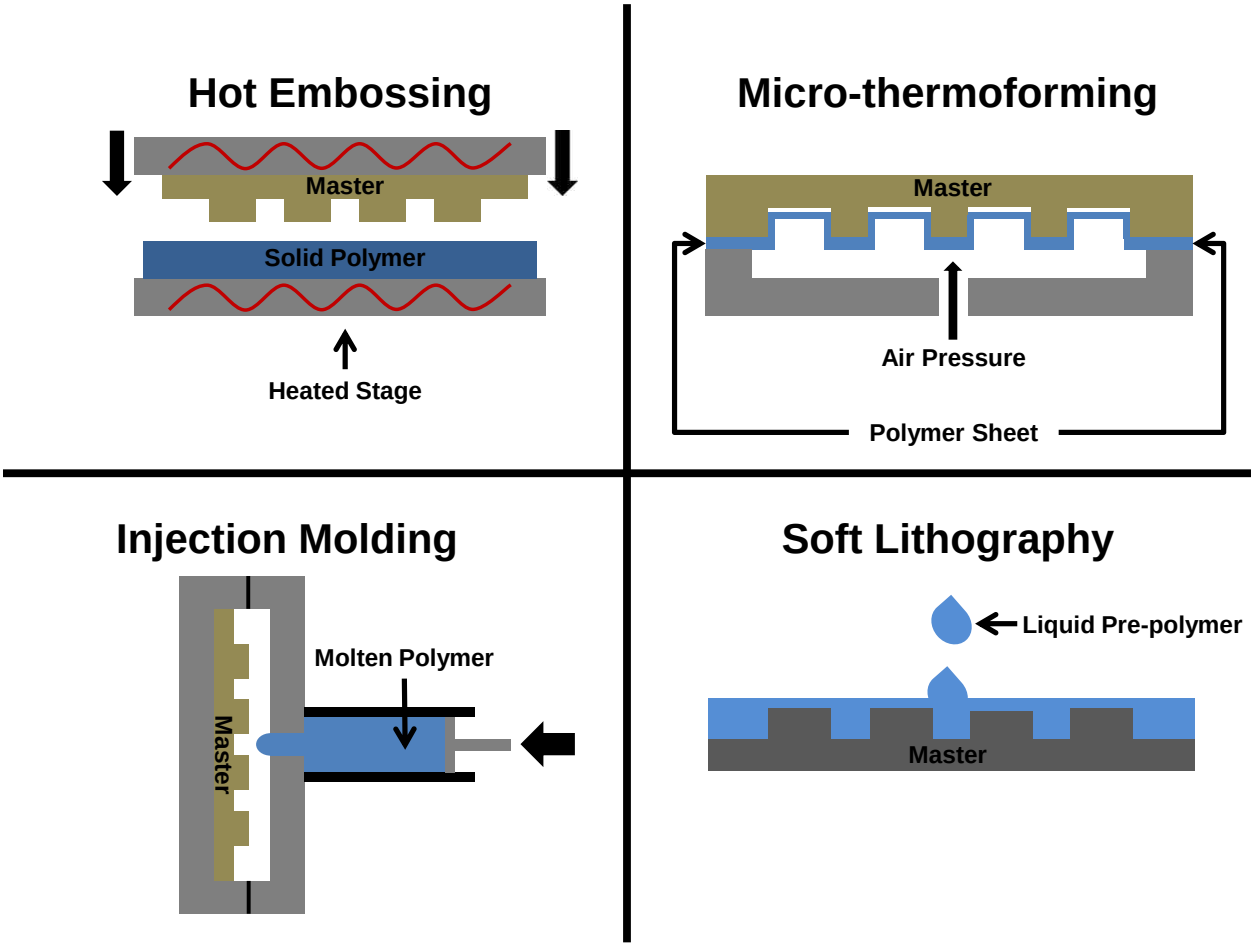

Scheme 3.1 Microfluidic device replication techniques

The last replication technique listed, soft lithography, puts less stress on the master, so molds can be fabricated using weaker materials. Silicon is commonly used as a base material, and positive impressions can be created on the surface using traditional silicon etching techniques,[146] or more often, by curing a polymeric material in the desired pattern.[147-148] The later technique is generally referred to as rapid prototyping, since it can be performed much more quickly than silicon etching. In a typical procedure, the silicon wafer is coated with a negative photoresist that will chemically crosslink upon exposure to UV light. Using a photomask where everything

but the desired microfluidic features are opaque gives a positive impression on the wafer after the uncrosslinked resist is washed away. The length and width of the microfluidic channels are determined by the photomask geometry while the channel height can be varied by coating the photoresist at different thicknesses. Masters fabricated using the previously discussed techniques may be used for soft lithography as well, as long as they have positive features.

Once the master has been fabricated, the replication of microfluidic features can be performed in the final device polymer. The replication method is generally determined by factors such as cost, the number of devices required, and most importantly, the physical properties of the polymer. Hot embossing, micro-thermoforming, and injection molding all require thermoplastic polymers, while soft lithography is generally performed using thermoset polymers, although thermoplastics can be used. These two classes are used to group polymers based on their general behavior at elevated temperatures, and simply put, will soften and eventually flow at high temperatures, while thermosets will decompose before softening appreciably when heated. This fundamental difference in thermal properties is determined by the chemical structure of the polymer. Thermoplastics are composed of linear polymer chains with no covalent bonding between them. Upon heating, the increased molecular motion of the individual chains allows them to move past each other easily which causes the material to become malleable. Thermoset polymers have connections between their linear portions called crosslinks, which restrict the large-scale molecular motion induced by heating and prevents the softening of the material. Some examples of thermoplastic polymers used to fabricate microfluidic devices are cyclic olefin

copolymer,[149-154] poly(vinyl chloride),[155-158] polystyrene,[152, 154, 159-161] polycarbonate,[152, 157, 159, 162-163] and poly(methyl methacrylate).[152, 157, 159, 162-167] A variety of factors can influence which thermoplastic material is chosen to construct devices including thermal properties, mechanical properties, optical properties, surface modification strategies, and personal preference. Some examples of polymers used to fabricate microfluidic devices using soft lithography are polyurethane-methacrylate (PUMA),[168-170] thermoset polyester (TPE),[171-173] Norland Optical Adhesive 81 (NOA81),[174-177] and poly(dimethylsiloxane) (PDMS).[106, 148, 178-179]

Hot embossing, micro-thermoforming, and injection molding all require thermoplastics since they use heat to imprint microfluidic features into a solid polymer substrate. Hot embossing was first introduced in the late 1990s and can be performed using a master mold or a wire.[143, 180] Both methods use elevated temperatures to soften a polymer in order to press a design into the surface. The wire method uses a heated wire that is pressed into the plastic to produce channels. While this method is relatively inexpensive and easy to perform, it can only produce devices with simple designs with poor reproducibility.[141] Using a master mold is much more common and can produce complex designs with high reproducibility. Once the master has been fabricated, it and the polymer are placed into the embossing machine and heated to a temperature where the polymer softens. The master and the polymer are then brought into contact under pressure and held there for a few minutes to transfer the positive design form the mold into the polymer. The assembly is cooled and separated to give back the master and the newly imprinted microfluidic device component. Devices fabricated using this

method are the exact inverse of the master mold, so reproducibility is excellent and the quality is limited by the fidelity of the method used to fabricate the master.[123]

Micro-thermoforming is another replication technique that uses heat to fabricate polymeric microfluidic structures. Some advantages of micro-thermoforming are short cycle times, light and flexible devices, and relatively low fabrication temperatures.[181] In this technique, a thin thermoplastic polymer film is pushed or pulled into the master mold (which can be a positive or a negative mold) using heat to soften the plastic and gas pressure. The resulting device components are composed of a thin layer of polymer with the microfluidic features protruding from the surface. During the molding process, the portion of polymer formed into the channels is stretched into a thinner layer than the original starting material, so the initial thickness of the polymer needs to be carefully chosen so that the final product is stable and rigid enough to handle fluid flow.[182] Injection molding is a commonly used method to fabricate many polymeric components on a large scale, but it has also been adapted to fabricate microfluidic devices. In this process, a thermoplastic polymer is heated to the melt stage then injected into a heated chamber with a positive master mold at high pressure. After cooling, the assembly is pulled apart to eject the molded microfluidic component and reset to produce another device. This process has been used to fabricate microfluidic devices since the late 1990s, but due to its complexity and startup expense, it is rarely used at the research level.[183] Early examples demonstrate some of the complexities associated with this technique since it is relatively easy to get replication errors if the mold temperature, polymer temperature, and demolding time are not carefully controlled and tested.[184] Despite these disadvantages, injection molding is likely the technique of

choice to mass-produce microfluidic devices in a thermoplastic polymer due to its high throughput.[185]

One microfluidic device replication technique that can be used with uncured thermoset or thermoplastic polymers is soft lithography. In this method, a reactive liquid pre-polymer is poured over the master mold and cured in place. The master and cured resin are separated to give the polymeric device with the features imbedded into the surface. The material used to construct the master is influenced by the final properties of the polymer as well as the curing conditions. Rigid masters fabricated using photolithography or machining techniques are suitable for elastomeric polymers, but polymers that become rigid with curing would be difficult to separate from an equally rigid mold. Polymer curing conditions can also affect the master mold since many polymers cure at elevated temperatures or using UV light. Soft lithography was first developed in the 1970s as an alternative to the variety of photolithographic techniques used for micro-fabrication,[186-188] but it has since become mostly associated with the production of microfluidic devices. The “soft” portion of the name indicates that flexible polymeric substrates are used to make and transfer features instead of using traditional methods and materials. Soft lithography methods have lower initial cost than the previously discussed replication techniques since they do not require any machinery, but they generally have a lower throughput due to the polymer cure time and lack of automation. Perhaps the most beneficial characteristic of soft lithography is the ability to use relatively fragile molds that can be rapidly fabricated and altered since the replication process is generally not as stressful to the master as other methods. The majority of microfluidic research is conducted in devices produced using soft lithography

since at the research level, device designs change frequently and relatively few replications need to be performed.[136]

Although other materials exist, PDMS is the dominant polymer used in soft lithography-based microfluidics. This is likely due to several factors including its low cost, optical properties, permeability to gases, ability to replicate submicron features, chemical inertness, ability to bond to a variety of substrates, and since it was introduced into the field of microfluidics relatively early.[106-107, 123, 141] Unlike most polymer materials, PDMS has a backbone chain composed of silicon and oxygen (see Scheme 3.2). Although they seem unusual, organic silicon compounds were first reported in 1863 by Friedel and Crafts,[189] and silicone polymers have been produced commercially since the 1940s.[190] The exact origin of PDMS is unknown, but it has been used in microfluidic devices since the late 1990s when Whitesides, Effenhauser, and others published several foundational papers.[106, 148, 179, 191-194] The general structure and curing reaction for commercially available PDMS are shown in Scheme 3.2. PDMS is sold as a two-part system where one part is the viscous base polymer and the other contains a short oligomer. In the curing process, the vinyl terminated polymeric chains are crosslinked with the silane-containing oligomers using a platinum-based catalyst to give the final material. While technically both the cured and uncured forms of PDMS are poly(dimethylsiloxane), henceforth, PDMS will be used to refer to the cured material. A typical procedure for curing PDMS involves mixing the oligomeric curing agent into the viscous polymer base and letting the reaction progress at elevated temperatures. The ratio of the two components varies by manufacturer, but for example, a ratio of 10:1 by mass (base to curing agent) is used in Sylgard® 184 which is a commonly used PDMS

system produced by Dow Corning. Curing of PDMS is typically done at elevated temperatures since room temperature curing is extremely slow (48 hours for Sylgard® 184 and 336 hours for Sylgard® 182). Despite its widespread use in microfluidics, PDMS has many shortcomings, including channel deformation due to its low elastic modulus, water vapor permeability, solvent adsorption, leaching of catalyst or oligomers, ineffective gas transport, and unstable contact angles after surface modification.[195]

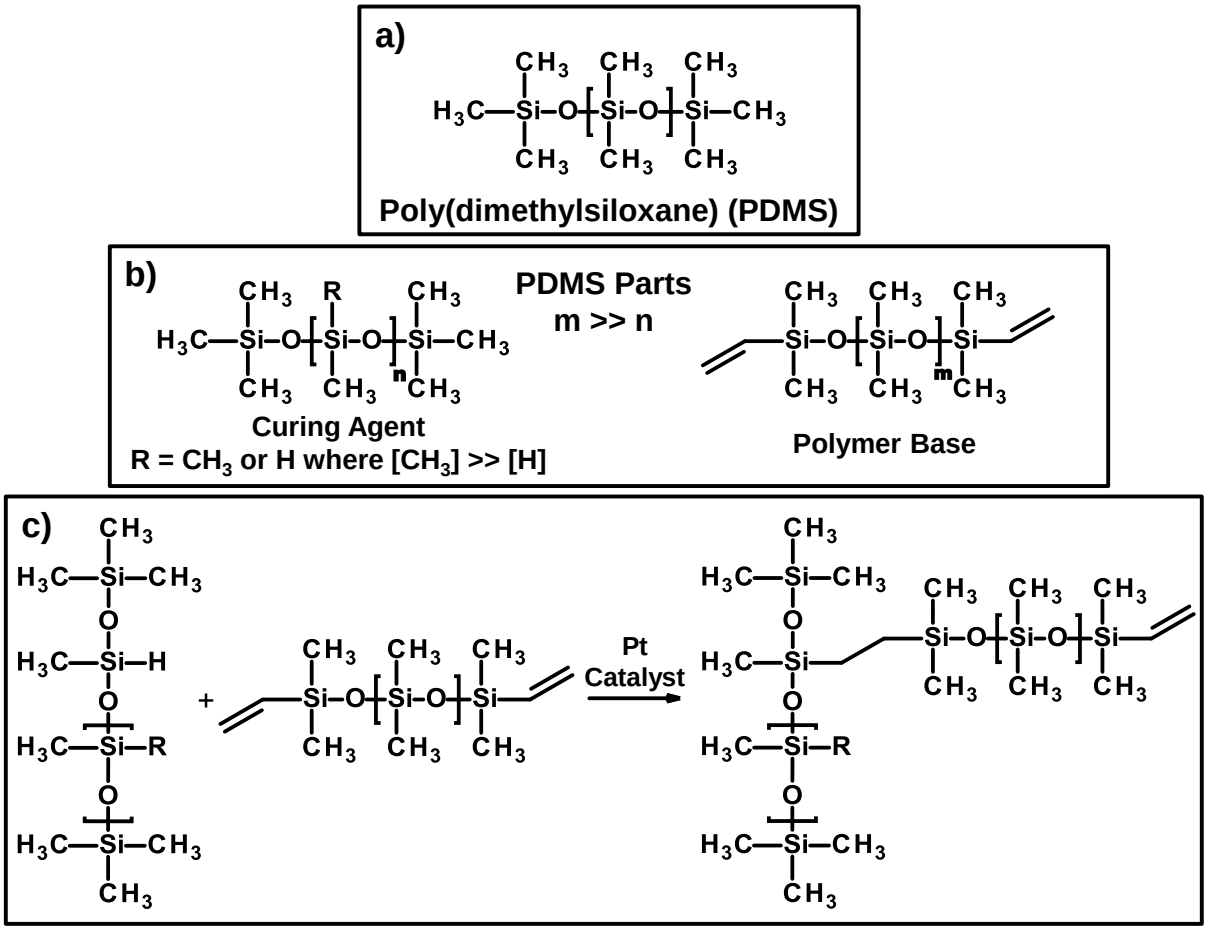

Scheme 3.2 PDMS structure and curing reaction

Alternatives to PDMS exist, but none have gained widespread acceptance. Recently, our group has developed a microfluidic resin system using thiol-acrylate chemistry that addresses many of the shortcomings of PDMS,[76] but in order to convince

researchers to use this new material, it needs to be well characterized. The benefits and shortcomings of this new thiol-acrylate material have been assessed and are presented here along with comparisons to PDMS. In addition, two microfluidic devices using this resin system have been developed to highlight the versatility of thiol-acrylate chemistry and demonstrate the usefulness of a PDMS alternative.

3.3 Thiol-Acrylate Microfluidic Resin (TAMR) Overview

The thiol-acrylate microfluidic resin (TAMR) developed in our group is a liquid two-part system that cures at room temperature in less than 24 hours. Once the two parts are mixed together, the working time is typically 20 minutes, after which the material will no longer flow. The cured resin is relatively hydrophilic without the need for surface modification, and it has a higher modulus than PDMS. Excess thiol or acrylate groups can be incorporated into the material, which allows for several potential surface modification strategies. This property can be exploited to adhere two pieces of resin with complimentary functional groups in order to fabricate microfluidic devices.

The first part of the two-part TAMR system contains the acrylate and the curing agent. Thiol-acrylate polymerizations are frequently conducted using amines as a catalyst or initiator (see Scheme 1.4), but since the fabrication of microfluidic devices requires the resin to cure on a flat mold, a volatile amine will evaporate from the surface and leave it tacky. In order to prevent this, the amine is covalently bound into the resin system so that it cannot evaporate. A Michael addition between the acrylate and a secondary amine is performed to produce a tertiary amine, which is covalently bound to the acrylate molecule (see Scheme 3.3). The Michael addition reaction does not require any additional solvent or reactants other than the amine and acrylate and is

performed at room temperature in 3 hours. This part of the TAMR system will be referred to as the amine activated acrylate (X-AA), where the X will refer to the amine used in that particular recipe. The second part of the TAMR system is the thiol, which is used without any modifications and will be referred to as its chemical name. When the two parts are mixed, the polymerization reaction begins and a highly crosslinked thiol-acrylate network will form (Scheme 3.3).

3.4 TAMR Preparation and General Curing Procedure

Part one of the TAMR system, the AA, is prepared by adding an amine, usually diethylamine (DEA), to pentaerythritol triacrylate (PETA) in a predetermined ratio that is designated as the percentage of acrylate groups that will react with the amine. For example, for a 20% DEA-AA, the ratio of the components would be:

$$\frac{\text{Moles of DEA}}{\text{Moles of Acrylate Groups}} = 20\% \qquad \text{Eq. 3.2}$$

PETA was added to a sealable container, followed by the necessary mass of amine. The amine addition needs to be performed rapidly to avoid significant evaporation of the amine. The two components were mixed well and stirred in a sealed container for at least three hours prior to use. The notation used here is different from that used by Bounds et al. who used the mol% of amine in the PETA-amine mixture relative to acrylate groups. This change was made to simplify calculations and to make the amount of acrylate groups consumed in the reaction more evident. For comparison, a 16.1% AA under the system used by Bounds et al. equates to a 19.2% AA using this definition.

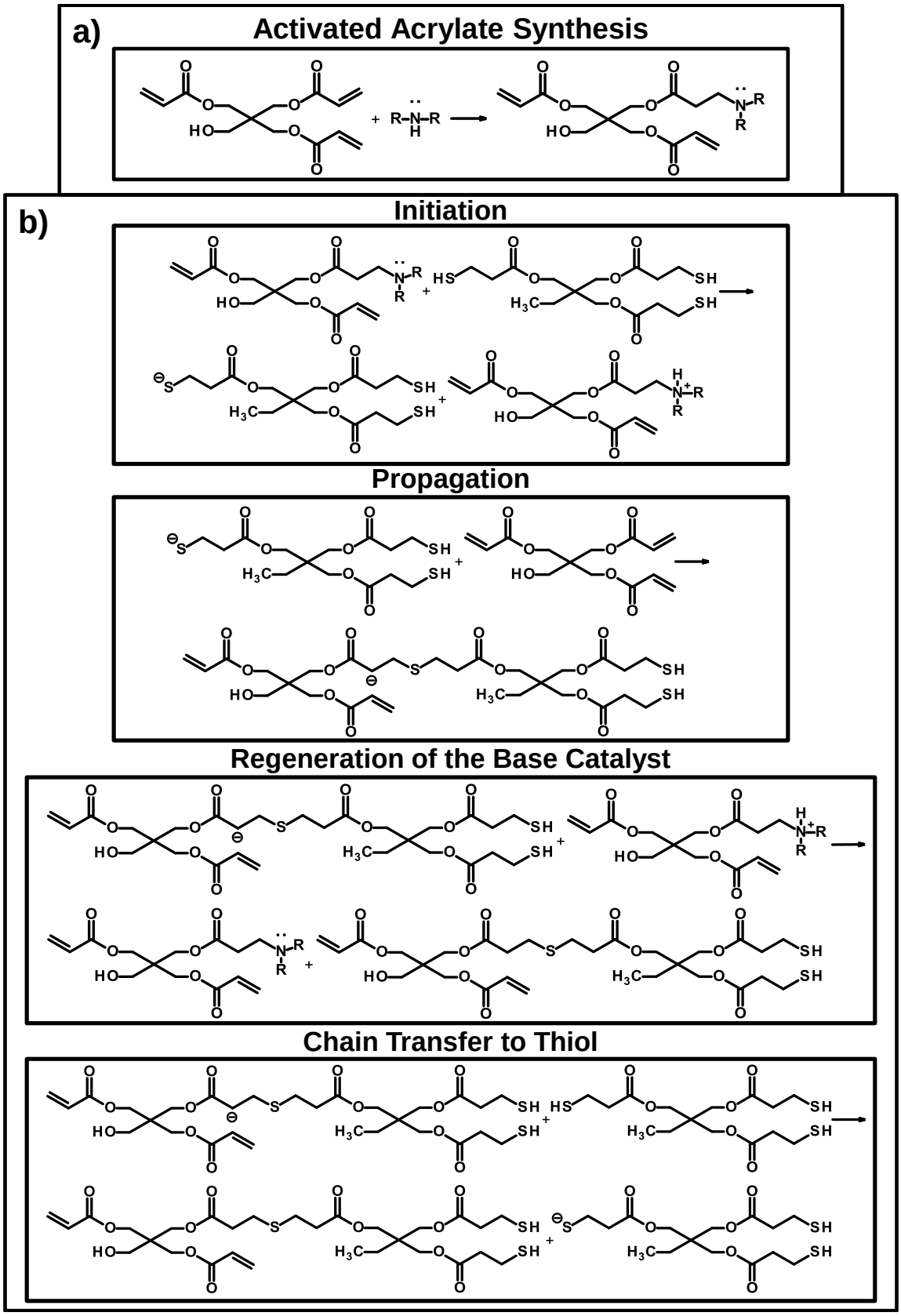

Scheme 3.3 TAMR a) AA synthesis and b) curing reaction with TMPTMP

The TAMR was cured by mixing the AA with trimethylolpropane tris(3-mercaptopropionate) TMPTMP in the desired ratio. The resin can be made using a 1-1 thiol:acrylate group ratio or with either thiol or acrylate groups in excess. Resin samples made with equal moles of thiol and acrylate groups are designated 1-1. Samples with excess functional groups are designated first by the percentage excess and then which group is in excess. For example, a sample containing 40% more acrylate groups relative to thiol groups would be designated “40% EA”, and a sample made with 20% excess thiol groups relative to acrylate groups would be labeled as “20% ET”. Once the required amount of TMPTMP was added to the AA, the two were mixed by hand thoroughly. This process frequently works air bubbles into the mixture, which need to be removed in order to ensure uniform samples. The mixture was placed into a centrifuge tube and spun for ~2 minutes at 4,000 rpm to force out the bubbles. The resin was then poured into a mold or another container to cure. Curing was performed at room temperature on the benchtop unless otherwise indicated.

3.5 TAMR Characterization

3.5.1 Introduction

When researchers choose a material to fabricate and perform experiment in a microfluidic device using soft lithography, many important properties of the material need to be considered. Many material characteristics are significant in nearly all devices, but some applications require specific qualities in a microfluidic resin that are more obscure or completely different from those needed typical examples. While no one material could satisfy all requirements for every application, a microfluidic resin that is highly tunable in a variety of areas would be highly desirable. The TAMR developed

by Bounds et al. could fit that description, but a detailed investigation into several key properties of the resin is needed to determine its utility to actual microfluidics users. In this study, several key properties of TAMR were investigated including: the cure kinetics, the hydrophilicity, the water absorption, the solvent absorption, the mechanical properties, the bonding mechanism, and ease of use. Each of these properties is important in nearly all microfluidic applications, so understanding how they relate to the chemical composition of TAMR will allow users to adjust the base formula to target whatever performance criteria they need and provide a viable alternative material in the field of microfluidics.

The curing behavior of any microfluidics resin is one of the most important features since it dictates the timescale on which devices can be fabricated and what equipment will be required. Within this broad category, several specific qualities include the ease of use, the working time, the cure time, and the cure temperature. The working time of a material is important since the user needs an adequate amount of time to mix the system and perform any other necessary tasks before pouring it onto the master mold. The problems associated with having a short working time are evident and will generally lead to wasted material and negatively affect user experience. While there are no apparent drawbacks to having a long working time, that ability generally increases the cure time of the material. The cure time is extremely important since it is the biggest influence on the rate at which devices can be fabricated. One of the benefits of soft lithography is the ability to change designs and reproduce new devices more quickly than with other fabrication methods, but if it takes several days for the microfluidic material to cure then that advantage is lost. Lastly, the cure temperature

dictates if heating equipment is required, which contributes to the overall cost of the material and impacts ease of use.

The hydrophilicity of a microfluidic resin is important in every experimental application since it affects fluid flow through the microfluidic channels in addition to a number of other considerations. If the material used to fabricate the device is incompatible with the fluid being pumped through the channels, increased pressure will be required in order to force the liquid through, which can lead to device failure, device deformations, equipment damage, and negatively impact ease of use. The hydrophilicity of the surface could also affect the experimental performance of the device, for example through its adsorption behavior towards biomolecules in bioassays[196-197] or by influencing how fluid droplets develop and behave in droplet generating devices.[198-200] A resin where the surface properties could be easily varied or modified would be ideal, as various applications can require large differences in hydrophilicity, sometimes even within the same device.

The absorbance of water and other solvents by microfluidic materials is a major concern when choosing what material to use or what experiments can be performed using a given resin. Absorbing liquids in a microfluidic experiment can alter the properties of the microfluidic material or create air pockets in the device that will interfere with the analysis. Microfluidic devices are not only used with aqueous biological systems but in applications that require the use of organic solvents or corrosive solutions, so many materials are not compatible with every type of experiment. A material that resists swelling in both organic and aqueous systems would be ideal and could allow for the development of new device designs and applications.

The mechanical properties of microfluidic materials used in soft lithography replication are most important when the device is removed from the master and when it is in operation. Flexible materials are easily removed from rigid masters, but will deform under pressure when in use inside a device, so applications involving higher pressures generally require a higher modulus material. Rigid materials are usually prepared using a flexible master mold, but damaging the master is more likely in these cases. One possible solution is to use materials that are balanced between flexibility and rigidity, but a better solution would be a material that could be removed from the master in a flexible state by then become more rigid through modification or further curing.

In addition to the cure time, the procedure used to bond two halves of a microfluidic device together can be a limiting factor in device reproducibility and replication time. In order to fabricate a usable device, the channel side obtained from the master is typically bonded to another flat piece of resin or another material, such as glass. The mechanism by which this bond is achieved varies with each microfluidic material, but a tight bond between the two device halves is crucial for device performance. The bonding procedure must also be reproducible to avoid wasting material on devices that were not adhered properly. The time and equipment needed to achieve bonding are also important due to their effect on overall cost and replication time. A material that can be bonded together quickly, reproducibly, and without the need for special equipment would be ideal for microfluidics.

Ease of use may be a largely subjective quality, but its importance to whether or not a material gets used is vital and should not be underestimated. PDMS, for example, is easy to use since it is a two-part system with a reasonable mix ratio (10:1 by weight)

and can be handled under normal atmospheric conditions. A resin with revolutionary properties may still fail to see use if, for example, it required mixing four parts in a 100:1:0.5:0.0001 ratio under an inert atmosphere. The cost, toxicity, cure time, working time, and bonding procedure all contribute to this quality as well.

In the following study, the properties which correlate to the microfluidic resin characteristics discussed above were determined for TAMR and compared to PDMS, which is the most commonly used material for soft lithography-based microfluidics. Along with the data, some qualities of TAMR relating to ease of use, general observations, and shortcomings will be discussed.

3.5.2 Materials and Methods

Materials

PETA stabilized with 300-400 ppm MEHQ was obtained from Alfa Aesar. TMPTMP was purchased from Evans Chemetics LP, Sigma Aldrich, and TCI America. DEA ≥99.5% was obtained from Alfa Aesar and Sigma Aldrich. Lauryl acrylate 90% (LA), poly(ethylene glycol) methyl ether acrylate (PEGMEA), triethylamine ≥99% (TEA), diethanolamine ≥98.5% (DEOA), and N-ethylethanolamine ≥98% (EEOA) were obtained from Sigma Aldrich. A Sylgard® 184 silicone elastomer kit was purchased from Electron Microscopy Sciences. See Scheme 3.4 for structures.

TAMR Preparation and Curing

The TAMR was prepared according to the general procedure described above. Curing of the TAMR was conducted following the standard protocol, while where the resin was cured varied by application and will be specified below.

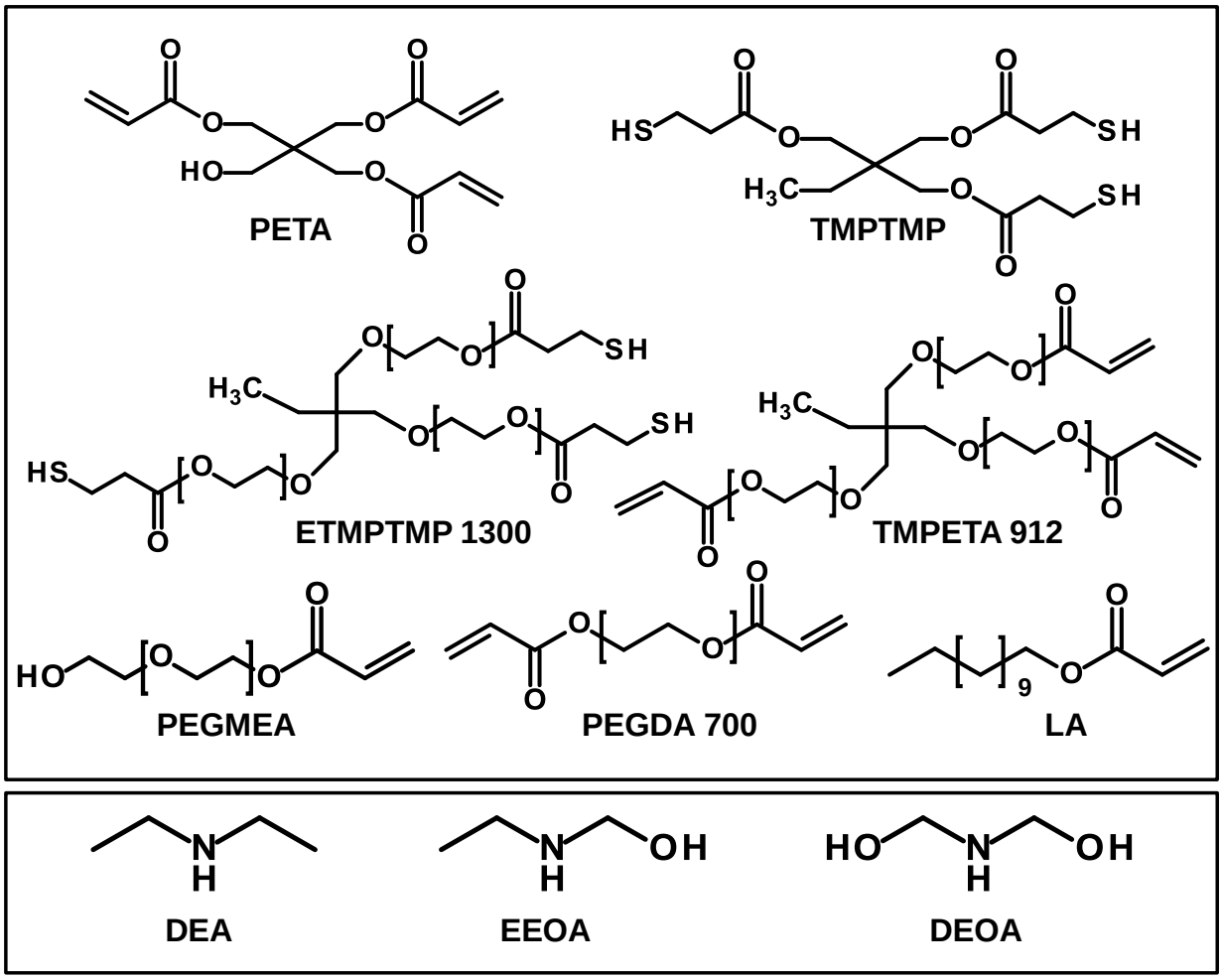

Scheme 3.4 Reagent structures

PDMS Curing

PDMS samples were made by adding the curing agent to the viscous base in a ratio of 1:10 by weight. The mixture was stirred well and placed under vacuum for several minutes to remove air bubbles. The PDMS was poured into the curing vessel and placed in an oven set at 70 °C to cure overnight.

TAMR Cure Kinetics

The TAMR was prepared according to the general procedure described above. The necessary amounts of AA and TMPTMP were combined in a weigh boat and mixed well by hand. A sample of the resin was removed and placed in a liquid cell on a Pike

Miracle single-bounce diamond attenuated total reflectance (ATR) cell attached to a Bruker Tensor 27 FTIR. The instrument was set to acquire a spectrum at regular time intervals (every minute for 2 hours or every 5 minutes for 15 hours). Data was acquired between 650 and 4000 cm^{-1} with a resolution of 4 cm^{-1}, 16 scans were taken for each spectrum, and all of the reactions were performed at room temperature. Once the FTIR data was acquired, the data was processed using Bruker's FTIR software package, Opus. A 9-point smooth was performed on the spectra and baseline correction was done using 10 iterations of the concave rubber band correction with 64 baseline points. After the smooth and baseline correction, the area under the peaks of interest was determined using the built in integration program. The bounds for each peak were determined visually and method B was used in the Opus integration protocol. Conversion of functional groups was determined according to Equation 2.1.

Water Contact Angle Testing

The TAMR was prepared and mixed according to the standard procedure described above. The resin was cured in polystyrene Petri dishes with a diameter of 5.5 cm or on a standard glass microscope slide. Once the resin had cured for the desired period of time, individual pieces were cut out of each dish. The sample pieces were placed on the stage of an AST Products VCA Optima contact angle goniometer and a 1 µL drop of nanopure water from a Barnstead NANOpure Diamond water system was placed on the surface at room temperature. After 10 seconds, the water contact angle was determined. Two contact angles were measured for each water droplet, three droplets were tested per sample, and three samples were used for each formulation for

a total of 18 contact angle measurements. The results were averaged, and the standard deviation was reported as error.

Water Absorption Testing by Mass

A variety of TAMR formulations were prepared as above and cured for 24 hours in a polystyrene Petri dish. Cylindrical pieces with a diameter of 1 cm and a height of ~4 mm were punched out of the TAMR using a biopsy punch. These samples were labeled, weighed, and submerged in distilled water. At regular time intervals, the samples were removed from the water, dried to remove surface moisture, weighed again, and placed back into the water. The visual appearance of the TAMR was noted as well.

Solvent Adsorption Testing by Size

TAMR samples were prepared and cured in cylindrical molds with a diameter of 3.5 mm and a height of 1 mm according to the standard procedure described above. After 24 hours of curing, the samples were removed from the mold, and the diameter of each sample was measured using a Nikon Eclipse 50i optical microscope and the NIS Elements software package. The samples were then immersed in solvent and stored at room temperature for 24 hours. After the soaking period had elapsed, the samples were placed in a glass Petri dish while remaining under solvent. The diameter of the samples was measured again using the microscope while the resin pieces were immersed in solvent. This was done to ensure there was no solvent evaporation out of the samples that would lead to changes in diameter and was adopted from a procedure used by Lee et a. to study the swelling of PDMS.[178]

Tensile Testing

TAMR was prepared according to the procedure above and cured in tensile test sample molds. PDMS was mixed in a 10:1 ratio of base to curing agent by weight, stirred well, placed under vacuum to remove bubbles, and poured into the tensile sample molds. The PDMS samples were cured overnight in an oven set to 70 °C. The molds were constructed from acrylic (PMMA) with the type 1 dimensions specified under ASTM D638. The molds were sprayed with a thin layer of boron nitride mold release to facilitate removal of the sample. Once cured, the samples were removed from the mold and placed into the grips of an Instron 5969 universal testing machine for analysis. A standard tensile test was performed with an extension rate of 5 mm/min, and the stress and strain on the sample were determined using Instron's Bluehill software package. The Young's modulus of the sample was reported as the slope of the initial linear portion of the stress-strain curve.

Bonding Scheme Testing

The bonding of TAMR to itself was tested using a simple microfluidic device design. TAMR was prepared and mixed according to the standard procedure described above. The channel half of the device was constructed by curing TAMR on a master mold made using silicon wafer and SU-8 by standard photolithography methods. The device pattern had 3 parallel channels which were 650 μm wide and 150 μm tall. The spacing between the center and outer channels was maintained at 450 μm for 1 cm. The flat portion of the device was fabricated by curing TAMR in a polystyrene Petri dish. Both the channel and flat pieces were cured for 1 hour in their respective molds, after which the TAMR was removed. Inlet and outlet holes were drilled at the end of each

channel using a 1/16” drill bit, and the resulting dust was blown away with compressed air. The channel side of the device was then slowly brought into contact with the polystyrene side of the flat portion of the device. The two halves were gently pressed together to ensure a good seal and exclude air pockets. The devices were left to finish curing at room temperature for 24 hours unless otherwise stated. After curing, the devices were plumbed using 1/16” outside diameter polytetrafluoroethylene (PTFE) tubing, and the connections were sealed at each port using a 5-minute epoxy. The center channel of the device was connected to a syringe filled with dyed water which was placed in a syringe pump. A 10 µL/min flow was introduced into the channel and steadily increased until failure occurred. The device was visually monitored for leaks, which would likely occur between the center and outside channels.

Oxygen Plasma Treatment

TAMR and PDMS samples were cut out and removed from a polystyrene Petri dish. The samples were laid on the sample tray polystyrene-cured side up and placed in the sample compartment of a Harrick Plasma PDC-32G plasma cleaner. The chamber was sealed an evacuated of air for 3 minutes. Next, the needle valve was opened and the plasma generator was turned on. The power used and the treatment time were varied and will be indicated below.

TAMR Surface Modification

19.2% DEA-AA samples made with 40% ET according to the standard procedure and cured for one hour at room temperature in a PS Petri dish. Samples were cut out of the Petri dish and then immersed in a modifying acrylate containing 1 wt% trimethylamine (TEA) to ensure the thiol groups at the surface could be deprotonated

and add to the acrylate. The samples were left in the acrylate solution for 1 hour, then removed and washed with water then acetone, twice each. The samples were left to finish curing at room temperature for at least 24 hours.

3.5.3 TAMR Variables

One of the things that makes TAMR so versatile is the ability to alter several key aspects of the resin quickly and easily, including: the amine concentration in the AA, the chemical structure of the amine in the AA, the ratio of thiol to acrylate groups, and the curing conditions. Previous work has shown that altering the amine concentration in the AA affects resin strength and gel time, but the other variables have not been extensively tested.[76] The effect that these additional changes have on the properties of TAMR was investigated and will be discussed in the sections to follow.

3.5.4 TAMR Cure Kinetics

The curing time and conditions are important factors to consider when choosing what material to use for making microfluidic devices. PDMS is typically cured at elevated temperatures for extended periods of time (65 °C for 8 hours for example) since the crosslinking reaction is extremely slow at room temperature. TAMR is able to cure at room temperature within a matter of hours, but recipe and curing conditions can affect this process. A detailed profile of the curing behavior of any microfluidic resin is essential information, and ideally, the curing behavior would be tunable. The curing reaction for a variety of TAMR formulations was monitored using FTIR to assess how recipe changes and curing temperature affect the kinetics. Figure 3.1 shows an example plot of functional group conversion versus time for a 19.2% DEA-AA 1-1 TAMR sample. Full conversion was achieved after 10 hours of curing at room temperature

with a final acrylate conversion of ~99% and a thiol conversion of ~88%. The difference between thiol and acrylate conversion is likely due to impurities in the TMPTMP, as discussed in the previous chapter. This difference can be addressed by adding excess acrylate groups, and Figure 3.2 demonstrates this by showing conversion profiles for 19.2% DEA-AA before and after the addition of 10% excess acrylate. Since the conversion profiles of thiol and acrylate line up after the addition of 10% EA, TMPTMP contains ~10% more thiol groups than the theoretical molecular weight and functionality predict.

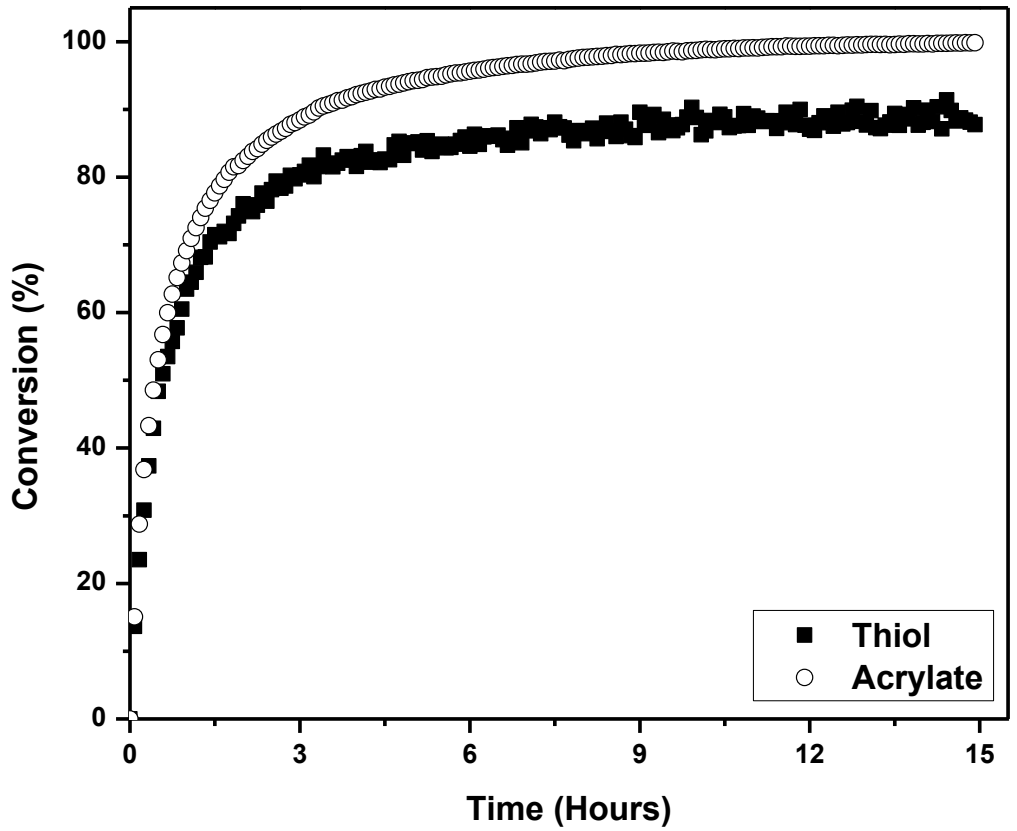

Figure 3.1 Conversion profile for 19.2% 1-1 TAMR

Dropping the amine concentration from 19.2% to 11.1% increases the cure time to ~12 hours at room temperature due to the lower base catalyst concentration present

in the 11.1% resin. Figure 3.3 shows the conversion profiles for 19.2% DEA-AA with 40% excess thiol and acrylate groups.

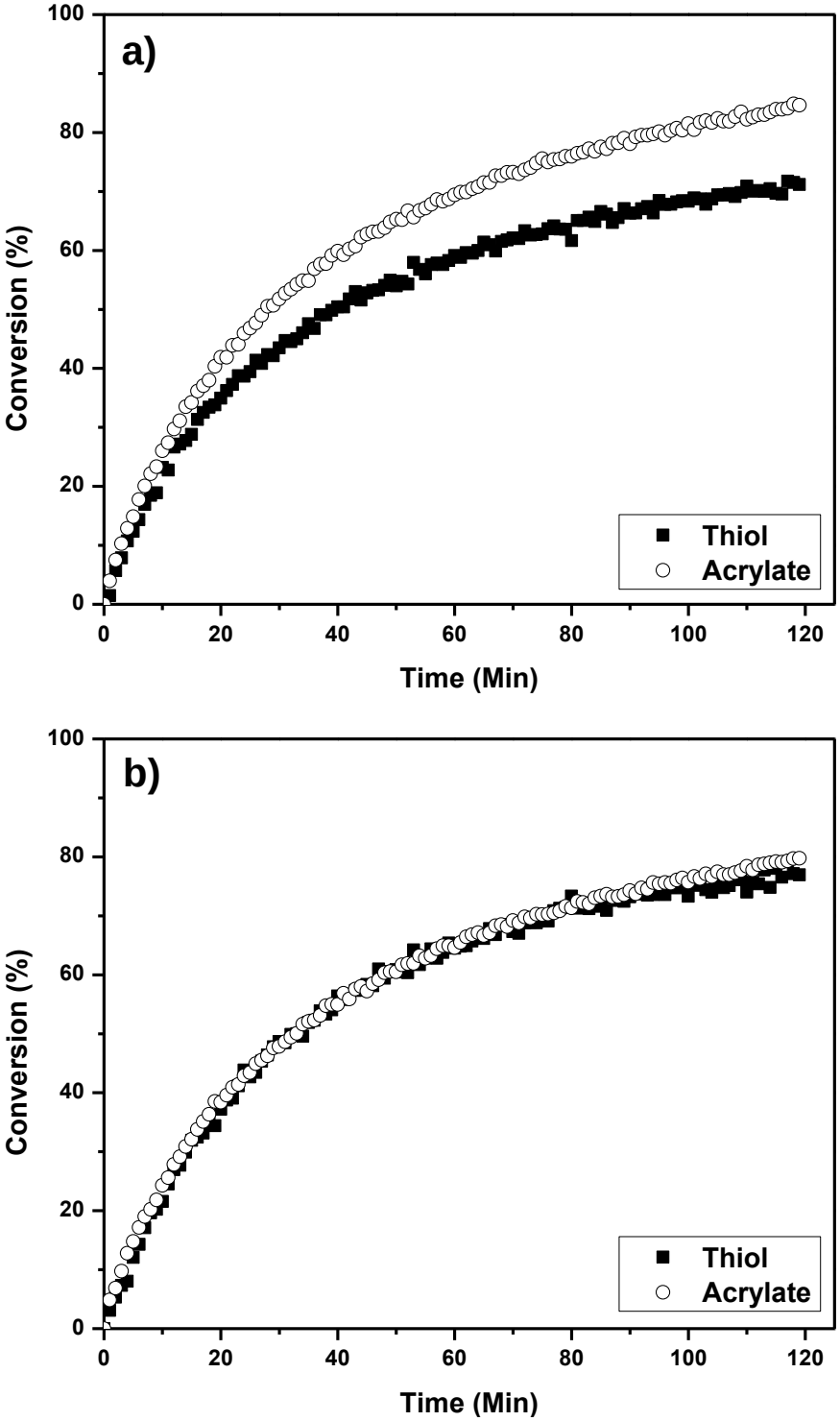

Figure 3.2 Conversion profiles for a) 19.2% 1-1 TAMR and b) 19.2% 1-1 TAMR with 14% EA groups to achieve 1-1 conversion

The 40% ET samples reached full conversion in ~4 hours with 100% acrylate conversion and 60% thiol conversion. The 40% EA TAMR reached 97% thiol conversion with 69% acrylate conversion and leveled off in ~6 hours. This result may seem odd at first, since the 40% ET sample gave nearly ideal conversion of both thiol and acrylate. However, since TMPTA is mostly pure, when it is the limiting reagent the corresponding thiol conversion should be in line with the theoretical value; whereas, when the thiol is the limiting reagent, the acrylate will react with however many thiol groups are present. This indicates that the actual thiol content present in TMPTMP samples is ~7-10% higher than the theoretical value, which is consistent with previous observations.

While a variety of TAMR formulations have been shown to cure efficiently at room temperature, the utility of the resin would be increased if the cure time could be shortened without sacrificing performance. Curing TAMR at elevated temperatures should decrease the cure time by increasing the rate of the polymerization reaction. In 19.2% DEA-AA 1-1 TAMR, increasing the cure temperature from room temperature to 50 °C decreased the cure time from 10 hours to 3 hours. Figure 3.4 shows the thiol and acrylate signals at several time points for a 19.2% 1-1 sample that was cured in an oven at 50 °C. This reduction in cure time is impressive, and these mild conditions should be easy to reproduce in any laboratory setting. Raising the cure temperature more should decrease the cure time even further, so it is conceivable that TAMR could be fully cured in one hour or less.

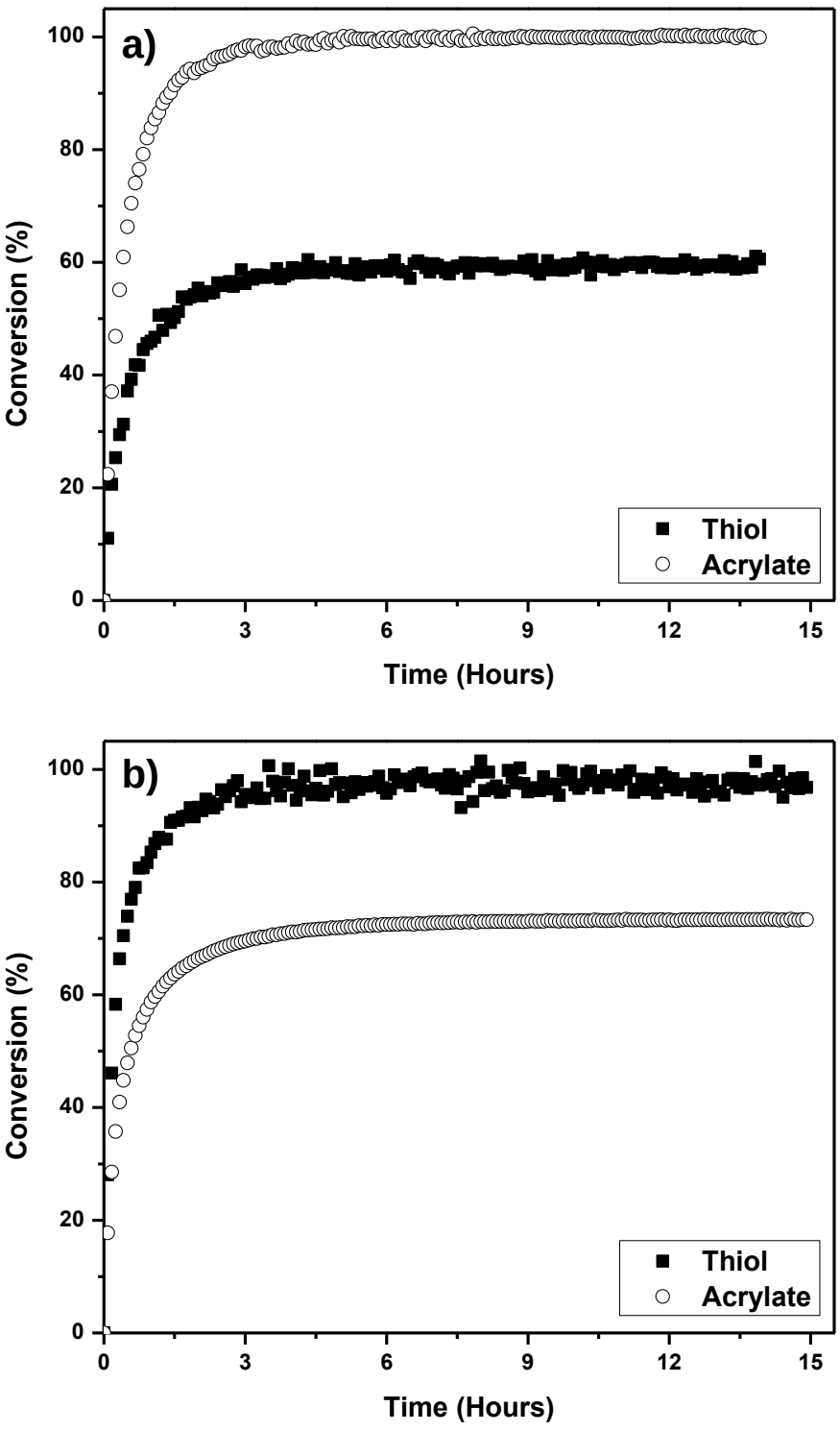

Figure 3.3 Conversion profiles for a) 40% ET and b) 40% EA 19.2% TAMR

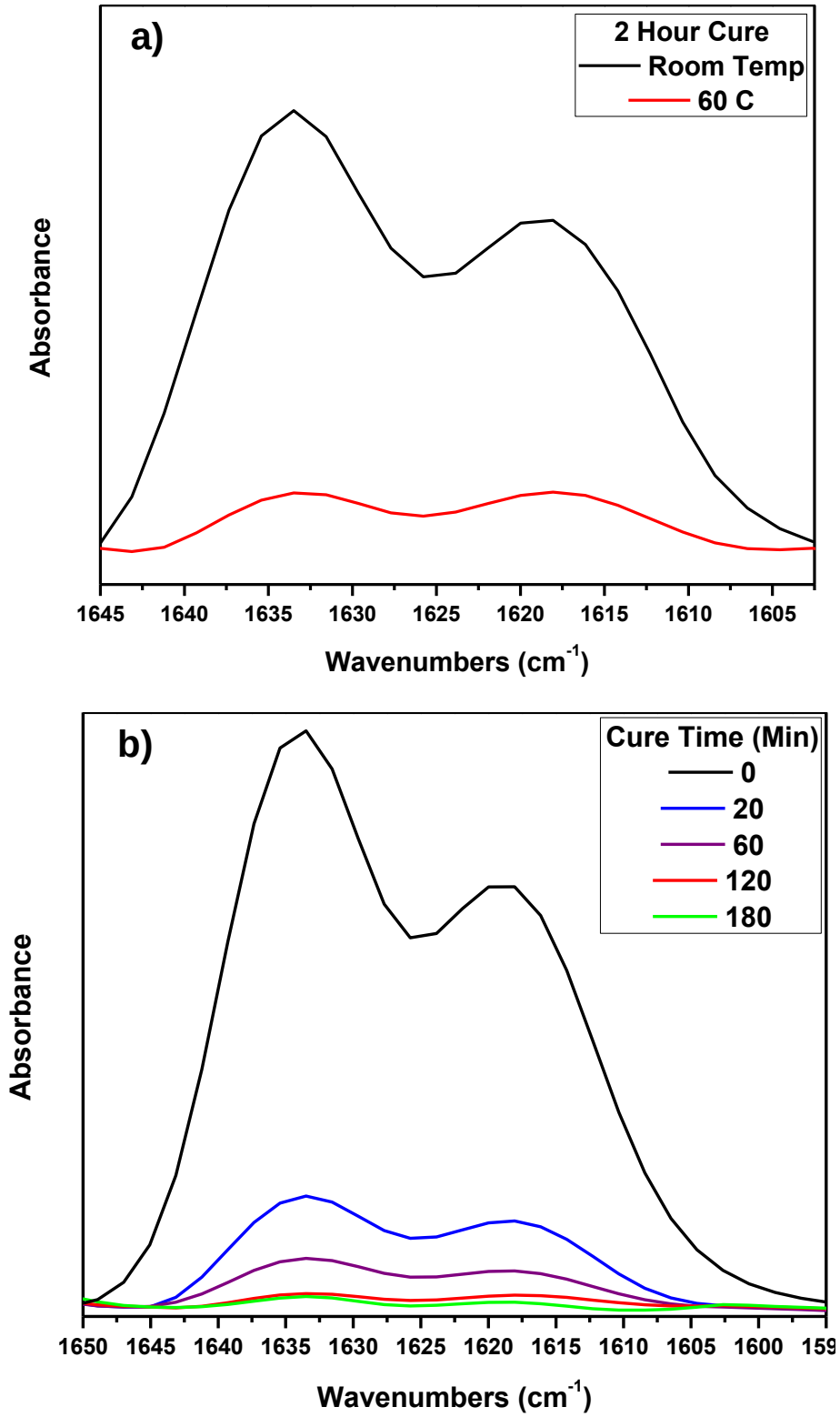

Figure 3.4 FTIR acrylate peaks for 19.2% 1-1 TAMR a) at 2 hours of curing at room temperature and 60 °C and b) over time at 60 °C

3.5.5 Hydrophilicity of TAMR

The hydrophilicity of materials used to construct microfluidic devices is of critical importance for a variety of applications. The most obvious examples that require aqueous conditions are biological systems, but other applications, such as droplet-generation, use water as well. Due to the high methyl group concentration at the polymer surface, cured PDMS has a water contact angle of ~110°, which is quite hydrophobic.[201] Modification of the surface using oxygen plasma is routine and can decrease the contact angle significantly by adding oxygen species to the silicon atoms located near the surface of the PDMS. However, immediately after plasma treatment the contact angle will start rising over time and will return to nearly the original value in a process called hydrophobic recovery,[195, 202-204] which is caused by the diffusion of short, uncrosslinked PDMS oligomers to the surface of the material.[205-206] In contrast, TAMR has a stable hydrophilic surface due to high ester group and amine concentrations in the polymer.[76] Previous work focused on one DEA-AA concentration, so gathering more data with different TAMR variations was needed.

The hydrophilicity of TAMR surfaces was measured using water contact angle testing. The samples were cured in a polystyrene (PS) Petri dish, which exposes one side of the resin to air and the other to PS during the polymerization process. The side where the water contact angle measurements were taken will be indicated in every case. Figure 3.5 shows the effect of amine concentration on the water contact angle for several TAMR formulations (PS side) at full cure. As expected, the 19.2% DEA TAMR has a lower contact angle than the 11.1% due to the increase in polar amine groups throughout the polymer matrix.

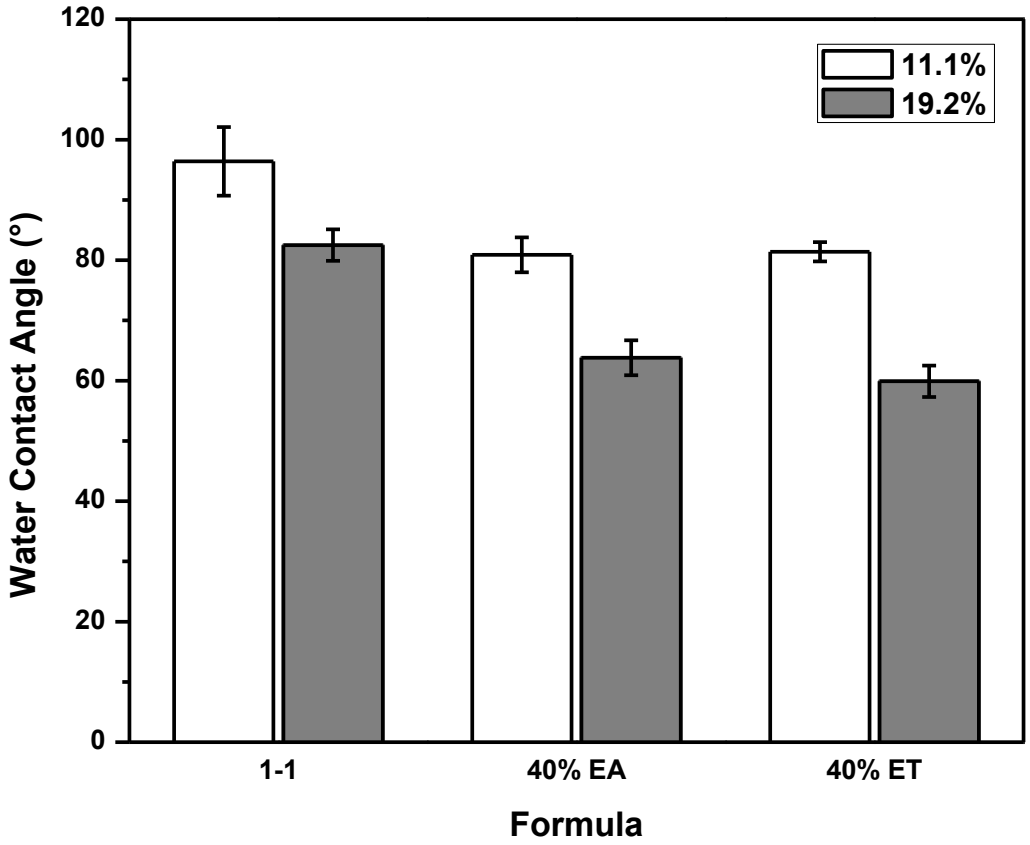

Figure 3.5 Water contact angles for 19.2% and 11.1% 1-1 TAMR on the PS surface

The formulations where excesses of either functional group were incorporated into the polymer also showed a decrease in contact angle relative to the samples where a 1-1 thiol to acrylate group ratio was used. In the case of excess acrylate, the overall amine concentration in the material is higher than either the 1-1 or ET samples since excess acrylate groups were added by using more DEA-AA. The samples with excess thiol likely showed a decrease in contact angle due to the polarity of the unreacted thiol group. All of the samples had contact angles significantly lower than unmodified PDMS, but the PS side of the 10% 1-1 samples did have a surprisingly high contact angle of ~96°.

The water contact angles were also measured for the 19.2% samples after 1 hour of curing instead of 24, and the results are displayed in Figure 3.6a. At 1 hour, the

1-1 sample still showed the highest contact angle at ~68°, but the difference between it and the samples with excess functional groups was smaller than at 24 hours. When comparing the 1 and 24-hour contact angles, there was a distinct difference between 1 and 24 hours of curing in the 1-1 samples (~14°), while the samples with excess functional groups essentially remained the same. The 11.1% DEA-AA samples were also tested, except due to the slower rate of reaction with the lower amine concentration, the contact angles were measured at 2 hours of curing to ensure the resin had fully gelled. Figure 3.6b shows that for the 11.1% samples, all three formulations showed an increase in contact angle with reaction time, and as with the 19.2% sample, the 1-1 sample increased the most (~24°). Although in both cases the water contact angle of the TAMR is increasing with reaction time, it is unlikely that the conversion from monomer to polymer has an appreciable change on the overall hydrophilicity of the material. Instead, the change in contact angle is due to longer exposure times to the curing surface, which in this case is polystyrene.

In order to test the effect of curing surface on the contact angle, the water contact angle of the side of the resin exposed to air was determined for the samples at both low cure time and full conversion. Figure 3.7 contains the air side contact angle results for both the 11.1% and 19.2% samples with 1-1, 40% EA, and 40% ET variations at the different cure times. It is obvious that the curing surface plays an integral role in both the contact angle of the material and how it changes over time since for the air-side of the samples, the contact angle decreased with cure time. This makes sense because the PS Petri dish surface has a relatively hydrophobic water contact angle of ~80°, and the air is more polar by comparison.

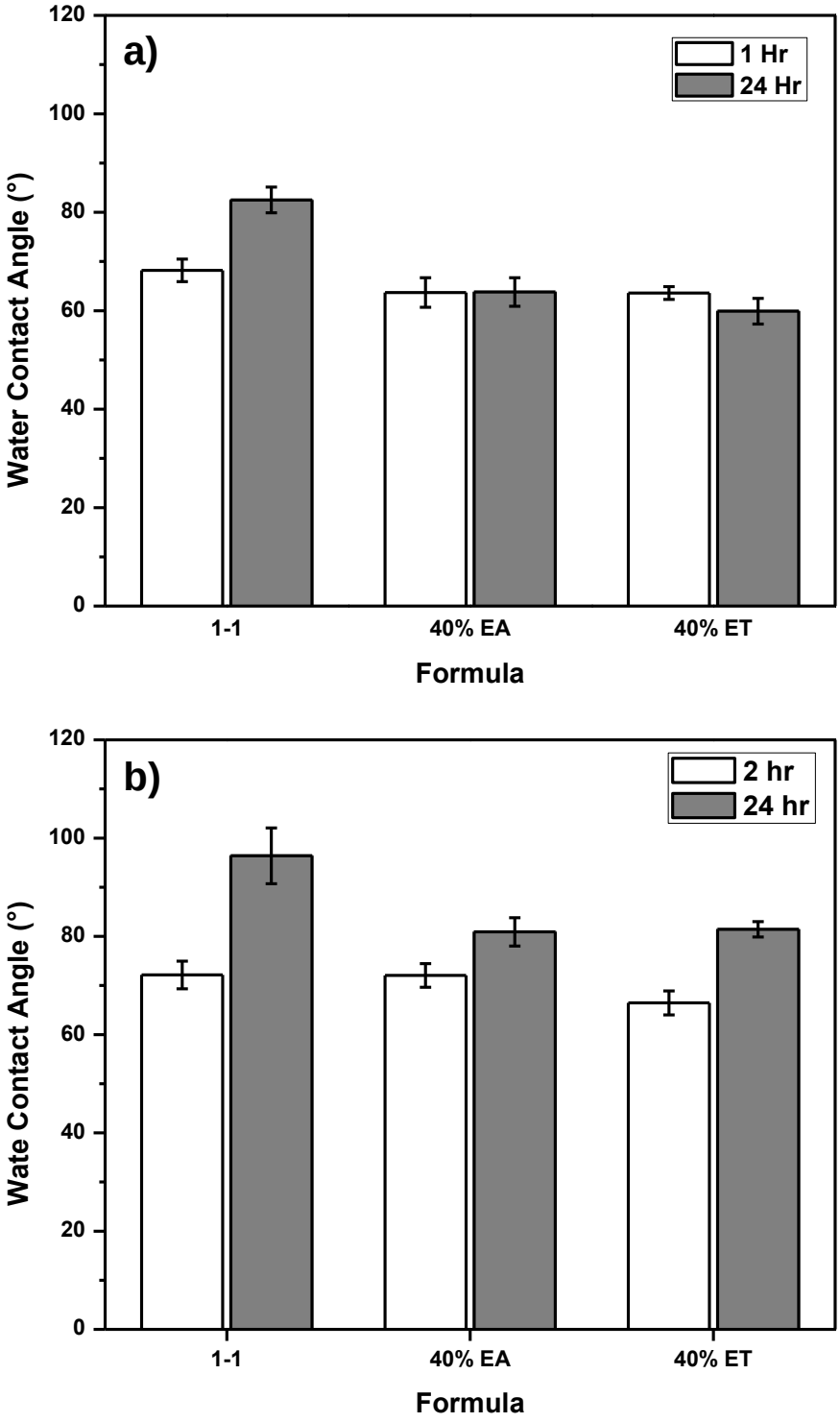

Figure 3.6 Water contact angles for a) 19.2% and b) 11.1% TAMR formulations over time on the PS surface

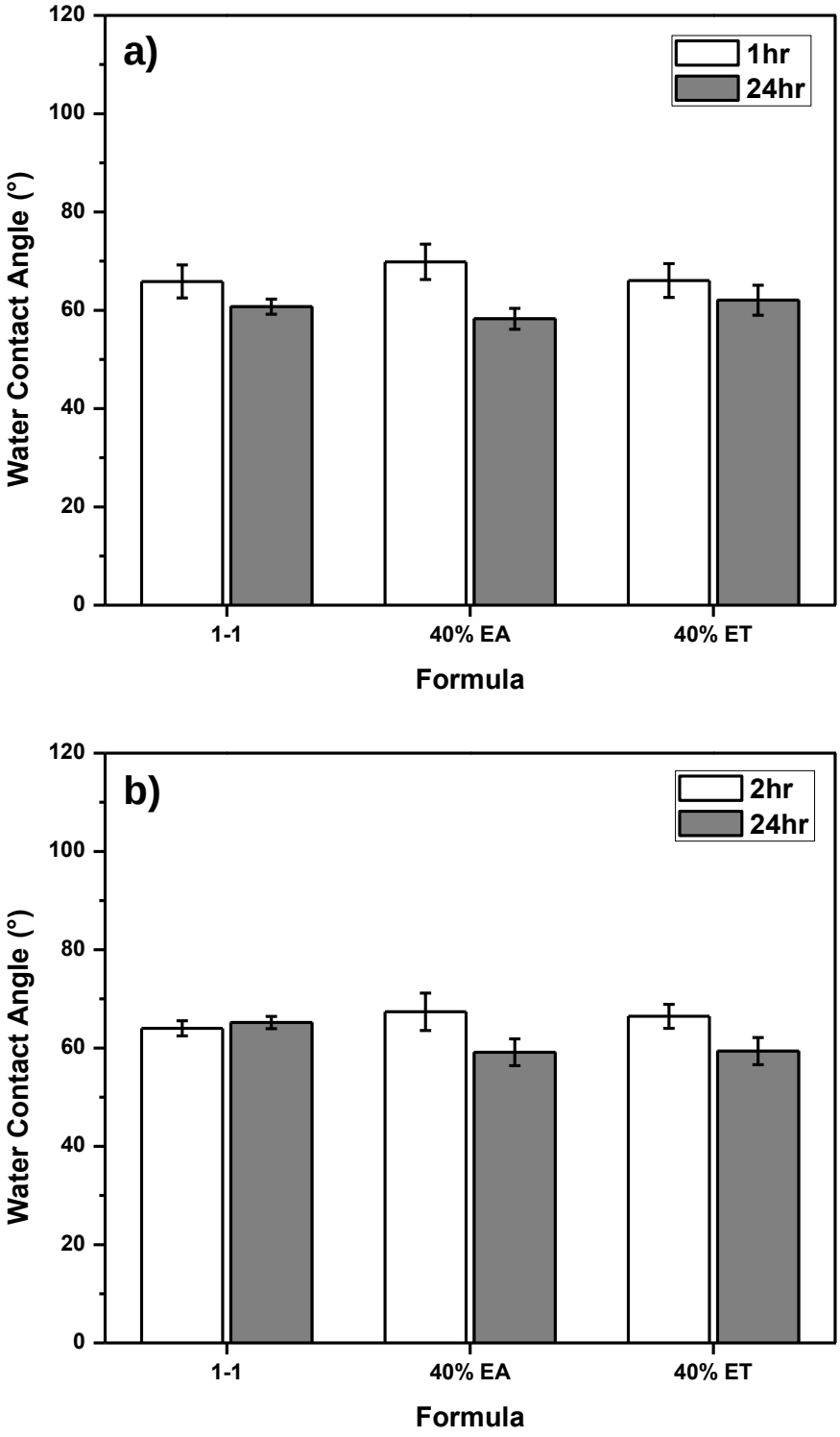

Figure 3.7 Water contact angles for a) 19.2% and b) 11.1% TAMR formulations over time on the air side

During the curing process, the hydrophobic segments of PETA and TMPTMP can orient themselves to be in contact with the PS while the more hydrophilic ester segments would be on the interior of the sample. As cure time increases, this orientation process continues, which increases the contact angle. The air-side of the resin could go through a similar process, but other possible explanations for the decrease in contact angle over time are oxidation processes or absorption of water vapor.

To investigate the effect of a hydrophilic curing surface on the TAMR contact angle, 19.2% 1-1 samples were cured on a glass microscope slide. The surface of the slide was determined to have a water contact angle of ~21°, which is due to the high oxygen concentration in the glass. Figure 3.8 shows the contact angle for 19.2% TAMR cured for 1 hour and 24 hours on the hydrophilic glass surface. At full cure, the contact angle is ~55° when cured on glass, which is nearly 30° lower than when the same sample was cured on the hydrophobic PS surface. As with the previous examples, there was a slight decrease in the contact angle with increased exposure time to the surface. The ability to vary contact angle by nearly 30° by altering the curing surface is extremely powerful since the same resin formulation could be used to achieve a variety of results. Larger differences in contact angle could potentially result from curing TAMR on surfaces with more extreme contact angles, such as fluorinated polymers or oxygen plasma modified glass surfaces, and the upper and lower contact angle limits for TAMR likely vary by resin composition. This property could be exploited to use TAMR as an adaptive surface that would take on a contact angle more compatible with whatever it was placed in contact with.

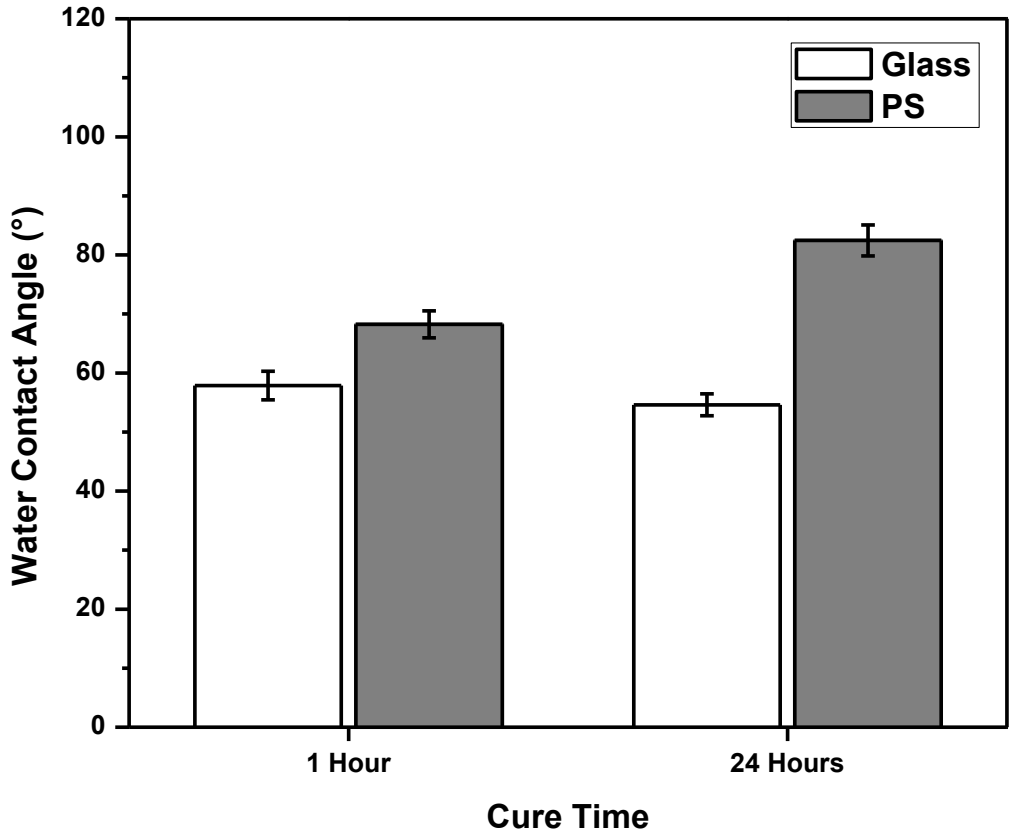

Figure 3.8 Water contact angles for 19.2% 1-1 TAMR cured on glass over time on the glass surface

3.5.6 TAMR Water Absorption

Since TAMR is more polar than PDMS, it was expected to absorb more water, and since microfluidics in aqueous systems is extremely popular, knowledge of the behavior of TAMR in water is of critical importance. Figure 3.9 shows results from a long-term study of the mass change of 11.1% and 19.2% DEA-AA based TAMR samples soaked in water. The inset on each graph shows the swelling behavior over the first 24 hours. The mass of 19.2% TAMR increased by 1.5% over 24 hours while the 11.1% increased by ~1%. In both cases, the 40% ET samples swelled the most, followed by the 40% EA sample, then the 1-1 samples, which follows the increasing crosslink density of the TAMR samples.

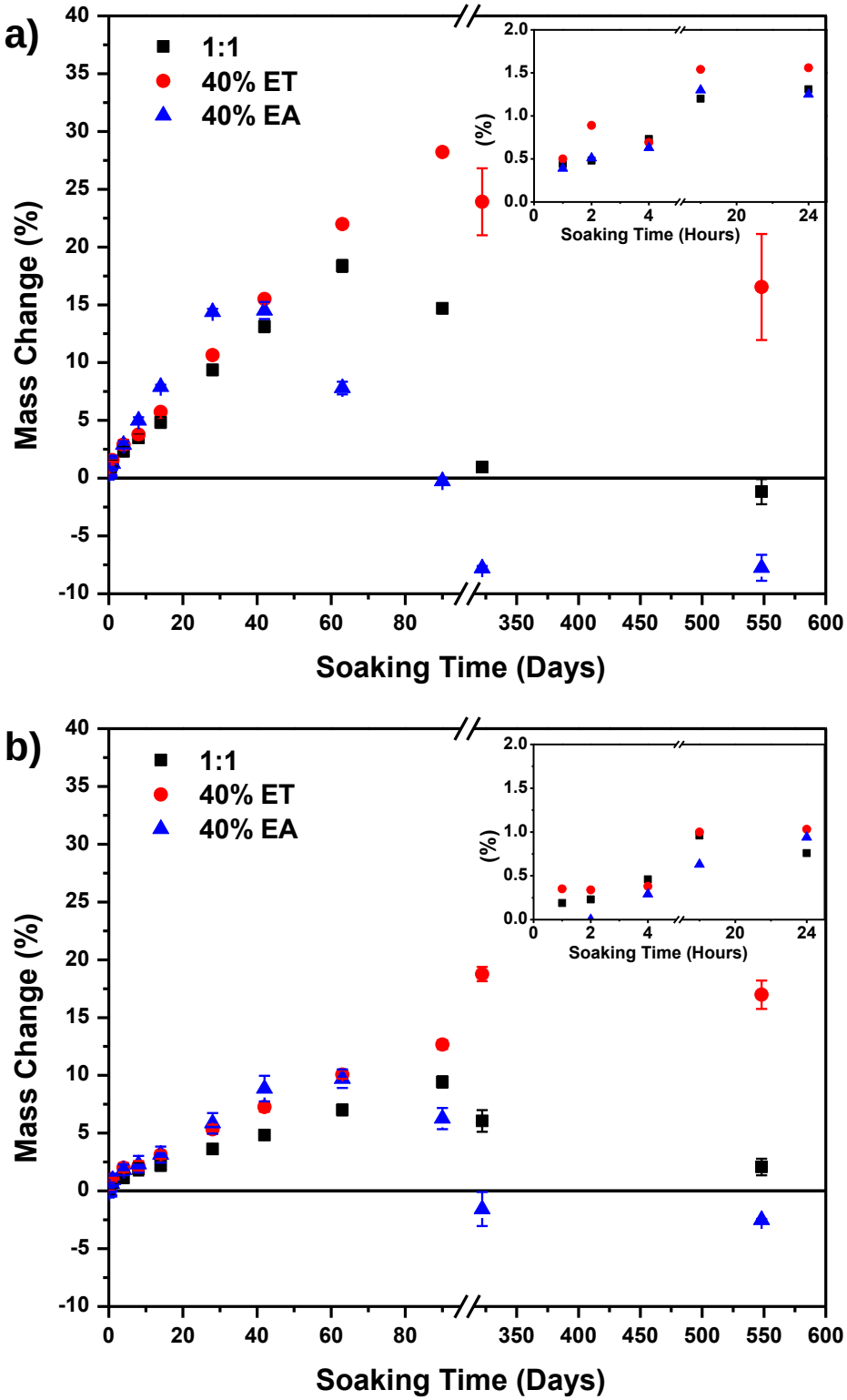

Figure 3.9 Mass change over time for a) 19.2% and b) 11.1% TAMR samples soaking in water (insets show absorption at low soaking times)

The ET samples likely have the lowest crosslink density due to the excess of monofunctional mercaptopropionic acid present in TMPTMP. The EA samples have lower crosslink density than the 1-1 samples due to the unreacted acrylate chain ends present in the network at full cure. Eventually all of the samples reached a maximum swelling amount then started to lose mass, with some samples decreasing below their initial masses. The decrease in mass is due to the hydrolysis of the ester bonds present in the polymer matrix, which is catalyzed by the incorporated amine. This explains why the 40% EA samples degraded the fastest followed by the 1-1 then the 40% ET since that is the order of decreasing amine content. Overall, the 11.1% samples swelled less than the 19.2% samples due to their increased crosslink density and decreased hydrophilicity.

The physical appearance of the TAMR samples was noted during the swelling data collection process. Over time, all of the samples became less transparent and started to cloud. The rate and intensity of the clouding paralleled the swelling rate for each sample. At 24 hours, the 19.2% 40% ET TAMR samples were noticeably more cloudy, and by 4 days they were completely opaque. At 8 days, all of the samples were cloudy, but both the 1-1 samples and 11.1% 40% EA samples were still translucent while the ET samples and the 19.2% 40% EA samples were opaque. At 28 days, all of the samples except the 11.1% 1-1 were opaque, but it eventually clouded fully between 42 and 90 days of soaking in water. The 11.1% samples were overall more resistant to clouding compared to the 19.2% samples due to the slower rate of water absorption. Despite this clouding behavior, except for a long-term aqueous study lasting more than 48 hours, each of the TAMR formulations tested remains usable.

An interesting phenomenon that was observed during the TAMR swelling and clouding studies was the formation of disc-shaped droplets inside of the resin pieces. Figure 3.10 shows several examples of these features imbedded in polymer samples.

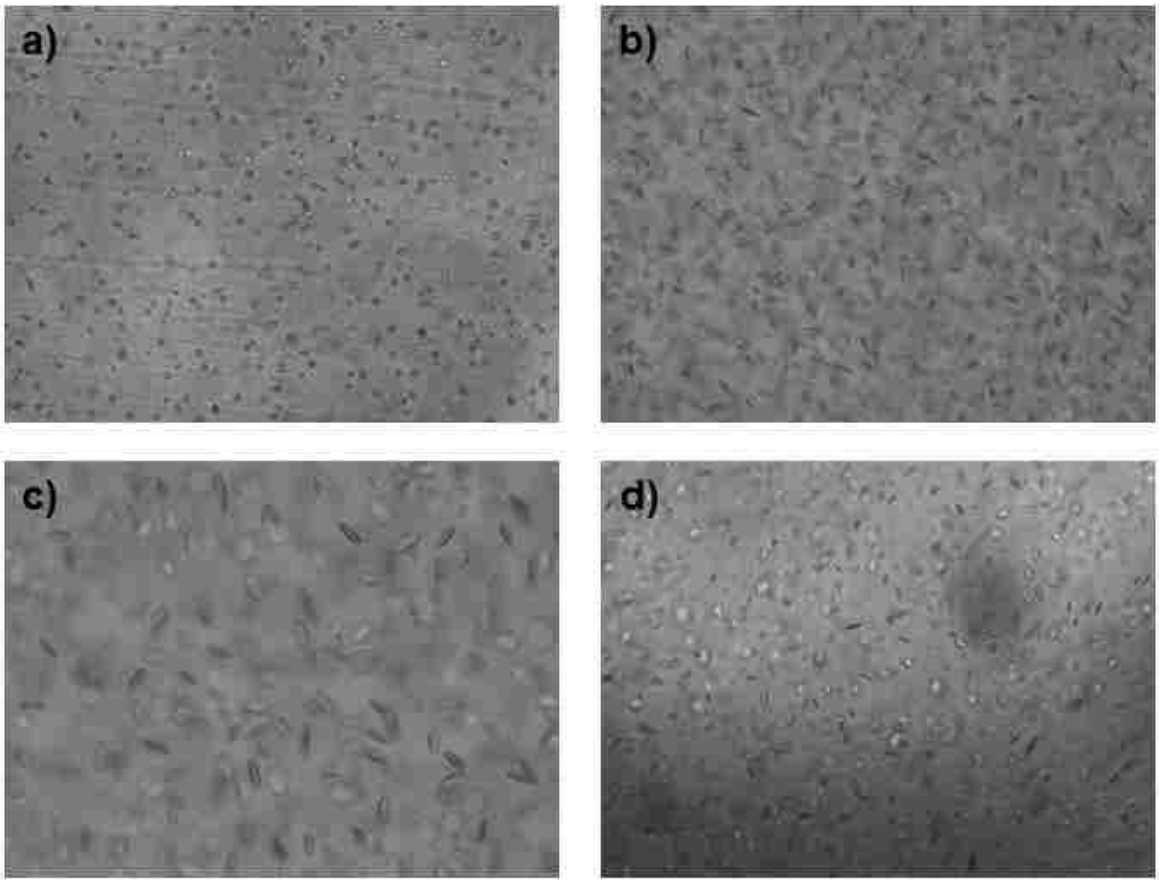

Figure 3.10 Disc-shaped water droplets in TAMR where the disc diameter is a) ~2-5 μm in 19.2% 40% ET and b-d) ~12-15 μm in 19.2% 40% EA

Generally, excess acrylate samples gave the most disc features, followed by 1-1 then excess thiol samples, which follows the decrease in amine concentration in the resin samples. The discs form slowly while the polymer is immersed in water and appear to increase in concentration before being obstructed by the clouding of the resin. Figure 3.11 shows a sequence of disc formation in a 19.2% 40% EA TAMR sample soaked in water. Samples with increased amine content (35.5%) showed some disc formation, but they were dominated by the overall clouding of the resin. When water

was mixed into the liquid resin before gelation, most of the water exists as large droplets, but this could be dependent on how aggressively the water is incorporated. The droplets and clouding can be removed by heating the resin samples in an oven to drive off the accumulated water. While a detailed investigation into this process was not performed, disc-shaped water pockets have been previously observed in a variety of polymers.[207-211]

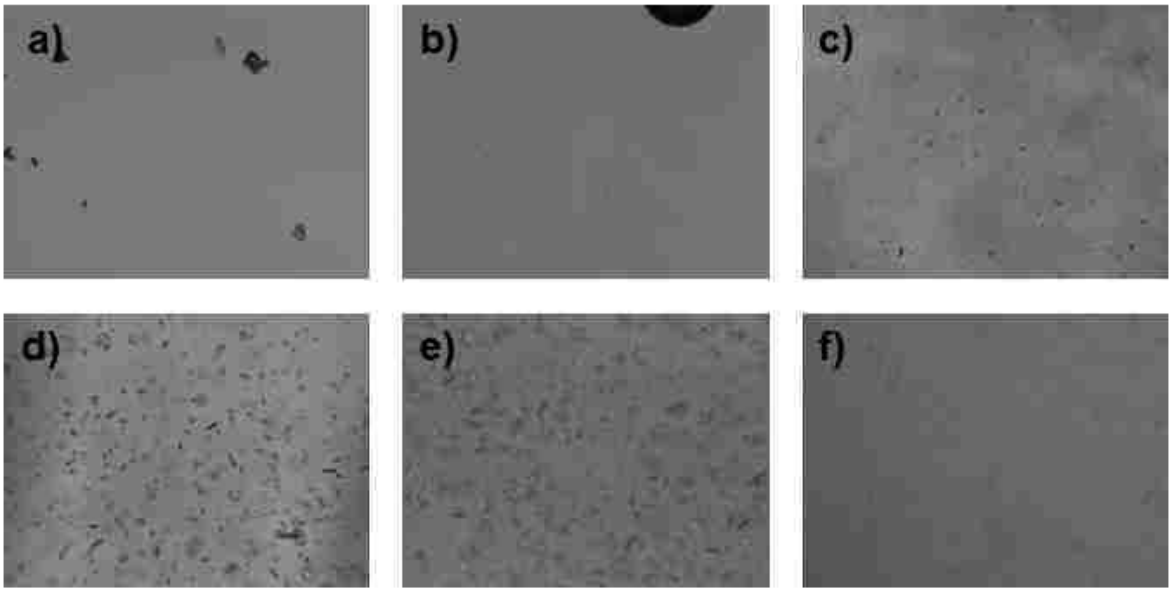

Figure 3.11 Evolution of water droplets over time in 19.2% 40% EA TAMR a) 2 hr, b) 24 hr, c) 48 hr, d) 120 hr, e) 168 hr, and f) 288 hr

Polycarbonate, polyester, and epoxy resins have been shown to develop disc-shaped features upon exposure to water. The driving force behind the disc formation in epoxy and polyester systems was identified to be water-soluble impurities present in the polymer matrix, and the disc formation process could be accelerated by the addition of salts such as KCl. A similar process is likely occurring in the TAMR samples where the incorporated amine is acting as the water-soluble “impurity” and driving the disc

formation since the number of discs appears to correlate well with the amine concentration.

3.5.7 TAMR Solvent Absorption

PDMS is known to swell dramatically in some solvents, especially nonpolar organic compounds and amines.[122, 178] As microfluidic applications involving organic solvents, such as the preparation of microparticles, become more popular, the need for materials that will not swell in these solvents increases The large number of methyl groups present in PDMS makes it hydrophobic, and although it is a thermoset, the crosslink density is low enough that it can swell significantly. TAMR should perform much better in nonpolar solvents due to its more hydrophilic nature, and it should perform better overall since it is highly crosslinked. A previous study showed that the mass increase of TAMR submerged in hexane was ~0.25% at 24 hours, while PDMS showed a mass increase of ~100%. In trimethylamine, PDMS swelled by nearly 250% in 24 hours while TAMR only swelled by ~0.7%.[76] While these results look promising, a wider variety of solvents needed to be screened to determine if TAMR preforms as expected.

The swelling behavior of TAMR in a variety of solvents is reported as the swelling ratio, which can be determined using the following equation:

$$S = \frac{D}{D_0} \qquad \text{Eq. 3.3}$$

where S is the swelling ratio, D is the sample diameter after 24 hours of soaking, and D_0 is the initial sample diameter. Table 3.1 contains the swelling ratios for 19.2% 1-1 TAMR in a variety of solvents and the swelling ratio for PDMS in those same solvents as reported by Lee et al.[178]

Table 3.1 Swelling Ratios for 19.2% 1-1 TAMR and PDMS

Solvent	TAMR Swelling Ratio	PDMS Swelling Ratio[a]
Water	1.01 ± 0.01	1.00
1 M HCl	1.05 ± 0.01	1.02 ± 0.01[b]
1 M NaOH	0.99 ± 0.01	1.01 ± 0.01[c]
Diisopropylamine	1.02 ± 0.01	2.13
Acetone	1.16 ± 0.01	1.06
Toluene	1.12 ± 0.01	1.31

a) Values reported by Lee et al.[178] b) 12 M HCl used c) 10 M NaOH used

Despite the long-term swelling behavior of TAMR in water, the swelling ratio of TAMR is comparable to PDMS in water at 24 hours. To test the stability of TAMR under corrosive conditions, samples were immersed in 1 M HCl and 1 M NaOH. The HCl samples had a higher swelling ratio than pure water; however, NaOH gave a swelling ratio slightly less than one, which means the samples decreased in size. One possible explanation for this could be the neutralization of charged, protonated amines in the TAMR network by the stronger $^{-}$OH base which led to a reduction in size due to the elimination of charge-charge repulsions. The swelling ratios for diisopropylamine and toluene are significantly lower in TAMR compared to PDMS, while the swelling ratio for acetone is higher. This is likely due to the polar nature of TAMR compared to PDMS. Although the TAMR samples did not swell dramatically in acetone, two of the six samples tested fractured in half during the testing process. One possible explanation is that a prior defect in those samples propagated as the network swelled. Overall, TAMR is more resilient to solvent swelling than PDMS, especially over 24 hours, but long-term exposure to the HCl or NaOH solutions will likely cause fairly rapid degradation of the material due to hydrolysis of the ester groups.

3.5.8 TAMR Mechanical Strength

The structural integrity of a microfluidic material is important in both the operation and construction phases of device use. When performing microfluidic experiments, the material used to fabricate the device must be able to withstand the pressures applied to the channel without failing or deforming. During the construction and assembly phase, the material should be tough enough to survive removal from the master mold, having tubing connected, the bonding procedure, and general handling by users. Elastomers like PDMS are ideally suited for soft lithography fabrication using rigid masters, like silicon wafers, since they can be removed from the mold easily, but their flexibility hinders their use for higher pressure applications where they will deform substantially.[122] Other microfluidic materials used for soft lithography, like PUMA, have high elastic moduli, but this means that they need to be cured on a flexible mold, like PDMS, instead of a silicon wafer. This requires an addition step in the mold making process compared to PDMS replication. A resin that is flexible enough to remove from a rigid mold while hardening to resist deformation would be ideal. TPE is an example of such a resin since it can be partially cured by UV exposure, removed from a rigid mold, then fully cured to give a stiff polymer. TAMR can also be removed from a rigid mold in a partially cured state then reach full cure over time to gain strength, which is primarily due to the high degree of crosslinking present in the system. The mixture will gel at relatively low conversion due to the high average functionality of two trifunctional monomers, which allows it to be removed from the mold, but the strength will continue to increase as conversion increases with time.

The elastic modulus of several TAMR formulations was determined at both low cure and full cure. Figure 3.12 contains the elastic modulus for both 19.2% and 11.1% TAMR with 1-1, 40% EA, and 40% ET formulations.

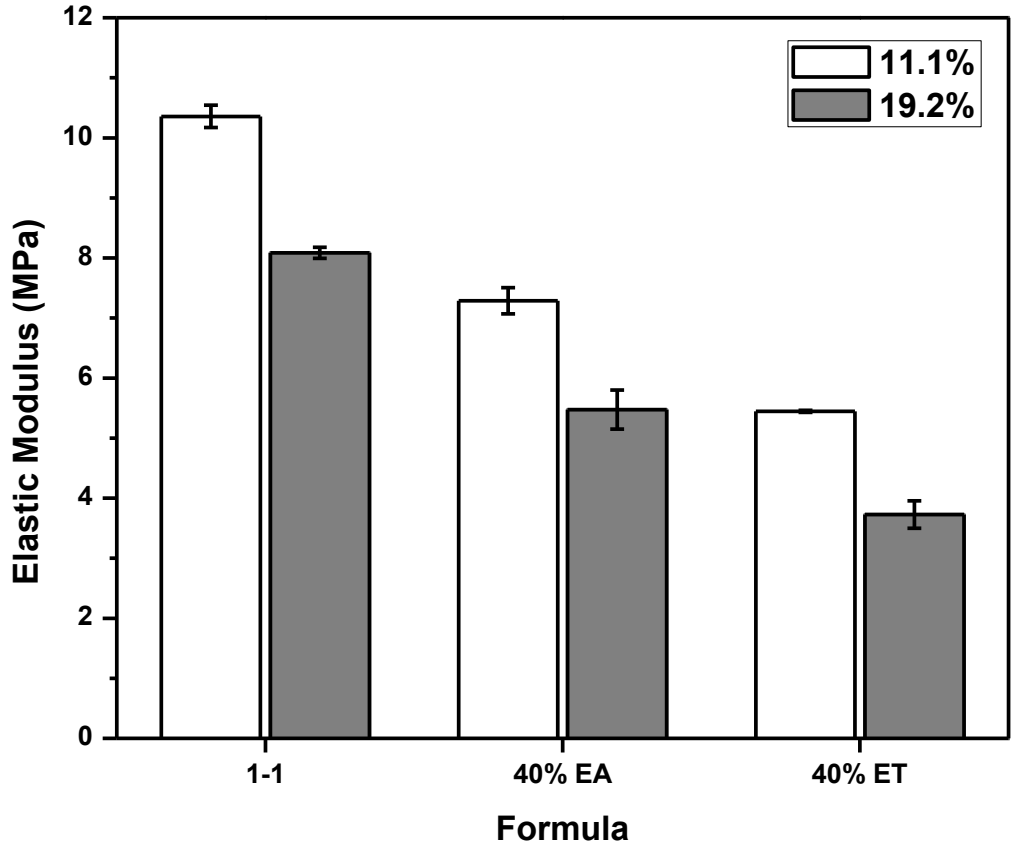

Figure 3.12 Elastic modulus for 19.2% & 11.1% TAMR formulations

As expected, the 11.1% samples all had higher moduli then their 19.2% counterparts due to the decreased crosslink density caused by the decrease in acrylate functionality associated with increased amine content. Both TAMR formulations have moduli that are significantly higher than PDMS, which was determined to have an elastic modulus of 1.21 ± 0.05 MPa for the recommended 10:1 cure ratio. The formulas containing excess groups have lower moduli than the 1-1 samples due to the overall lower crosslink density associated with the presence of a significant portion of unreacted groups in the polymer matrix, but all of the samples had higher moduli than

PDMS. The 40% ET samples had a lower modulus than the excess acrylate samples due to the lower crosslink density produced by the monofunctional mercaptopropionic acid impurity present in TMPTMP. In order to see what effect the small difference in the final thiol and acrylate conversions had on the modulus of the cured TAMR, 14% EA groups were added to a 19.2% 1-1 sample. Using FTIR conversion plots of samples made using those same ratios, it was determined that 14% EA groups was enough to give a true 1-1 thiol-acrylate group ratio. The modulus of samples made using the true 1-1 ratio was found to be 8.5 ± 0.3, which is slightly higher than the unmodified 19.2% 1-1 samples. The increase in modulus is not dramatic since the monofunctional impurities are still present to reduce overall crosslinking density, but adjusting the formula to give a true 1-1 ratio is a viable way to gain a modest increase in modulus.

Figure 3.13 shows the elastic moduli for both amine concentrations at 1 and 24 hours of curing for all three formulations. Although the samples completely gel and can be handled easily, the modulus at 1 hour of curing was considerably lower than the modulus at 24 hours for each sample, which facilitates easy removal of the resin from rigid masters. As shown earlier, TAMR can also be cured at elevated temperatures to speed the polymerization reaction. In order to confirm that the heating process did not affect the structural properties of the resulting material, the elastic modulus was determined for 19.2% 1-1 TAMR cured for 3 hours at 50 °C. When cured for 24 hours at room temperature, the TAMR had an elastic modulus of 8.09 ± 0.09 MPa, and when cured for 3 hours at 50 °C, the resin had a modulus of 8.1 ± 0.2 MPa. This confirms that the increased temperature sped up the reaction rate while not affecting the mechanical properties of the resulting polymer network.

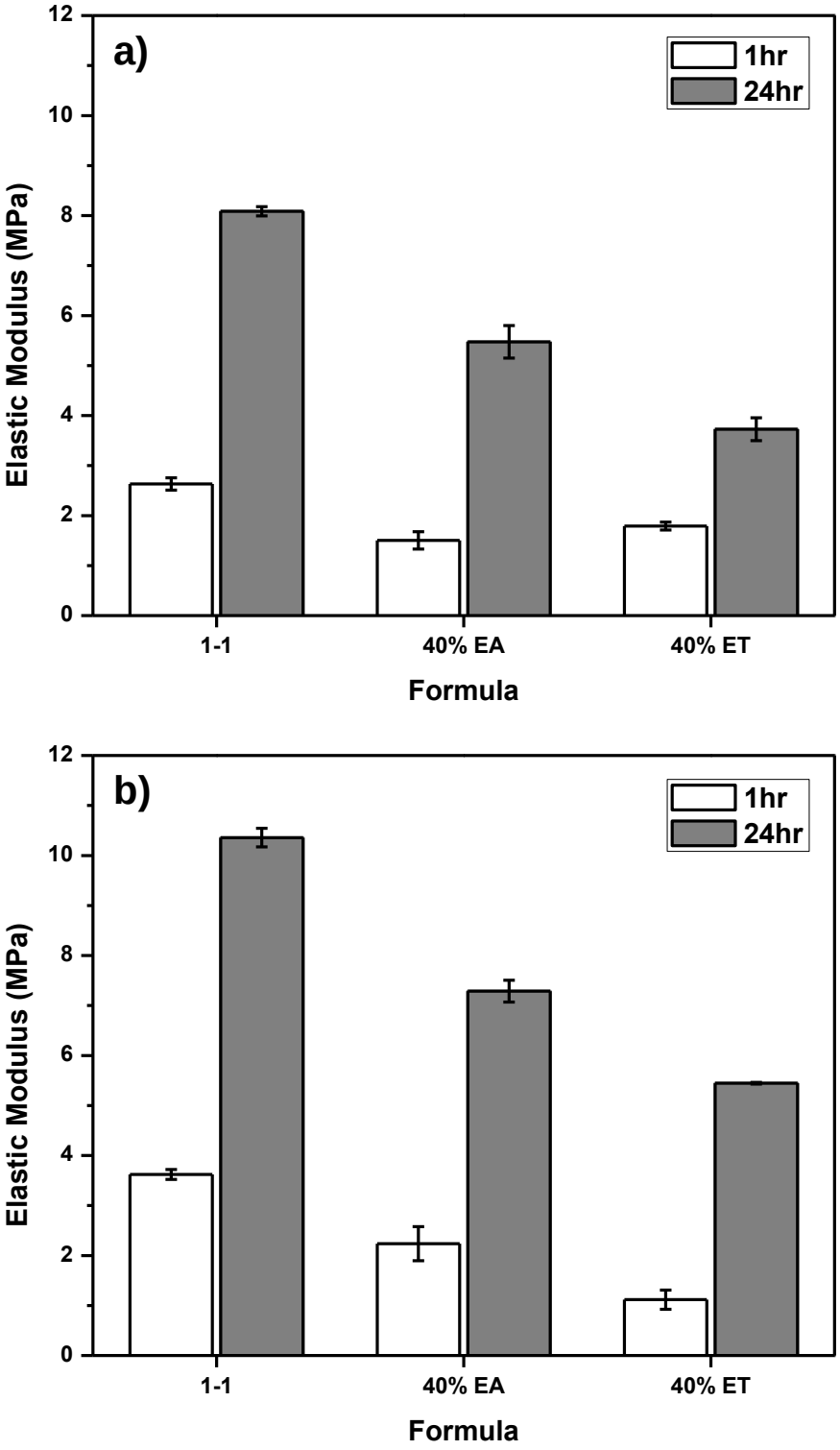

Figure 3.13 Elastic modulus for a) 19.2% and b) 11.1% TAMR formulations over time

Several small modifications were performed on the 19.2% TAMR system in an attempt to raise the modulus. First, for the 40% EA sample, instead of using more 19.2% DEA-AA to raise the acrylate content to 40% above the thiol group content, unaltered PETA was used. This should increase the modulus due to the higher average functionality in the unmodified PETA compared to the AA mixture where 19.2% of the acrylate groups have been reacted with an amine. Figure 3.14a gives the results for the typical 19.2% 40% EA sample and one prepared using unmodified PETA. While the results are far from dramatic, substituting PETA for the DEA-AA gave a modulus increase of 13.3%. Next, instead of using DEA as the amine in the AA, EEOA and DEOA were used in an attempt to add hydrogen bond donors to the polymer system and increase the modulus. While TAMR contains an abundance of hydrogen bond acceptors due to the ester group associated with each thiol and acrylate, there are relatively few hydrogen bond donors. Figure 3.14b compares the modulus for the 19.2% AAs using DEA, EEOA, and DEOA. Switching from DEA to EEOA (adding one hydroxyl group) gave a modest modulus increase of ~10%. Adding a second hydroxyl group by switching to DEOA caused a sharp drop in the modulus of ~20% instead of the expected increase, but in addition to the low modulus, the DEOA samples were cloudy upon curing even though the AA mixture was clear. This is likely due to the hydrophilic DEOA promoting the AA to absorb a large amount of water vapor from the air which phase separated as the polymerization occurred and caused the cloudiness. As seen in a variety of other polymer systems,[210, 212-213] the excess water domains throughout the polymer matrix led to a reduction in elastic modulus through the formation of microcavities which caused premature fracturing of the polymer.

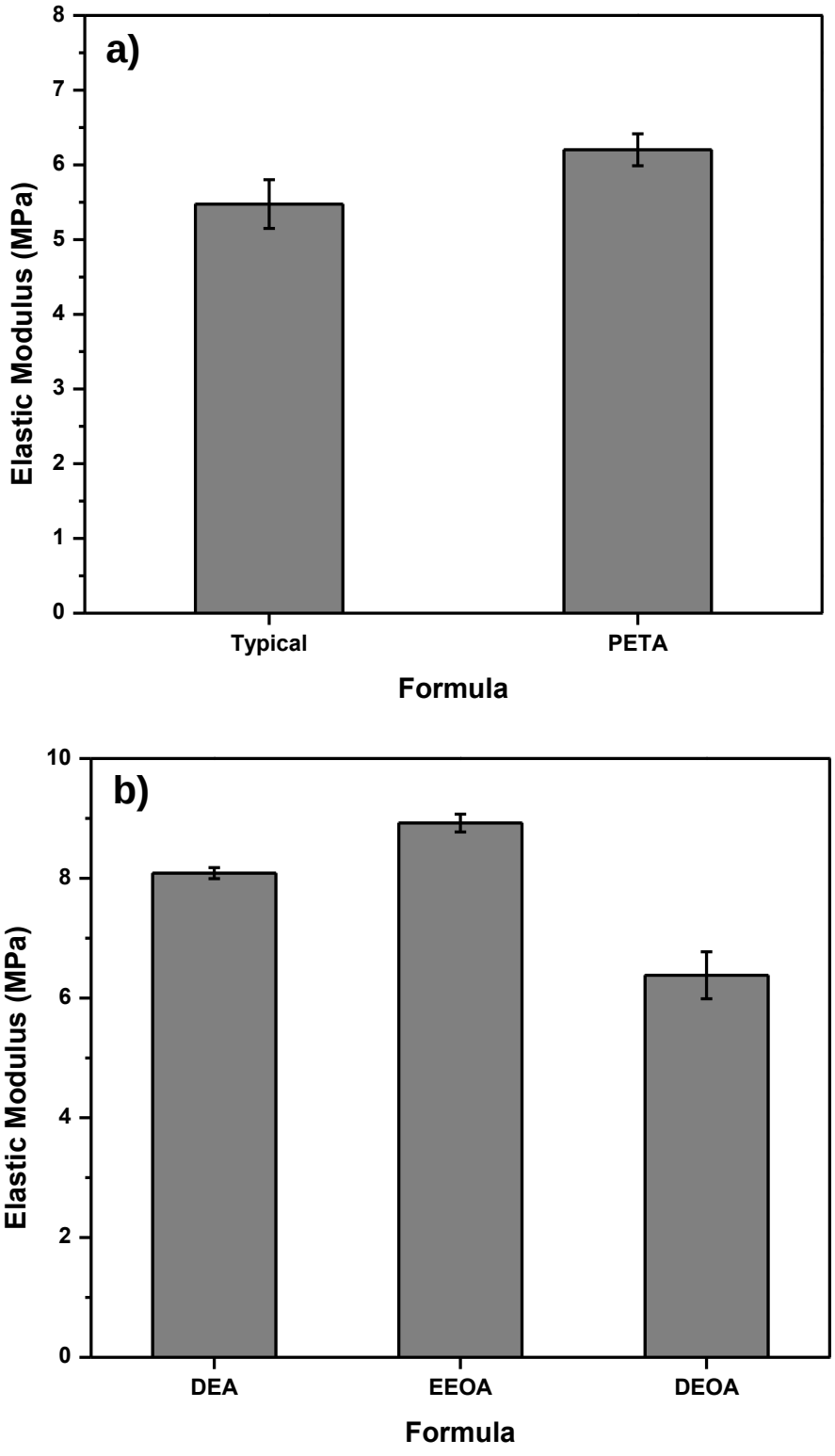

Figure 3.14 Elastic modulus for 19.2% a) 40% EA TAMR made with excess PETA and b) 1-1 with different amine AAs

3.5.9 TAMR Bonding Strength and Mechanism

Bonding strength is an important characteristic of any microfluidic material due to the high pressures and small bonding areas present in many devices. PDMS is typically bound to glass or itself using an oxygen plasma treatment, which facilitates the formation of Si-O-Si linkages between the two surfaces. TAMR can bond to itself by incorporating excess functional groups into each side of the device and bringing them into contact. Earlier work has shown that the bond strength between the two surfaces increases with increasing excess functional group content, and the bonding mechanism was theorized to be an interfacial thiol-acrylate reaction between groups on the opposing surfaces.[76] In order to confirm this and investigate what conditions are important for achieving a strong bond, several TAMR formulas were used to fabricate a series of test devices. Four devices were fabricated per test variable, so the reproducibility of device fabrication will also be evaluated. The first device tested was constructed using 19.2% DEA-AA TAMR with 40% EA groups for the channel half and 40% ET for the flat half of the device. The original device fabrication procedure called for a weight to be placed on top of the device after the two halves were put together, so in order to test if this was necessary to get a strong bond between the device layers, the weight was omitted during the curing process. Of the four devices constructed, three were fully functional. In the one nonfunctional device, a piece of debris, likely from the hole drilling process, was trapped between the device halves and spanned the gap between the center and one of the outside channels. This caused an inadequate seal between the center and outside channels and so fluid crossed over the channel boundary at this point. This method of failure is due to operator error and can be

prevented by more thorough dust removal with compressed air and device inspection before bonding. The other three devices performed impressively and were able to withstand 10 mL/min of flow without failing, which was the maximum possible flow rate with the syringe pump. One of the devices was tested on another syringe pump and was able to handle 26 mL/min without failing. Clearly compressing the two device halves during the bonding process is not necessary to achieve a strong bond, which is important for devices with small features that could be damaged easily.

The effect of the amine content in the AA on the bond strength between TAMR layers has not been previously investigated. Another set of test devices was fabricated using 11.1% DEA-AA to determine if the lower amine content would affect the device strength. All four of the test devices were functional and each withstood the maximum flow rate of 10 mL/min without failure. One device was fabricated and tested only 30 minutes after the bonding procedure was performed. This device was able to withstand 10 mL/min but failed after fluid was manually forced through the channel. The importance of having a fluid tight channel even when the TAMR has not fully cured will be discussed in Section 3.5.10.

As shown in a previous section, TAMR can be fully cured in three hours at 50 °C without affecting the mechanical properties of the finished material. While this is an important observation, an even more important test is to determine if devices can be fabricated in this manner instead of waiting 24 hours for bonding to occur. Four devices were fabricated by curing the halves at room temperature for the first hour, preparing and bonding the two halves, then finishing the cure at 50 °C for three additional hours. All four devices were useable and withstood 10 mL/min like the 19.2% devices cured at

room temperature for 24 hours. This cuts the fabrication time for a device from 24 hours down to 4 hours or less, which means devices can be fabricated and used in the same day, and even faster fabrication times are likely possible if higher cure temperatures were used. The initial one-hour cure before removing the device halves from the mold and performing the bonding procedure could be done at elevated temperatures to decrease the time required, but the time savings would likely not offset the potential problems, such as uneven curing due to temperature variances and overshooting the optimal resin cure window.

The increase in bond strength with increasing functional group excesses observed in a previous study[76] is compelling evidence that suggests the TAMR adhesion mechanism is in fact covalent bonding between the complimentary functional groups on each surface, but changing the concentration of excess functional groups also changes other resin properties. Examples of extremely strong adhesion between surfaces without covalent bonding are a common phenomenon seen in adhesives like poly(vinyl acetate) glues. This type of adhesion involves many weak forces, such as van der Waals forces and hydrogen bonding, summing together to produce a high overall strength and is referred to as the adsorption theory of adhesion.[214] The adhesive strength of these systems is determined by factors such as the surface free energy, the modulus, and the wettability of the material. In TAMR, the two surfaces should have good contact, since they are chemically very similar and are bonded together at low modulus, and they have many opportunities to form hydrogen bonds and dipole-dipole interactions due to the prevalence of ester, amine, and hydroxyl groups in the system. In order to determine if the main adhesive mechanism is covalent bonding

or the sum of weak interactions, devices were fabricated using 1-1 19.2% DEA-AA TAMR for both halves instead of the excesses of complimentary functional groups. During device construction, the two resin halves adhered to each other, and leak testing showed that these 1-1 devices performed as well as the devices made using excess groups since each was able to withstand a slow rate of 10 mL/min without failing. The adhesion between the two 1-1 surfaces is largely due to the summation of weak forces, but some covalent bonding could be present since not all of the functional groups have reacted at 1 hour of curing.

Since none of the devices failed in the flow tests due to poor bonding, the devices were physically pulled apart to evaluate how well they had adhered. Two separate mechanisms of failure were observed in the devices: cohesive and adhesive failure. In devices that failed cohesively, the bond between the two layers could not be broken before the actual material began to fail. Adhesive failure occurred when the device halves could be separated cleanly without fracturing the bulk material. All of the devices made using excess functional groups failed in a cohesive manner while the 1-1 devices failed adhesively. Examples of the two failure types can be seen in Figure 3.15. The cohesive failure specimen shows fracturing where the resin broke in the middle of the channels, so there are channel components on both halves of the device, while the adhesive failure specimen separated cleanly and only has channel components on one side of the split. The 1-1 devices, likely bond together well enough for most microfluidic applications, but the excess functional group strategy is required to make the strongest devices. The cohesive failure of the excess-bonded devices confirms that the primary bonding mechanism between the two device haves is covalent bonds between thiol and

acrylate groups on the opposing device halves. Unlike PDMS, TAMR devices can be fabricated and bound together to achieve cohesive failure without the need for specialized equipment like a plasma generator.

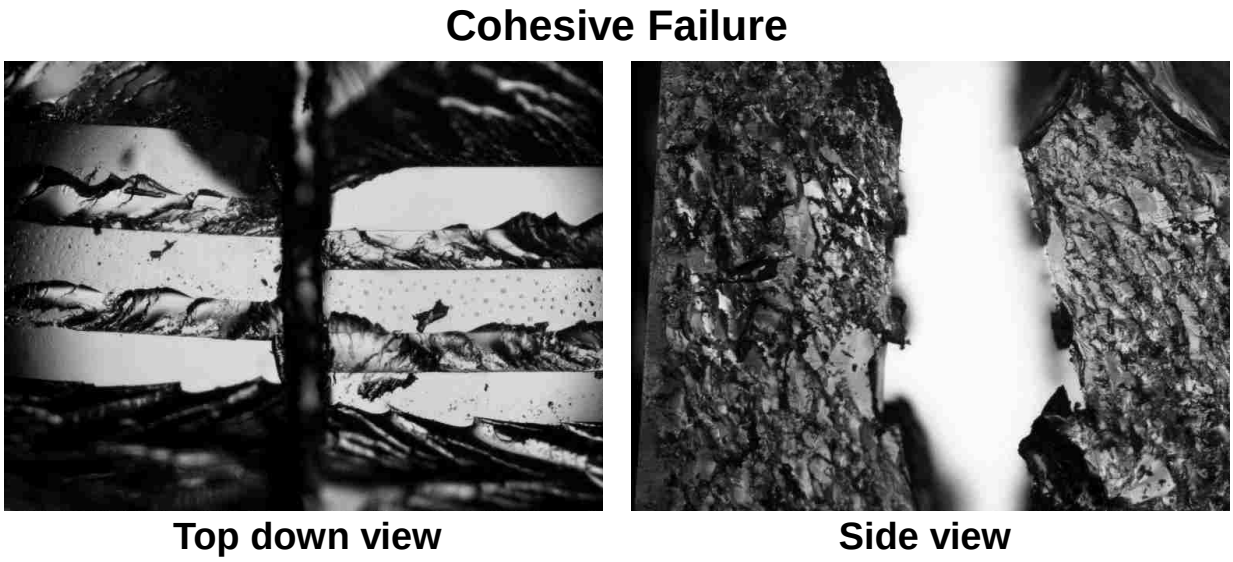

Figure 3.15 Microfluidic device failure modes

3.5.10 TAMR Surface Modification

Although a range of properties can be targeted by changing the TAMR formulation, selective modification of the surface of the resin would be advantageous. The surface of PDMS can be modified by exposing it to oxygen plasma then to a silane, which will covalently bond to the surface via and Si-O-Si bond. The chemical structure of the silane can be adjusted to achieve a range of surface properties and chemistries. Plasma treatment of the PDMS surface is also used to bond devices together and increase the hydrophilicity of the material. While surface modification of PDMS is possible, it requires an oxygen plasma generator, which is not a ubiquitous piece of lab equipment. Surface modification of TAMR should be possible by making use of excess functional groups incorporated into the resin to perform thiol-acrylate coupling reaction with a modifying monomer. For example, a TAMR sample made with excess thiol could be exposed to a fluorinated acrylate to produce a highly hydrophobic surface. Bounds et al. have previously attempted this technique, but they performed the surface modification procedure after curing the TAMR for 24 hours. While there is still an abundance of available functional groups in TAMR samples made with excess thiol or acrylate, even at full cure, they might not be readily accessible for modification. The surface reorientation process described earlier in Section 3.5.5 could account for why their modification procedure was unsuccessful if most of the functional group sites were oriented to the interior of the polymer. Other possibilities for the lack of surface functionalization observed at 24 hours of curing include the low mobility of the excess groups at full cure or air oxidation of the surface groups. The ability of TAMR surfaces to be modified with liquid monomers was evaluated by monitoring the water contact

angle change after exposure to both hydrophilic and hydrophobic compounds after one hour of curing at room temperature. The TAMR surface was also modified using oxygen plasma treatment in order to compare to PDMS.

Table 3.2 contains the results of the thiol-acrylate surface modification procedure. The 19.2% 40% ET samples were allowed to cure for one hour, and then they were immersed in either LA or PEGMEA with 1 wt% TEA for 1 hour. After washing the samples thoroughly with water and acetone, they were left to fully cure.

Table 3.2 Water Contact Angles of Modified 19.2% 40% ET TAMR

Modifying Acrylate	**PS Side Contact Angle**	**Air Side Contact Angle**
PEGMEA	43 ± 4°	45 ± 3°
-	60 ± 3°	62 ± 3°
LA	84 ± 5°	77 ± 3°

The water contact angle was reduced from 60° in a normal 19.2% 40% ET sample cured on PS to 43° for the PEGMEA modified sample, and raised to 84° in the LA sample which indicates that the modification procedure was successful. The PS side of the TAMR showed slightly better modification results for both the LA and PEGMEA likely due to oxidation at the air interface. The washing procedure should have been sufficient to remove any non-covalently bound acrylates, but further studies need to be performed to optimize the modification procedure and ensure the change in contact angle is due to the covalently bound modifying groups. This liquid modification strategy can be used to selectively modify individual microfluidic channels since TAMR devices capable of containing fluid can be manufactured at low cure times.

In order to determine if TAMR samples could be modified using oxygen plasma, samples of 19.2% 1-1 TAMR cured for 1 hour and fully cured PDMS were exposed to 5 minutes of plasma on the medium setting. Table 3.3 contains the water contact angles

of the samples exposed to oxygen plasma that were obtained within 20 minutes and after being stored at room temperature for 5 days.

Table 3.3 Oxygen plasma treatment of TAMR and PDMS

	19.2% 1-1 TAMR[a]	**PDMS**
Immediate	46 ± 6°	23 ± 7°
5 Day Storage	33 ± 5°	101 ± 4°
14 Day Storage	50 ± 8°	105 ± 1°

a. TAMR samples treated at 1 hour of curing at room temperature

The high uncertainties associated with these measured water contact angle values are due to several drops with much higher contact angles than the others. This could be due to an inconsistency in the plasma field since both the PDMS and TAMR samples were affected. Compared to unaltered samples, the water contact angle of TAMR was decreased by ~20° using plasma treatment, and although TAMR is not as responsive to plasma treatment as PDMS is, this could be an effective surface modification technique for TAMR. Over the 5-day storage period, the water contact angle of the PDMS samples increased by nearly 80°. This is due to the process of hydrophobic recovery where uncrosslinked PDMS oligomers migrate to the surface of the resin and raise the contact angle. The TAMR samples actually showed a decrease in contact angle over the 5-day storage period. This is likely due to the absorption of water at the hydrophilic surface or possibly surface reorganization where the polar ester, amine, and hydroxyl groups oriented towards the oxygen-rich surface. After 14 days of storage on the benchtop, PDMS continued to recover its hydrophobicity and the contact angle increased to 105°, but the TAMR sample also showed an increase in contact angle by rising to 50°. Why the contact angle increased between 5 and 14 days is unclear.

3.5.11 General TAMR Usage Observation

While performing all of the more detailed TAMR analysis experiment discussed above, several interesting observations were made that were not investigated further but still deserve mentioning. When making the AA, several interesting color changes were observed as the acrylate is initially clear, but when DEA is added, the mixture takes on a purple-brown color that fades over time into a yellow hue. One possible explanation is that the color comes from the inhibitor MEHQ since when put into solution at neutral pH it is clear but raising the pH with NaOH produces a dark red-brown color. The deprotonation of the acidic phenol group in MEHQ frees up a pair of electrons to resonate around the aromatic core, which changes the absorption properties of the molecule and produces the color change. In the AA synthesis, a strong enolate base is produced which could deprotonate the MEHQ and get the same effect. The color fades over time since as the reaction progresses, the enolate concentration drops. Efforts to observe this phenomenon by UV/Vis spectroscopy have been unsuccessful up to this point, but should be achievable.

Once it has been produced, the AA has been used successfully after 6 months, but long term storage stability has not been investigated. One interesting phenomenon observed when testing a 19.2% DEA-AA that was stored for ~20 months on the benchtop in a plastic jar was that a 1-1 sample made with TMPTMP gelled in ~5 minutes instead of the usual 18-20. Figure 3.16 shows example conversion versus time plots for freshly prepared 19.2% DEA-AA and a 19.2% DEA-AA that was stored for over a year when cured with TMPTMP at a 1-1 ratio at room temperature. It is evident that the faster gel time is, at least in part, due to an increase in the polymerization rate. This

increase in rate can be attributed to the absorption of water, which increases the polarity of the mixture and, as shown above, speeds the rate of the thiol-Michael addition. Therefore, for long-term storage, AA should either be kept in a well-sealed airtight container or stored under dry conditions to maintain its original properties.

Once cured, the long-term storage properties of TAMR vary by formulation. As discussed earlier, all TAMR samples will absorb water and cloud over time so dry storage is preferable. Yellowing of the resin is observed after several months of sitting on the benchtop, and this phenomenon can be accelerated by storing the samples at higher temperatures, where the samples eventually turn orange. This is most likely due to the oxidation of the bound amine, and many commercial adhesives and coatings made using amines have similar issues. Eventually, samples stored in the open atmosphere will develop a film on the surface. This is a commonly observed phenomenon in epoxy resins, called bloom or blush, that develops when amines react with carbon dioxide in the air to form ammonium bicarbonates, which absorb water and cause the greasy film.[215] Eventually, after 3-4 years of storage in the open air at room temperature, the TAMR will degrade back into a viscous gel due to the hydrolysis of the ester linkages prevalent throughout the matrix. The rate of the ester hydrolysis will increase with increasing amine content in the resin as well as with increasing water content. Based on all of these observations, the best way to store TAMR samples long-term would be under dry conditions and under inert atmosphere if yellowing is a concern.

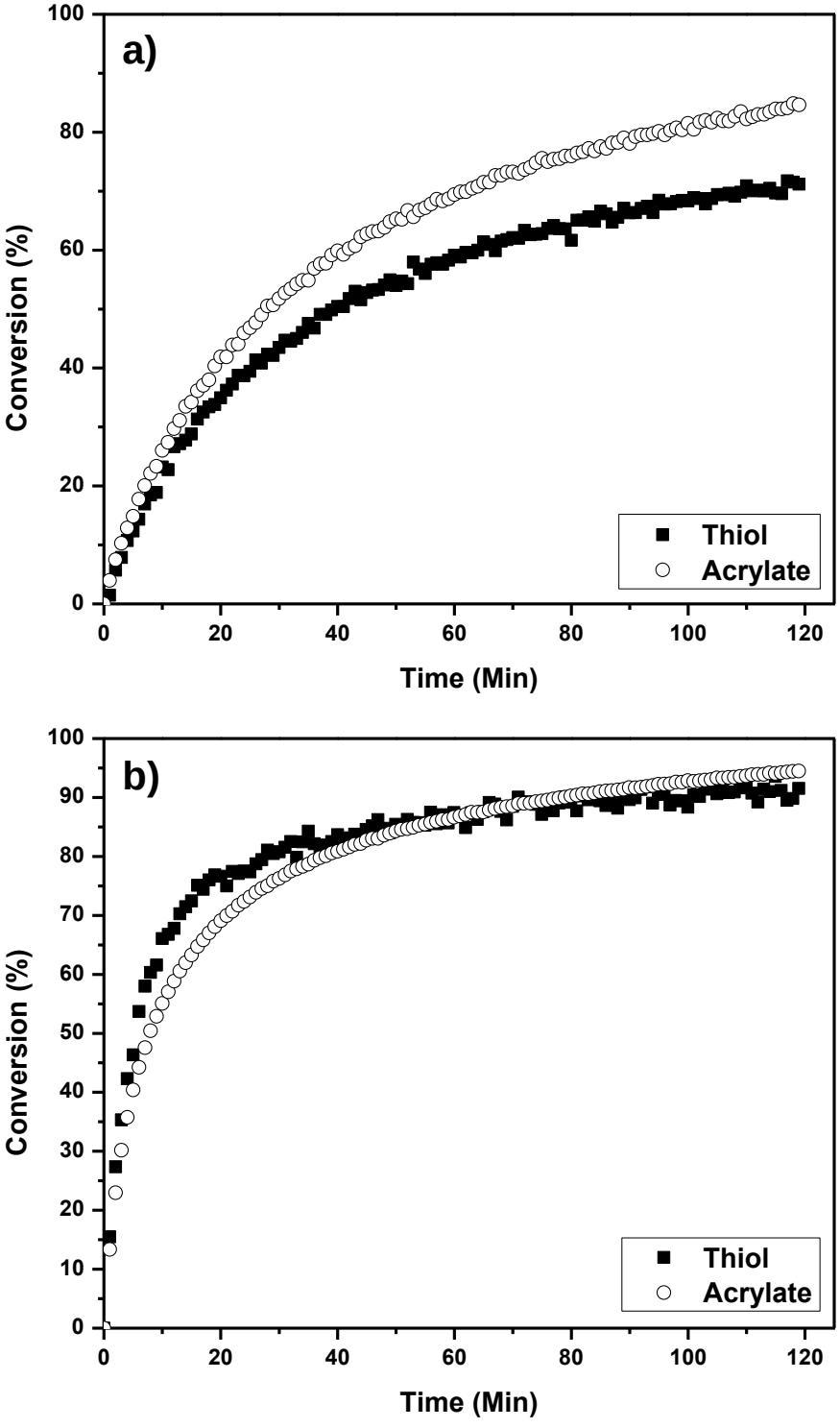

Figure 3.16 Conversion profiles for normal and aged 19.2% 1-1 TAMR

The ability to replicate small features (~50 μm or less) in TAMR has never been reported. Figure 3.17a shows the replication of small cell trapper arrays in 19.2% 1-1 TAMR which measure 60 x 35 μm. Obviously TAMR is able to replicate the features with high fidelity, but the uncropped image shown in Figure 3.17b illustrates one current problem with TAMR. When PDMS is used to replicate these features, it is put under vacuum for 30 minutes or more to remove bubbles and dissolved gasses after it has been mixed. Using 19.2% TAMR, the resin will gel in ~20 minutes, so putting it under vacuum for 30 minutes would be impossible. Altering the recipe by making a 2.9% DEA-AA raises the gel time to 1.5-2 hours, but even leaving it under vacuum until it gels after pouring it onto the master just raises the bubbles out of the features and into the bulk resin. This could be due to the increasing viscosity of TAMR while it is curing or to the solubility of gases in the resin, but this is one area that needs improvement before TAMR can be used in devices with small features.

The ease of use for a microfluidic material is one of the main factors researchers will consider before using a resin system. Both TAMR and PDMS have their strengths and weaknesses when it comes to ease of use. In terms of resin preparation, PDMS is bought as a two-part system with no synthesis required, and while making the AA is not difficult, it is an extra step not present with PDMS. One advantage of TAMR is that since the user is making the system, they have control over every aspect of the process. The mixing process is quite similar for both systems although PDMS is generally made in a set 10:1 ratio while TAMR recipes tend to be closer to 1:1, but it depends on the formulation. The PDMS base component is extremely viscous and cannot be pipetted easily while both TAMR components flow well.

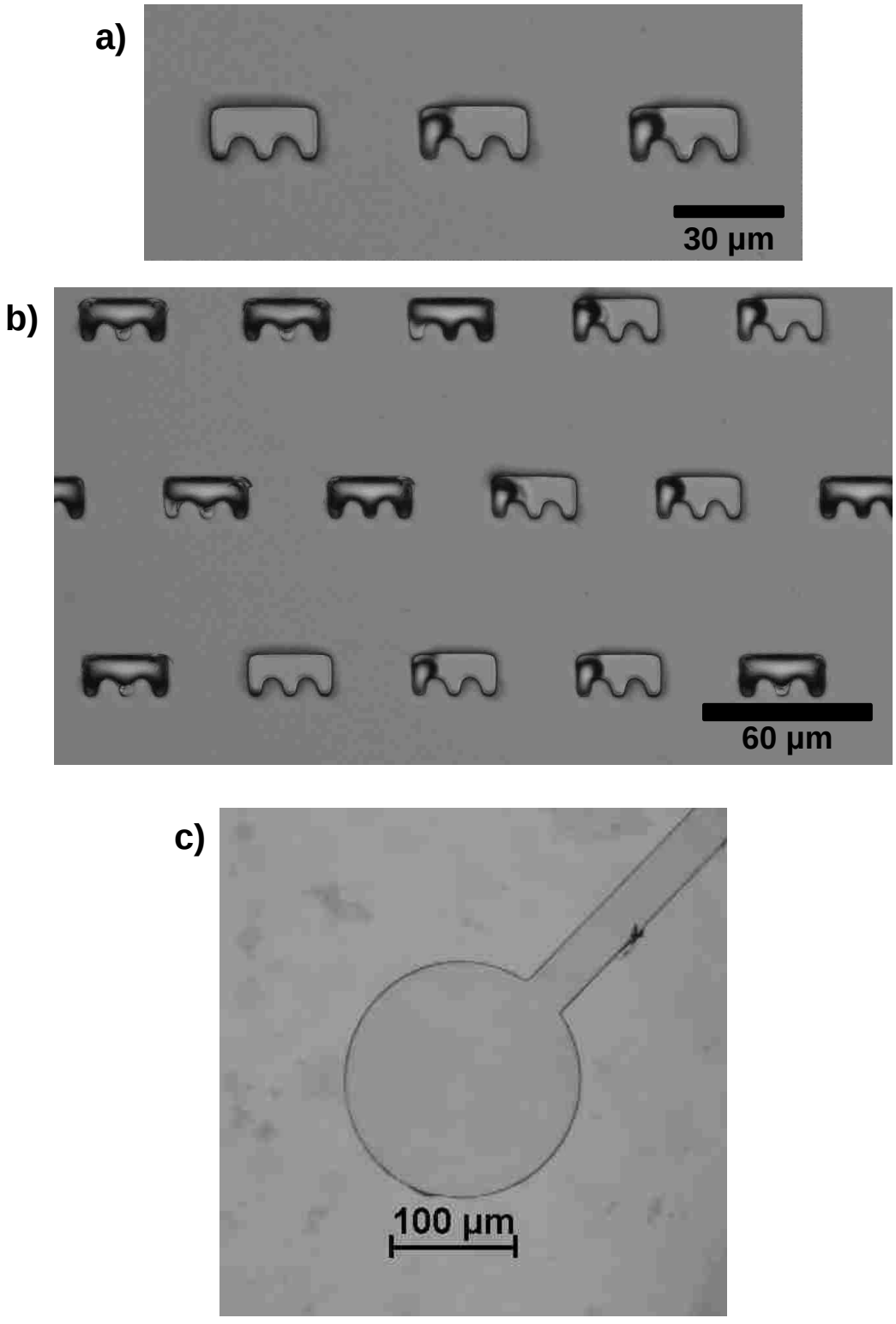

Figure 3.17 Replication of small microfluidics in TAMR a) cell trappers, b) cell trappers with bubbles, c) microfluidic channel and port

The resin curing procedure is where TAMR really shines since it can be cured at room temperature in 24 hours, while PDMS would take several days to cure. Both resins can be cured at elevated temperatures for faster results though. The device fabrication procedure highlights some of the biggest flaws in both PDMS and TAMR. In order to flow liquids through the microfluidic channels, holes need to be made at the ends of the channels so tubing can be connected. While in PDMS these holes can be punched out with a needle or biopsy punch, TAMR will crack under those conditions. In order to get holes in the TAMR pieces, they have to be drilled out, which in itself is not that bad until you consider the amount of dust that the drilling process produces. The drilling dust sticks to the TAMR and needs to be blown off with compressed gas or rinsed off. When the time comes to bond the two device halves together, one weakness of PDMS is exposed. In order to bond PDMS to itself or glass, a plasma generator is required to modify the surfaces, which must be put into contact immediately to stick together, but TAMR can be bonded to itself without any surface modification treatments. Once the holes have been produced, the tubing can be sealed using uncured PDMS or TAMR which is cured in place around the tubing. Overall, PDMS requires more time to cure the resin, but once it is cured, it can be stored for long periods before fabricating a device. TAMR cures quickly, but devices need to be put together after 1 hour of curing so the components cannot be stockpiled for bonding later. While TAMR has several drawbacks that need to be addressed, the advantages it has over PDMS in certain areas could make it a useful material in the field of microfluidics.

3.5.12 Conclusions

Several key properties of TAMR have been investigated and the performance of the resin has been evaluated. It has been shown that 19.2% 1-1 TAMR fully cures in ~10 hours at room, but it can be successfully cured at 50 °C in 3 hours. The hydrophilicity of the resin was determined for a variety of formulations and was found to depend on the resin composition as well as the curing surface. This property could potentially be exploited to modulate the water contact angle of cured TAMR by as much as 30° without changing the resin formulation. The absorption of water by cured TAMR samples was quantified by mass, and it was determined that the ET samples absorbed water the fastest, followed by EA, then 1-1 samples. Formulations with lower amine content absorb water more slowly and do not cloud as quickly compared to higher amine content resins. Degradation of TAMR was observed after immersion in water for extended periods of time, and the rate of degradation was shown to parallel amine content. Disc-shaped droplets were observed in the resin, which were attributed to the accumulation of water around the highly polar, protonated amine groups in the resin. The absorption of a variety of solvents by TAMR was quantified by changes in the size of resin samples. Acetone was able to swell TAMR most significantly, but overall TAMR performed better than PDMs due to its high crosslink density. The elastic modulus of several TAMR samples was determined at both low and high cure. On average, TAMR samples tripled in modulus between 1 hour and 24 hours curing, and samples made using lower amine concentrations were found to be stronger due to the higher crosslink density. The TAMR bonding procedure was refined by determining that weight was not necessary to get a strong bond between the two device halves. The bonding

mechanism was confirmed to be the covalent bonding of thiol and acrylate groups across the resin pieces, but devices of adequate strength can be fabricated using only 1-1 resin. Finally, several general observations were made about the use of TAMR including the storage stability, problems with bubbles, and ease of use. While more characterization remains to be done, this information should provide researchers with enough information to make a more informed decision about using TAMR in future microfluidic applications.

3.6 Fluorescence-Based Detection of Pathogens

The following section has been adapted from Ref. 77 with permission from The Royal Society of Chemistry.

3.6.1 Introduction

The detection and identification of disease causing organisms is of crucial importance to world health. Whether testing for *E. coli* in a meat packing plant or tuberculosis in the developing world, the timely discovery of pathogens can help medical personnel treat infected individuals quickly or prevent a devastating outbreak. The ability to test for a variety of organisms on-site, using a low cost and disposable point-of-care (POC) diagnostic device would be of great use to mankind. POC testing is not a new concept, and several examples of POC tests include at home pregnancy tests or blood glucose monitors. POC diagnostic devices give rapid results since they do not require processing by an off-site laboratory, and ideally, they can be used by individuals with minimal training. Over the past few decades, there has been a push to develop POC devices to detect disease causing organisms,[216-222] and despite many

advances, a small, disposable, and low-cost device capable of detecting a variety of pathogens remains a largely unrealized goal.[223-224]

Many of the most successful POC diagnostic devices capable of detecting pathogens are based on microfluidics.[225-227] These two areas, microfluidics and POC diagnostics, share many of the same goals, including the miniaturization of complex components, the reduction of sample volume, and the production of low-cost and disposable devices. One common way to perform POC diagnostics on a microfluidic device is an enzyme-linked immunosorbent assay (ELISA), which has many variations. The concept of an ELISA test is to use the specific relationship between antigens and antibodies to trap and detect pathogens or their components. First, an antibody or antigen is bound to the wall of the microfluidic channel. This bound biomolecule will capture any corresponding groups present in the solutions flowed through the channel. Next, a blocking compound is used to cover the channel walls where no compound is attached to prevent non-specific binding between the test compound and the microfluidic device material. Commonly used blocking compounds are bovine serum albumin (BSA) and casein, and they are generally put into solution and flowed through the channel. Finally, the analyte solution is put through the channel, and if any compounds specific to the bound biomolecule are present, they will attach. After the attachment step, various means of detecting the bound analyte exist, but most use fluorescence.

One way to detect a pathogen is to capture the whole organism. This can be accomplished by attaching an antibody specific to that organism onto the channel surface. The antibody will specifically bind to the antigens present on the surface of the

pathogen and capture it for detection. Alternative methods for confirming the presence of specific pathogens detect just the structural components of the organism. These methods do not require the whole cell, and since one organism contains a large number of the compounds of interest, these methods can typically confirm the presence of the organism at lower concentrations. One example are gram-negative bacteria, such as *E. coli*, which have lipopolysaccharides (LPSs) on their surface, which consist of a polysaccharide chain that protrudes from the cell and a lipid segment that anchors the structure into the cell membrane. *E. coli* serotypes are categorized and named by their LPS structures. For example *E. coli* O157:H7 is a pathogenic strain that frequently causes outbreaks in the United States.[228] The number and letter combinations listed after *E. coli* designate the serotype, or subgroups of the bacterium. The O in the serotype designation refers to the O-antigen, which is the end polysaccharide portion of the LPS. The H refers to the H-antigen, which characterizes the flagellum of the bacterium. The O-antigen has been used to classify *E coli.* serotypes since the 1940s, and there are ~180 O-antigen and ~50 H-antigen designations in use currently.[229] These LPSs can be captured via interactions with a compound like polymyxin B (PMB), which is an antibiotic peptide.[230-233]

Similarly to the field of microfluidics as a whole, many of the POC systems developed using microfluidics are fabricated with PDMS, which can be attributed to its relatively low cost, optical clarity, gas permeability, chemical inertness, ability to replicate submicron features, and the ability to bond it to glass or itself using a surface modification process.[148, 234-235] Despite these advantages, PDMS has several limitations that hinder the development of POC diagnostic devices targeted at

pathogens. First, as discussed in section 3.5.5, PDMS has a hydrophobic surface which can cause biomolecules, such as enzymes or antibodies, to denature.[236-237] In their natural aqueous environment, proteins are folded so that the hydrophobic segments of their amino acid chains are oriented inward, and the hydrophilic segments are on the exterior. When put in contact with a hydrophobic surface, like PDMS, the protein can change its conformation so that the once buried hydrophobic portions are exposed to the surface. This change in morphology can cause the loss of protein activity, in the case of an enzyme, or a loss of binding specificity for a particular antigen in the case of an antibody. Although PDMS has a hydrophobic surface after curing, the surface can be modified to become more hydrophilic. The most common technique to accomplish this involves treatment of the surface with oxygen plasma, which is initially effective, but the hydrophilic surface in only transient as it quickly reorganizes to become hydrophobic again.[238-239] Other surface modification techniques have been proposed and investigated with varying degrees of success, but they are generally more complex and less widely adopted compared to oxygen plasma treatment.[240] Second, the typically unreactive surface of PDMS caused by its relatively simple chemical structure hinders the attachment of bio-sensing receptors. As seen in Scheme 3.2, PDMS has a backbone composed of alternating silicon and oxygen atoms with methyl groups at each available position of the silicon. This lack of functional groups prevents the attachment of biomolecules using traditional techniques. The PDMS surface must be modified in order to facilitate attachment of the biomolecule, which is often a complicated process.[241-243] Last, traditional blocking methods used in other microfluidic devices are ineffective in PDMS.[244] Other techniques involving surface modification of

the PDMS have been developed to combat this, but none are as simple as traditional blocking using casein or bovine serum albumin.[245-247]

3.6.2 TAMR POC Diagnostic Device Prototype Overview

The POC device prototype presented here was constructed using TAMR and was designed to detect *E. coli* by two different methods. Scheme 3.4 illustrates detection strategy one where whole *E. coli* O157:H7 bacteria were captured using an antibody bound to the TAMR surface.

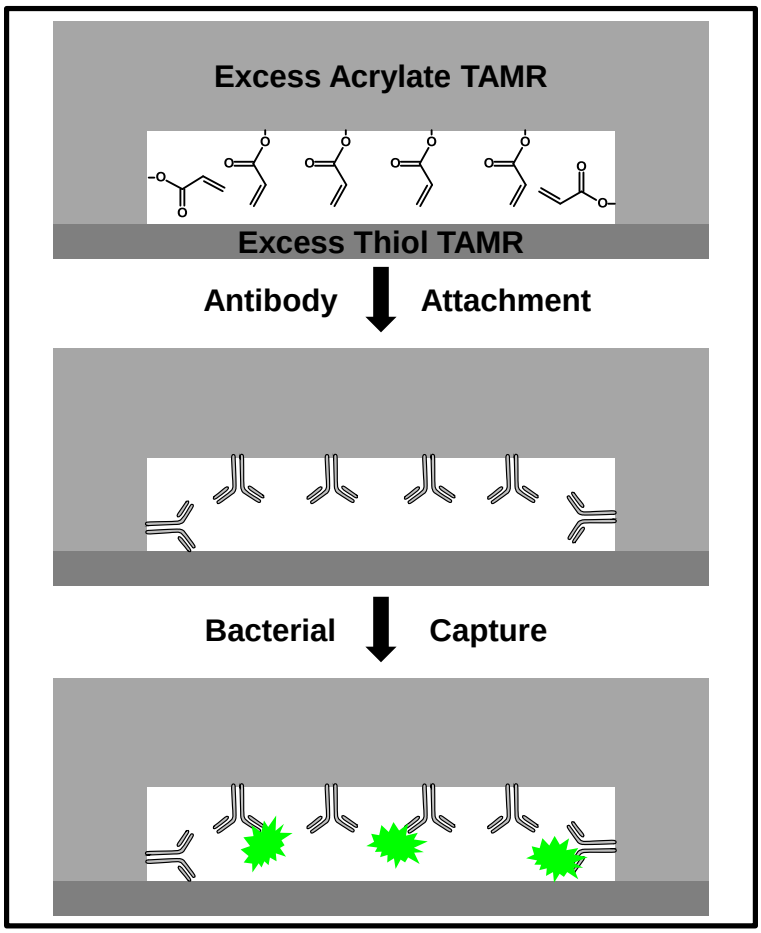

Scheme 3.4 Bacterial capture in a TAMR microfluidic device

Bonding was achieved through Michael addition reactions between amines or thiols present as side groups in the peptide chain of the antibody and the excess acrylate groups present on the microfluidic channel surface. Detection of the bacteria

was confirmed by modifying them with a fluorophore then monitoring the increase in fluorescence in the channel. In the second detection strategy, the presence of *E. coli* O55:B5 was confirmed by capturing the LPSs associated with that organism. PMB was attached to the microfluidic channel surface via a Michael addition, and fluorescently labeled LPSs were captured and detected using fluorescence.

3.6.3 Materials and Methods

Materials

PETA stabilized with 300-400 ppm MEHQ was obtained from Alfa Aesar and TMPTMP was purchased from Evans Chemetics LP. DEA ≥99.5% and casein blocking buffer were obtained from Sigma Aldrich. PDMS was prepared using a Sylgard® 184 silicone elastomer kit obtained from Elsworth Adhesives. Both phosphate-buffered solution (PBS) and PBS with Tween 20 (PBS-T20) were purchased from Amresco Inc in powdered form. *E. coli O157:H7* antibodies were obtained from Kirkegaard & Perry Laboratories both labeled with fluorescein isothiocyanate (FITC) and unlabeled. *E. coli O55:B5* lipopolysaccharides labeled with Alexa Fluor® 568 dye and polymyxin B labeled with BODIPY® FL were purchased from Life Technologies. With the exception of the powdered PBS and PBS-T20, which were reconstituted into working solutions, all reagents were used as received.

Microfluidic Device Manufacture

First, 19.2% DEA-AA was made according to the procedure described previously in section 3.4. To make the flat, bottom side of the device, the 19.2% DEA-AA was mixed with enough TMPTMP to give a mixture containing 40% excess thiol groups. For the top side of the device containing the microfluidic channels, 19.2% DEA-AA was

mixed with enough TMPTMP to yield a mixture containing 40% excess acrylate groups. Both compositions were stirred thoroughly, to ensure a homogeneous mixture, and then centrifuged at ~5,000 rpm for 3 minutes to remove bubbles introduced during the mixing process. The flat bottom half of the device was fabricated by curing the 40% ET resin in a polystyrene Petri dish. The microfluidic channels were introduced into the top half of the device by pouring the 40% EA resin over a positive master machined out of PMMA and allowing it to cure. The microfluidic channels were straight, rectangular channels with circular inlet and outlet ports at each end. Both samples were allowed to cure for 1 hour at room temperature before they were removed from their respective surfaces. After removal, holes were drilled at each end of the channels incorporated into the top half of the device using a Dremel press and a 1/16" bit. The TAMR slab was rinsed with ethanol and blown dry with nitrogen to remove any residue left behind from the drilling process. The final microfluidic device was constructed by bringing the top and bottom halves into contact with each other. Air bubbles between the two halves were pressed out by hand to ensure a good seal, and the device was left to fully cure for 24 hours under a load of ~1.4 kg/in^2.

PDMS Preparation

PDMS was prepared by mixing the elastomer base with the curing agent in a 10:1 ratio by weight. The two components were stirred well, poured into a polystyrene Petri dish, degassed at 24 in Hg for 30 minutes, and finally cured on a hot plate for 4 hours at 55 °C.

Fluorescent Labeling of *E. coli* O157:H7

A live culture of *E. coli* O157:H7 was prepared by inoculating Luria-Bertani broth for 12 hours at 37 °C. At 12 hours, agar plating of the culture showed an average concentration of 10^9 colony-forming units per mL (cfu/mL). To label the bacteria, the cells were washed twice with PBS by centrifuging 1 mL of the culture at 12,000 rpm for 2 minutes, replacing 0.9 mL of the supernatant with PBS, and re-suspending the bacterial pellet by vortex mixing. The fluorescent dye, TAMRA-SE (2 µL, 5 mg/mL), was mixed with the washed culture and allowed to incubate for 30 minutes at 37 °C. The previously described washing procedure was repeated four times to remove any excess dye.

Functionalization of the Microfluidic Channel

Tubing with an outside diameter of 1/16 inch was pretreated with casein blocking agent for 1 hour and rinsed with PBS prior to use. One end of the tubing was inserted into the holes drilled into the microfluidic device, and the other end was attached to a syringe pump. The microfluidic channels were washed with 1 mL of deionized water then filled with a 50 µg/mL antibody solution or a 100 µg/mL PMB solution. The device was incubated for 16 hours at 4 °C and then washed with 2 mL of PBS-T20 followed by 1 mL of PBS at a rate of 10 µL/min. The channels were then blocked by filling them with casein blocking agent and incubating for 1 hour at room temperature. The channel was washed using PBS-T20 and PBS in the same manner described above.

Bacterial Capture

Solutions of TAMRA-SE labeled *E. coli* O157:H7 were made at 10^5, 10^6, and 10^7 cfu/mL, and 1 mL of each was pumped through a channel functionalized with antibody at 10 µL/min. The channel was then rinsed with 3 mL of PBS at 10 µL/min.

LPS Capture

Solutions of *E. coli* O55:B5 LPS were prepared at both 100 µg/mL and 1 µg/mL. One mL of each solution was pumped at 10 µL/min through a channel functionalized with PMB. The channel was then rinsed with 3 mL of PBS at 10 µL/min.

PDMS and TAMR Fluorescence

PDMS and a TAMR device were prepared as above and placed on a fluorescent microscope. The focus was set to the upper surface of the material being tested, and images were taken using a variety of different fluorescence filter sets at five different locations across the material. The average intensity of each image was calculated using ImageJ.

Fluorescence Measurements

Fluorescence intensity was used to track changes in the microfluidic channel over the course of the experiments. The fluorescence intensity from a piece of the TAMR device with no channel was used as an internal standard for each data point. The difference between the fluorescence intensity obtained in the channel and the background intensity was determined. This process was repeated five times per sample, the results averaged, and the standard deviation calculated. The average fluorescence intensity obtained was normalized in order to make the data more readable.

3.6.4 Background Fluorescence in TAMR and PDMS

In order for TAMR to be used in any fluorescence-based microfluidic assays, the background fluorescence of the resin needs to be minimal for a variety of fluorescence filter sets. The fluorescent response obtained from TAMR was compared to PDMS, a widely used microfluidic material, for the 4',6-diamidino-2-phenylindole (DAPI), FITC, tetramethylrhodamine isothiocyanate (TRITC), Texas Red, and Cy5 filter sets and the results displayed in Figure 3.18.

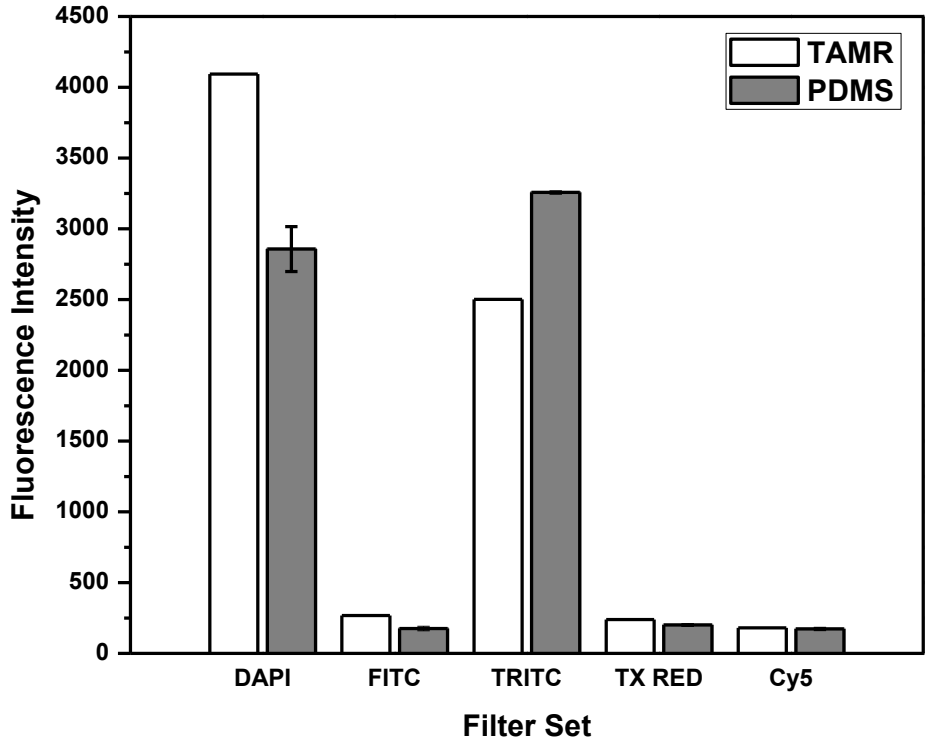

Figure 3.18 Background fluorescence in TAMR and PDMS

Both TAMR and PDMS had similarly minimal fluorescence for the FITC, Texas Red, and Cy5 filter sets. For the TRITC filter PDMS had a significantly higher fluorescence intensity than TAMR, while for DAPI, TAMR was more intensely fluorescent than PDMS. Both materials fluoresced more intensely for DAPI and TRITC

than for FITC, Texas Red, or Cy5. Based on this data, TAMR should perform similarly to PDMS in fluorescence-based microfluidic assays.

3.6.5 Specific Detection of *E. coli* O157:H7 Using Antibodies

The attachment of anti-*E. coli* O157:H7 to the channel surface of the TAMR microfluidic device was determined by functionalizing one channel with fluorescently-labeled antibody according to the procedure described above and comparing it to a control channel with only the casein blocking agent. Figure 3.19 shows the fluorescence intensity of the control and functionalized channels as a function of rinsing time with PBS-T20 at 10 µL/min.

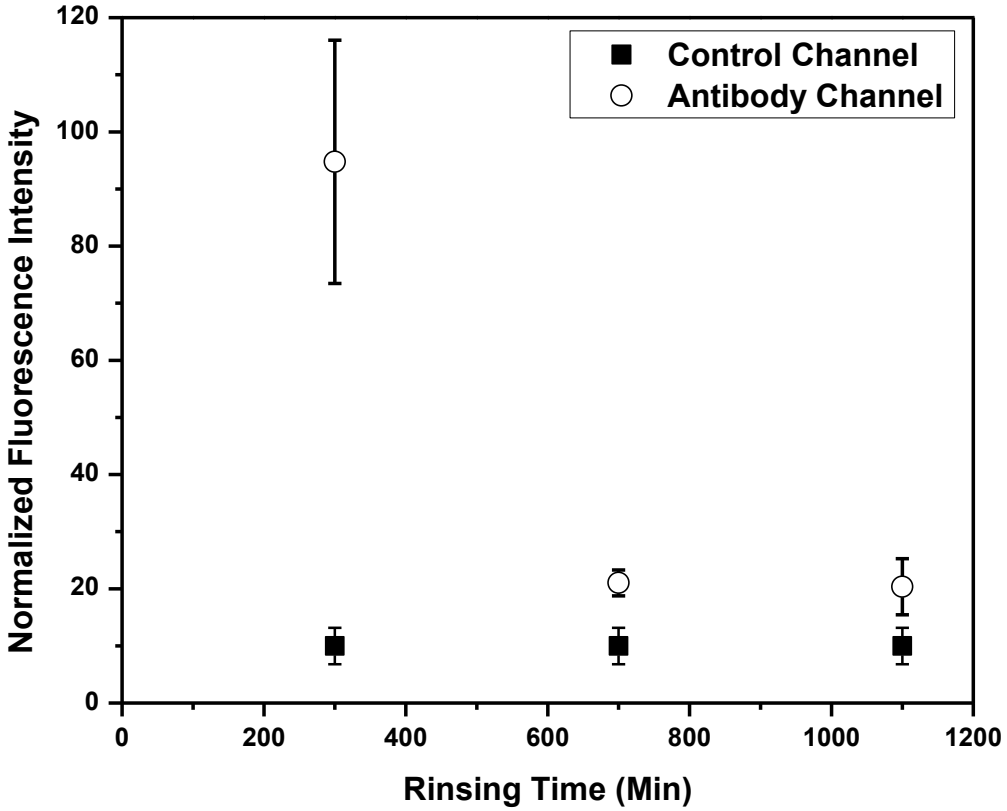

Figure 3.19 Antibody attachment to the TAMR surface

At five hours of rinse time, the fluorescence intensity of the antibody-functionalized channel is ~10 times that of the control channel. However, as rinsing

time increases, the fluorescence from the functionalized channel decreases significantly. This indicates that many of the antibodies were not covalently bound to the channel surface. Despite this, even after 18 hours of rinsing, the functionalized channel maintained higher fluorescence intensity than the control channel, which indicates that a portion of the fluorescently labeled antibody was covalently linked to the TAMR surface or at least strongly attached.

Next, the ability of casein to block the non-specific binding of bacteria to the channel surface was determined. Figure 3.20 shows the fluorescence intensity for the as prepared channel, the channel after casein blocking, and the channel after exposure to 10^5 and 10^7 cfu/mL of fluorescently labeled *E. coli* O157:H7.

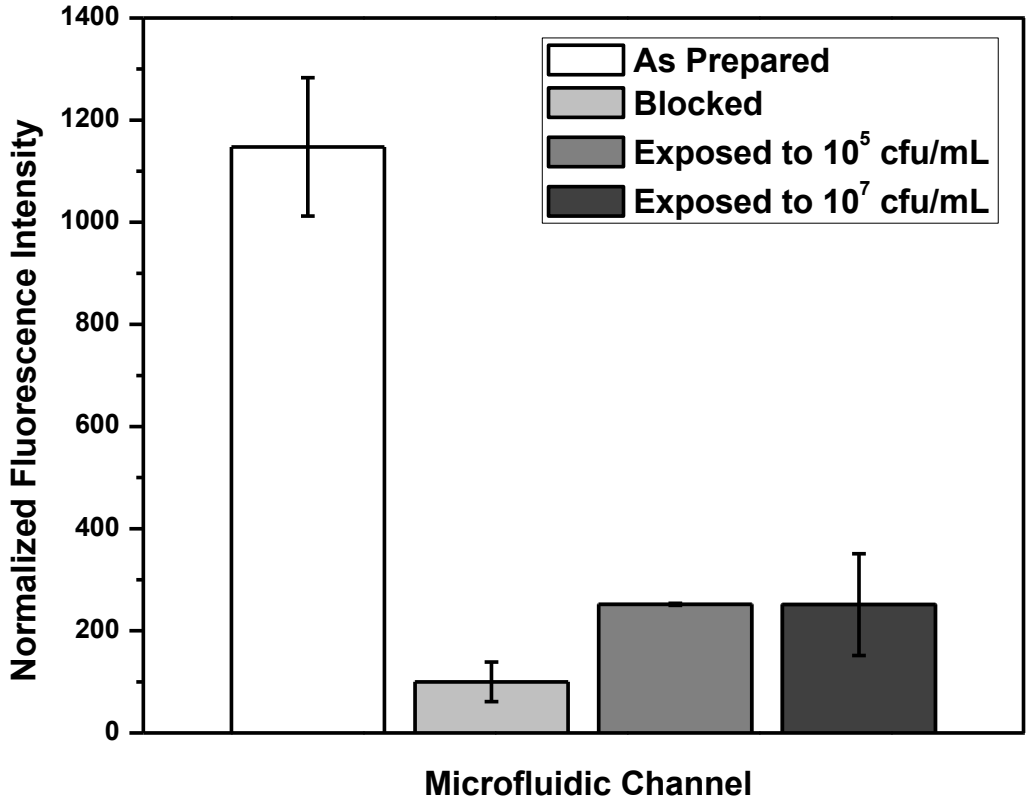

Figure 3.20 Blocking non-specific binding of bacteria with casein

Blocking the TAMR channel with casein led to a significant drop in the background fluorescence of the resin, which is likely due to the casein absorbing the fluorescence excitation light or the light emitted from the TAMR. Upon exposure to the solution containing 10^5 cfu/mL of *E. coli*, the fluorescence signal increased due to non-specific binding of the bacteria to the blocked channel walls. Exposing the channel to a higher concentration of bacteria (10^7 cfu/mL) showed no increased signal, which indicates that the non-specific binding sites were saturated.

The specific binding of fluorescently labeled *E. coli* O157:H7 to antibodies attached to the surface of the microfluidic channel was assessed by flowing solutions of increasing bacterial concentration through the channel and monitoring the fluorescence. As shown in Figure 3.21, as the bacterial concentration was increased from 10^5 to 10^6 to 10^7 cfu/mL, there was a corresponding stepwise increase in the fluorescence signal from the fluorophore used to label the bacteria. This indicates that the antibodies bound to the channel surface successfully captured bacterial cells because, as shown in the previous figure, the nonspecific bonding sites were saturated at 10^5 cfu/mL and showed no increase in fluorescence with increasing bacterial concentration. The high standard deviation associated with the fluorescence intensity for the 10^7 cfu/mL solution is due to the accumulation of bacteria captured near the channel inlet that lead to a fluorescence gradient along the channel when the data was collected.

3.6.6 Detection of *E. coli* O55:B5 Lipopolysaccharides Using Polymyxin B

The viability of an alternative method to whole cell capture using antibodies was tested which relies on the capture of the LPSs associated with a bacterium using an antimicrobial peptide attached to the microfluidic channel surface.

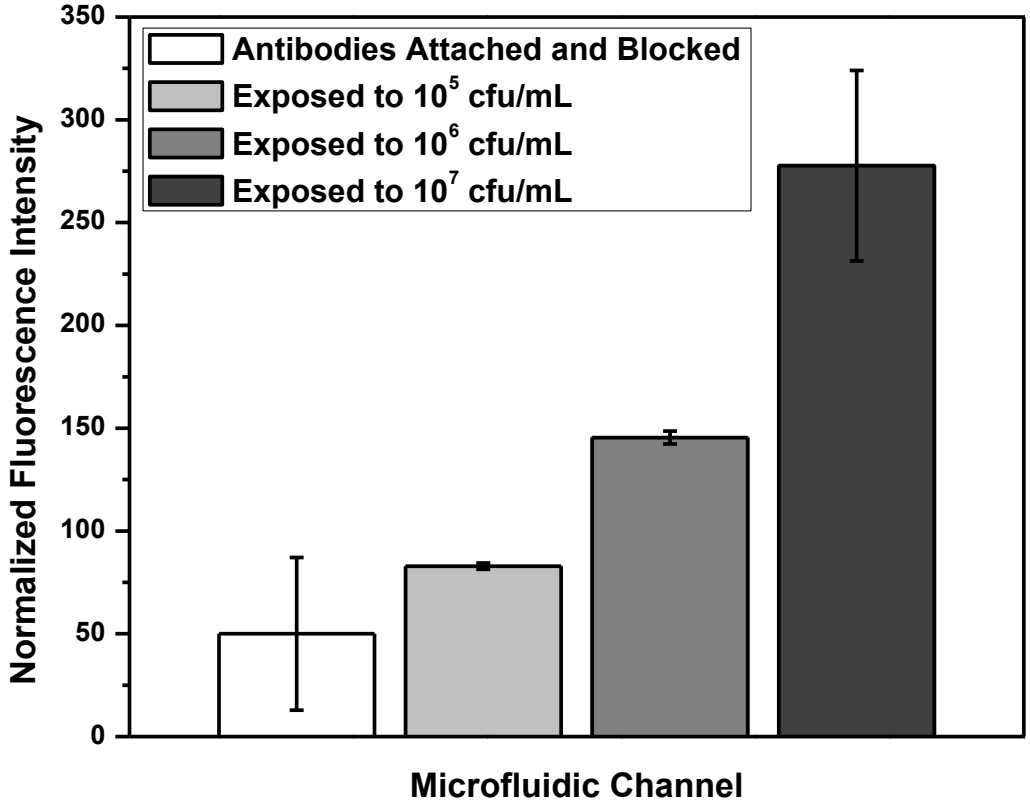

Figure 3.21 *E. coli* capture in the TAMR device

The first step was to evaluate the performance of casein as a blocking agent against the non-specific binding of LPSs. Figure 3.22 shows the fluorescence signal obtained from the bare channel, the channel after casein blocking, and the blocked channel after exposure to a 1 µg/mL solution of fluorescently-labeled *E. coli* O55:B5 LPS, all using the Texas Red filter set.

As seen previously, blocking the channel with casein led to a significant drop in fluorescence. Exposure of the casein-blocked channel to the LPS solution gave a slight increase in signal due to a small amount of the labeled LPS non-specifically binding to the channel surface. These results indicate that casein can be used to block the majority of non-specific LPS binding in the TAMR device. Attachment of PMB to the

channel surface was confirmed by the increase in fluorescence signal obtained from performing the functionalization procedure using PMB labeled with FITC.

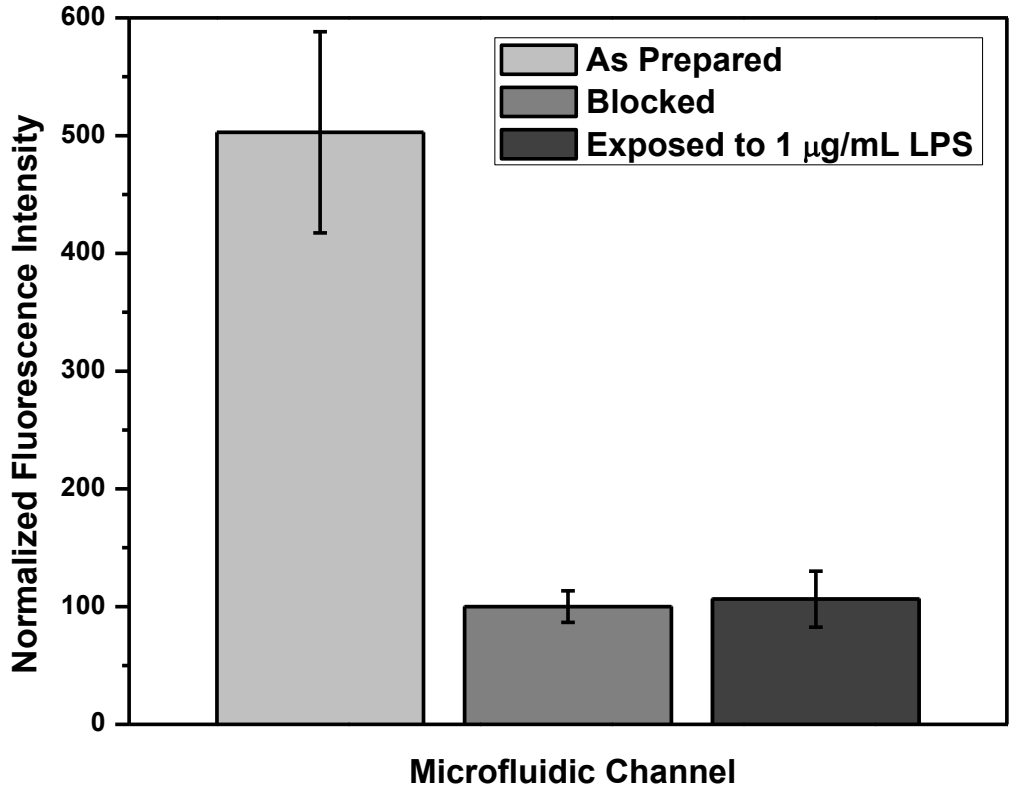

Figure 3.22 Blocking the non-specific binding of LPS with casein

The capture of *E. coli* O55:B5 LPSs using the PMB-functionalized channel was monitored using the Texas Red filter set, and the results are displayed in Figure 3.23. After exposing the channel to a 1 μg/mL solution of labeled LPS, there was a dramatic increase in the fluorescence, and flowing through a 100 μg/mL solution showed a further increase in signal. This indicates that the LPSs were successfully trapped using the PMB attached to the channel surface. The increased error for the more concentrated LPS solution is again due to a fluorescence gradient starting at the channel inlet.

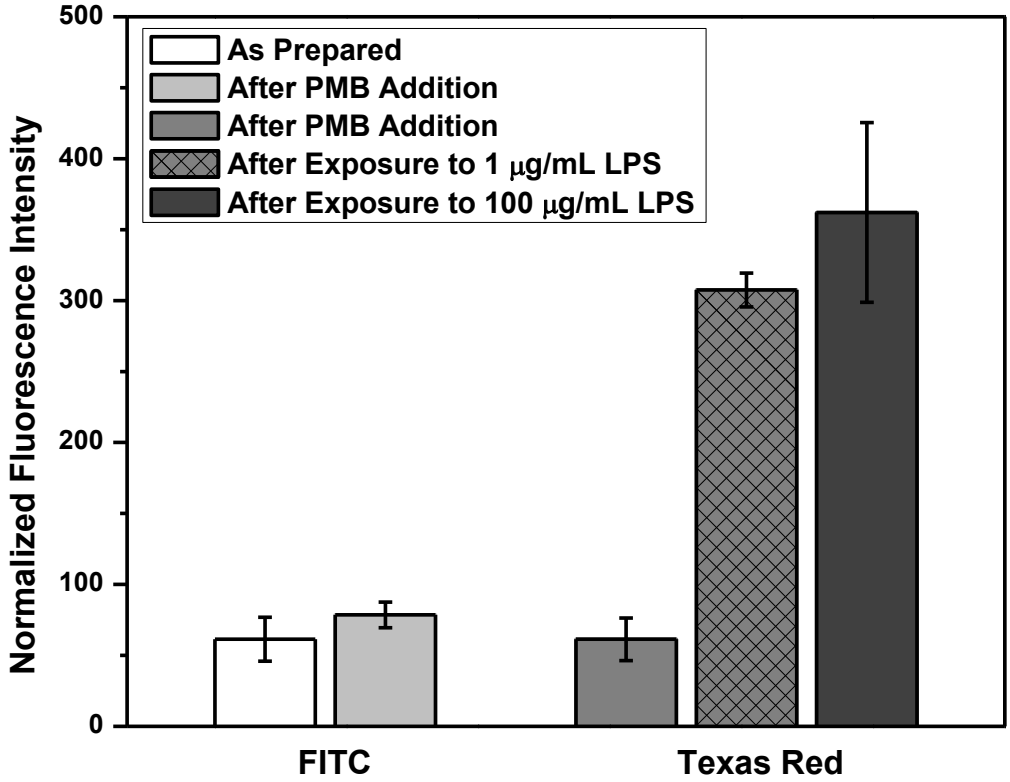

Figure 3.23 *E coli* LPS capture in the TAMR device

3.6.7 Conclusions

These examples demonstrate that TAMR can be used to construct working microfluidic devices using soft lithography techniques. The fluorescent response of the resin was determined using a variety of different filter sets commonly used by researchers, and the results were comparable to PDMS. Casein was found to be an effective blocking agent that not only suppressed the non-specific binding of bacterial cells but also reduced the background fluorescence signal from the resin during assays. The hydrophilic and functional group rich surface of TAMR allowed for the successful attachment of proteins in one step. While many of the antibodies were non-covalently bound to the channel surface, the presence of a detectable signal even after 18 hours of rinsing indicates some were bound to the resin walls. *E. coli* O157:H7 was successfully detected down to 10^5 cfu/mL using an antibody assay, and the presence of *E. coli*

O55:B5 LPSs were confirmed down to 1 μg/mL using PMB. Further optimization of the procedure and signal amplification techniques could be used to significantly decrease the limits of detection presented here, but these results confirm that TAMR can be utilized for the construction of microfluidic device based biological assays.

3.7 A Gradient Generating Microfluidic Device

3.7.1 Introduction

Algal blooms are characterized by a rapid increase in algae population and proliferation in either freshwater or marine ecosystems. Although many of these events pose no threat to humans or aquatic organisms, certain species of algae will produce harmful algal blooms (HABs) that can greatly affect the environment due to the production of toxins or simply through the effects of their extreme biomass.[248] Humans can be affected by HABs by ingesting foods contaminated with algae toxin, direct contact with water where the toxin is present, or through breathing aerosolized toxins. Some examples of the effects of algae toxins are neurotoxic shellfish poisoning, which is caused by brevetoxins, paralytic shellfish poisoning which is caused by saxitoxins, and amnesic shellfish poisoning caused by domoic acid.[249] One thing that makes these toxins so harmful is the absence of known antidotes to these compounds. In addition to physically harming people, HABs can also impact the economy through fish kills and seafood contamination as well as destabilize ecosystems through the effect of toxins and the depletion of oxygen from the water during the bacterial degradation of algal biomass.[250]

Algal blooms can occur naturally, and they have been reported for centuries, but unfortunately, it is widely agreed that HABs have grown more frequent in recent

years.[250-253] Humans have directly impacted the increase in HABs through the introduction of nitrogen and phosphorus into the environment from the use of fertilizers. These excess nutrients, along with climate change, have caused HABs to occur more frequently and last longer.[251-252] Detecting, identifying, and forecasting HABs is complicated due to the large number of variables that influence the formation of these events. Factors such as nutrient concentration, water temperature, water salinity, pH, dissolved oxygen, and light levels all play a role in the formation and longevity of HABs. In order to these variables systematically, further experimentation needs to be conducted in carefully controlled laboratory settings.

One technology that maximizes control over experimental conditions and throughput while minimizing reagent use is microfluidics. This relatively new field of study has been used to study a variety of biological systems, and algal growth kinetics[254] and oil production screening[255] studies have already been performed using microfluidic systems. One example of an algae behavior that is important to understand in order to predict and model HABs is chemotaxis, or the movement of the cells in response to chemical cues. It is crucial to understand what types of nutrients and what concentration will draw in certain species of algae. Microfluidic devices have already been developed to study chemotaxis in bacterial systems using devices that generate chemical gradients.[256-258] The most important aspect of these devices is that the channel where the algae are located must be flow-free so the cells are free to respond to the chemical gradient.

One design for these devices uses a PDMS upper portion, that contains the microfluidic channels, and a lower portion comprised of a hydrogel, such as agarose,

through which the chemical gradient is established via diffusion. The center channel of the device contains the algae and is maintained in a flow-free state, while the gradient is established using the outside channels. One channel acts as the nutrient source and contains a nutrient-rich solution while the other channel serves as a sink and contains a buffer solution with no nutrients. The nutrient will diffuse into the hydrogel layer of the device and towards the sink channel, which establishes a linear nutrient concentration gradient across the center channel of the device. The algae in the center channel are monitored to determine whether they respond to the chemical stimulus by tracking their movements.

One of the problems with gradient-generating microfluidic devices constructed using the two-layer PDMS and agarose design is that a fluid tight seal is difficult to establish between the two surfaces. One method is to use an external support structure to clamp the hydrogel and PDMs layers together. This can produce a working device, but the system is quite sensitive to the pressure applied by the support since too much pressure will force the hydrogel into the microfluidic channels while too little pressure will give a leaking device. A device where the rigid microfluidic layer could bond to the hydrogel without external support would make fabrication much easier and improve device reproducibility and reliability. Using thiol-acrylate chemistry, a gradient-generating microfluidic device was constructed by coupling TAMR to a thiol-acrylate based hydrogel without using external support structure. Scheme 3.5 displays a schematic of how the device is set up and an actual thiol-acrylate device with red dye in the channels to improve visibility.

a)

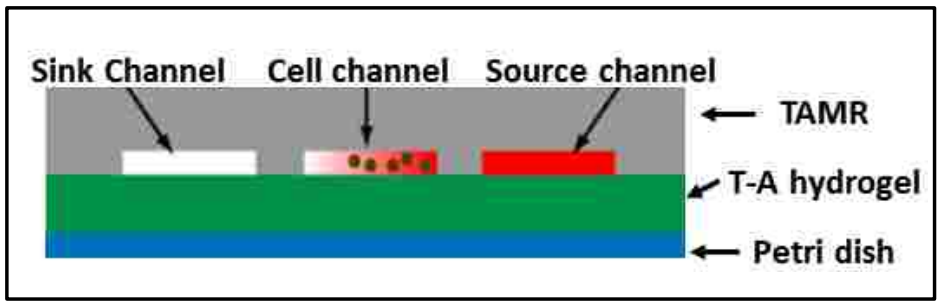

b)

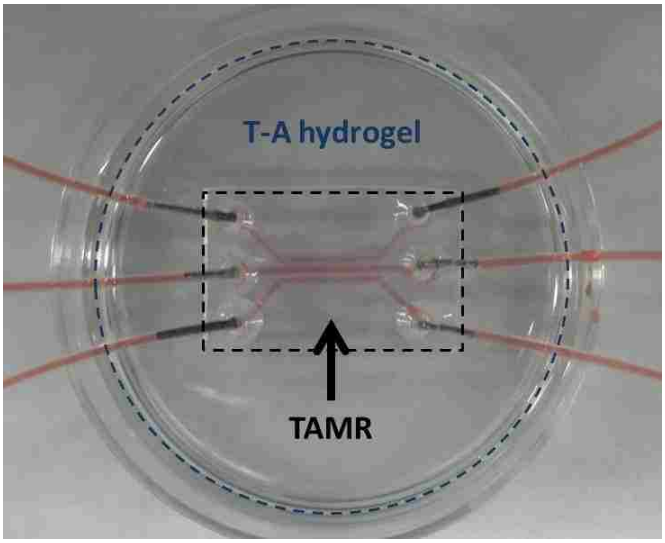

Scheme 3.5 a) Thiol-acrylate gradient generating microfluidic device overview and b) a thiol-acrylate device

3.7.2 Materials and Methods

Materials

PETA stabilized with 300-400 ppm MEHQ was obtained from Alfa Aesar. TMPTMP was purchased from Evans Chemetics LP and Sigma Aldrich. Ethoxylated trimethylolpropane tri(3-mercaptopropionate) 1300 (ETMPTMP 1300) was generously donated by Evans Chemetics LP. Poly(ethylene glycol) diacrylate average M_n 700 g/mol (PEGDA 700) and trimethylolpropane ethoxylate triacrylate average M_n ~912 (TMPETA 912) were purchased from Sigma Aldrich. DEA ≥99.5% was obtained from Alfa Aesar and Sigma Aldrich. See Scheme 3.4 for structures.

TAMR Microfluidic Channel Casting

Microfluidic channels were imbedded into TAMR by casting from a silicon and SU-8 master fabricated using standard photolithography techniques. TAMR was prepared according to the general procedure described earlier. The AA was mixed with enough TMPTMP to give a 1-1 ratio of functional groups, and after centrifugation, the resin was poured onto a clean silicon wafer with channel features while it sat in a polystyrene Petri dish. Between 15 and 17 grams of total material was enough to completely cover the wafer in a layer 2-3 mm thick without spilling over onto the Petri dish. After curing for 1 hour, the resin was peeled off the silicon wafer and cut into individual chips. The TAMR pieces were allowed to continue curing at room temperature until 24 hours of total cure time had elapsed to ensure maximum conversion of functional groups. Inlet and outlet holes were introduced at the appropriate places on the device using a drill equipped with a 1/16 inch drill bit. Excess dust and residue from the drilling process was blown away using compressed air, and the devices were stored under dry conditions until used.

Hydrogel Fabrication

Thiol-acrylate hydrogels were fabricated by adding the PEGDA 700 and TMPETA 912 (if applicable) to a centrifuge tube, followed by the ETMPTMP 1300, and then the aqueous component (typically PBS or TAP). Care was taken to mix each layer as little as possible during addition to prevent local gelation from occurring when the curing agent was added. (If the components are mixed together while they are being added to the tube, the curing agent will be encapsulated in gel immediately upon addition. This causes the majority of the mixture to remain unreacted with clumps of

hydrogel spread throughout.) The hydrogel was cured by raising the pH of the solution to between 7.5 and 8 by adding 0.01 mmol NaOH per gram of monomer/buffer. This amount of NaOH gives a gel time of approximately 15 seconds, but it can be adjusted to increase or decrease gel time if desired. Once the base was added, the mixture was vortexed for ~5 seconds, inverted several times, and vortexed again to ensure thorough mixing. The solution was poured into a Petri dish and allowed to cure at room temperature for at least 5 minutes prior to use. Hydrogels were labeled as the weight percent polymer content and the mole percent of acrylate groups from TMPETA 912 if applicable. For example, a 22% hydrogel would contain 22 weight percent polymer in buffer solution with no TMPETA 912, and a 15% 50% 912 hydrogel would contain 15 weight percent polymer with 50% of the total acrylate groups coming from TMPETA 912.

Construction of the Microfluidic Device

The cured TAMR pieces with the imbedded microfluidic channels were combined with the thiol-acrylate hydrogel to give a gradient generating microfluidic device. Both components were prepared as described above. The TAMR half of the device was plumbed with 1/16 inch outside diameter Teflon tubing at the inlet and outlet ports. The seal between the tubing and cured TAMR was generally fluid tight, but the connection could be sealed using additional liquid TAMR that was applied around the tubing and allowed to cure in place. Two pieces of tubing could be connected together using 22 gauge needles after the tip was removed. The tips of the needles were cut off using a pair of wire cutters, and the syringe fitting was pulled off. The cutting process collapsed the end of the needle, so it was filed down until the opening was reformed. The metal

tube that resulted from this process was pushed into the end of the Teflon tubing, and the resulting connection was liquid tight without the need for any sealant. Once the necessary tubing was connected to the TAMR piece, it was placed on a freshly prepared thiol-acrylate hydrogel cured in a Petri dish. The TAMR half of the device must be placed on the hydrogel cautiously in order to get a good seal between the two surfaces and since excess pressure could force the pliable hydrogel up into the microfluidic channel, which would block it. The device was left to sit for 5 minutes prior to use to ensure a good bond between the hydrogel and TAMR layers.

Hydrogel Swelling Studies

Thiol-acrylate hydrogels were prepared according to the procedure above and cured in molds measuring 7 x 14 mm. After ~5 minutes, the gels were removed from the molds, weighed, and immersed in PBS. The gels were taken out of the PBS, dried of excess surface moisture, and weighed again. The percentage swelling was calculated as the weight at 24 hours of soaking minus the initial weight, divided by the initial weight. Three replicates were run for each formulation with a minimum of three samples each, the values averaged, and the standard deviation reported as error.

Microfluidic Gradient Characterization

A TAMR gradient-generating microfluidic device was prepared according to the procedures above. The top channel of the device was connected to a 10 μM solution of rhodamine 6G prepared in N-free TAP media, and the bottom channel was connected to unaltered N-free TAP media. The center channel was filled with N-free TAP media, and the surface of the hydrogel was also covered with N-free TAP to prevent evaporation from the hydrogel over the course of the experiment. The top and bottom

channels were infused with their respective solutions at a rate of 15 μL/min. Images were taken of the device using a fluorescent microscope with the rhodamine filter. The diffusion of the solution containing the fluorophore was tracked by measuring the fluorescence intensity across the center channel of the device.

3.7.3 Thiol-Acrylate Device Development

The initial goal of this project was to develop a microfluidic device that contained a rigid upper component that would bond to a porous hydrogel component. This device would be analogous to a device currently in use by our collaborators, which uses PDMS and agarose. TAMR was chosen as the top layer of the device since it is more hydrophilic than PDMS and can be fabricated with excess functional groups that could promote adhesion. The first attempts focused on using TAMR in combination with agarose as the hydrogel, as it is well characterized and is the same hydrogel used in the device developed by our collaborators. No adhesion was obtained using unmodified agarose and efforts to produce hybrid systems by incorporating thiol and acrylate monomers were also unsuccessful. Alternative hydrogels, such as polyacrylamide were tested, but no bonding was achieved. The breakthrough came when a thiol-acrylate hydrogel was developed, based on a report from Pritchard et al.,[78] using a trifunctional thiol and a difunctional acrylate that both contained poly(ethylene glycol) chains to improve water solubility. When TAMR was brought in contact with this hydrogel, there was an immediate attraction between the two surfaces. If the two layers were left in contact for a few minutes, efforts to detach the TAMR from the hydrogel led to cohesive failure of the hydrogel, which indicates a strong bond between the two surfaces. The reasons for why bonding is achieved between the TAMR and thiol-acrylate hydrogel and

not the other hydrogels have not been investigated, but one possibility involves the free versus bound water in the hydrogels. In hydrogel systems, water is theorized to exist in two main states: bound water that is interacting with the polymer chains and free water, which occupies the space between the chains.[259] When agarose was prepared between 1 and 3 weight percent in water, a film of liquid water is observed on the surface. This film could prevent interactions between the TAMR surface and the agarose chains and is due to a process called syneresis, where water is expelled from the gel.[260] In contrast, the thiol-acrylate (TA) hydrogels have a surface that is completely dry to the touch and have a much lower water content (typically ≤85% compared to agarose at ≥97%). In addition, the TA hydrogels are chemically crosslinked gels while agarose is a physically crosslinked gel that is held together by polymer chain entanglements and interactions between groups along the backbone. This means that the amount of water the TA gels can hold is limited by the crosslink density of the network, while agarose gels will continue to absorb water until they disintegrate. It is possible that the majority of the water in the TA hydrogels is bound water due to the relatively high polymer content of the system and the strong interactions between water and the ethylene glycol repeating groups present in the monomers. This allows for interactions between the TAMR surface and the hydrogel polymer to develop and bind the two together. It is unlikely that covalent bonding between thiol and acrylate groups from each surface is responsible for the hydrogel bonding since this phenomenon was observed for 1-1, 40% EA, and 40% ET TAMR formulations all at full cure.

The TA hydrogels were initially cured using DEA, as is typical for TA polymerizations. The theory was that the DEA would act as a nucleophile and bind into the polymer network via a Michal addition, similarly to the AA reaction in TAMR, and not leach out. In actuality this process is likely unreliable as the amine will generally be protonated in an aqueous environment, which prevents it from acting as a nucleophile in the Michal addition. Hydrogels were successfully fabricated using DEA, but the process was inconsistent due to the high volatility of DEA and the small reagent volumes need to gel the mixture. In response, an alternative strategy was developed that used an AA mixture similar to the TAMR system. A 66.6% DEA-AA was produced and used to cure the hydrogel, which improved reproducibility and ensured the amine was covalently bound into the polymer network. While this strategy was effective, in order to simplify the system and avoid any biocompatibility issues, the hydrogel curing agent was changed to NaOH. In the hydrogel system, it is the overall pH of the mixture that determines whether or not the polymerization reaction occurs, so the identity of the base is unimportant.

The water content of the hydrogel can be adjusted easily to achieve a wide range of physical properties, but for the microfluidic device, the hydrogel must be stable enough to support the rigid upper layer while allowing for the rapid diffusion of small molecules in solution. The two main hydrogel concentrations used in this study were 22 and 15 weight percent polymer. When the concentration was lowered to 10%, the hydrogel was not rigid enough to consistently support and bond to the TAMR portion of the device. Higher concentrations than 22% were not considered due to decreased diffusion at higher polymer content. The original hydrogel formula was made using

PEGDA 700 and ETMPTMP 1300, but in order to increase crosslink density, trifunctional TMPETA 912 was added to the system. A 1-1 ratio between acrylate and thiol groups was maintained while the number of acrylate groups contributed by the trifunctional monomer was altered.

3.7.4 Hydrogel Swelling Studies

Initial experiments showed that the TA hydrogel was not fully saturated at 22% and would swell when put into contact with buffer solution. This is a problem in the microfluidic device because the swelling alters the channel geometry, which can induce flow in the center channel or even completely block the channel. The swelling behavior of the hydrogel was determined for a number of different formulations to find a system that would swell minimally but still be rigid enough to support the channel layer of the device. The initial 22% hydrogel formula produced a gel that swells by 80 ± 5% when immersed in buffer solution over 24 hours, and decreasing the polymer content to 15% caused the gel to swell by 87 ± 15%. Unfortunately, due to the high variance in the swelling for the 15% samples no conclusions can be made as to the effect of hydrogel concentration on the swelling in this system. It is likely that the lower monomer concentration hydrogel would swell more than the higher one, which seems counterintuitive at first, but the increasing the monomer concentration increases chain interpenetration and typically gives a tighter network that absorbs less.[261] Instead of altering the polymer content in the gel, another way to change the gel properties is to alter the polymer network structure by incorporating an ethoxylated triacrylate into the system while replacing some of the diacrylate with triacrylate in order to maintain a 1-1 thiol-acrylate ratio. When 50% of the PEGDA 700 acrylate groups were replaced with

TEMPETA 912 acrylate groups, the gel only swelled by 30 ± 3%. This is due to the increased crosslink density of the network restricting the amount of water that can be absorbed by the gel.

3.7.5 Microfluidic Gradient Characterization

The concentration gradient produced across the center channel of the device was characterized using a fluorophore solution. The shape and concentration range of the gradient are important since the algae will not respond to a shallow gradient and a high stimulus concentration can overwhelm them. The ideal chemical gradient would a fairly steep gradient that developed and reached a steady state quickly. Figure 3.24a shows the diffusion profile over time for a 22% hydrogel obtained by taking the fluorescence intensity along a line drawn across the center channel of the device. The right hand side of the graph corresponds to the part of the device closest to the source channel. The gradient obtained is relatively shallow and slowly increases in intensity over the course of the 12-hour experiment due to the swelling of the gel ans slow diffusion of fluorophore through the gel. In order to combat this, the polymer concentration in the hydrogel was reduced from 22% to 15% in an attempt to increase the diffusivity of the fluorophore through the gel, and the results from this change are shown in Figure 3.24b. While a steady-state concentration gradient was not achieved during the experiment, a steeper gradient profile was developed in a shorter period of time than when using the 22% gel. This is due to the faster diffusion of the fluorophore through the gel, but the gradient leveled off over time.

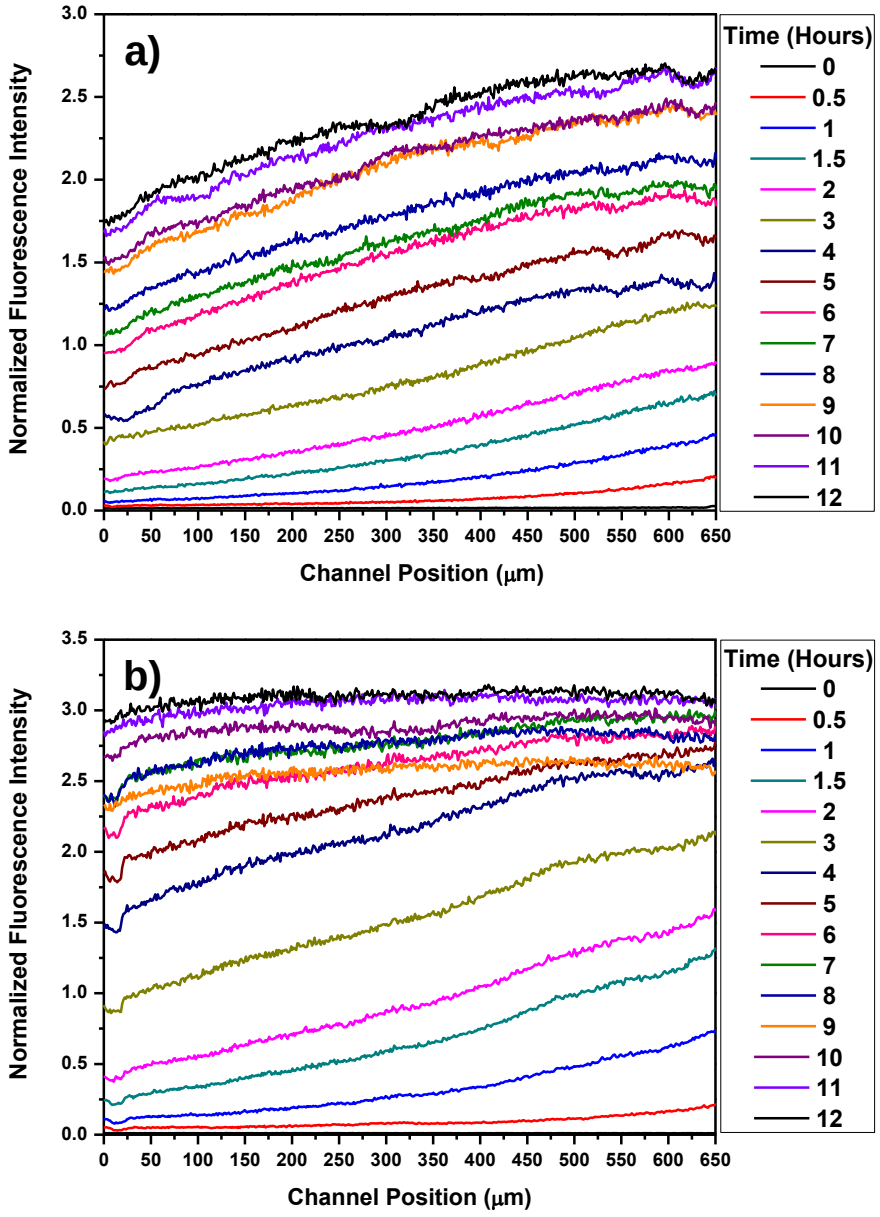

Figure 3.24 Concentration profiles in thiol-acrylate devices with a a) 22 % hydrogel and b) 15% hydrogel

The results from increasing the crosslink density of the gel by incorporating TMPETA 912 in a 15% 50% 912 hydrogel are displayed in Figure 3.25. The increase in crosslink density appeared to slow the formation of the gradient down, but gave a steeper gradient that eventually reached a steady state after 7 hours. Decreasing the

hydrogel thickness by about half with the 15% 50% 912 hydrogel gave the steepest and smoothest gradient profile, but the effect was minimal.

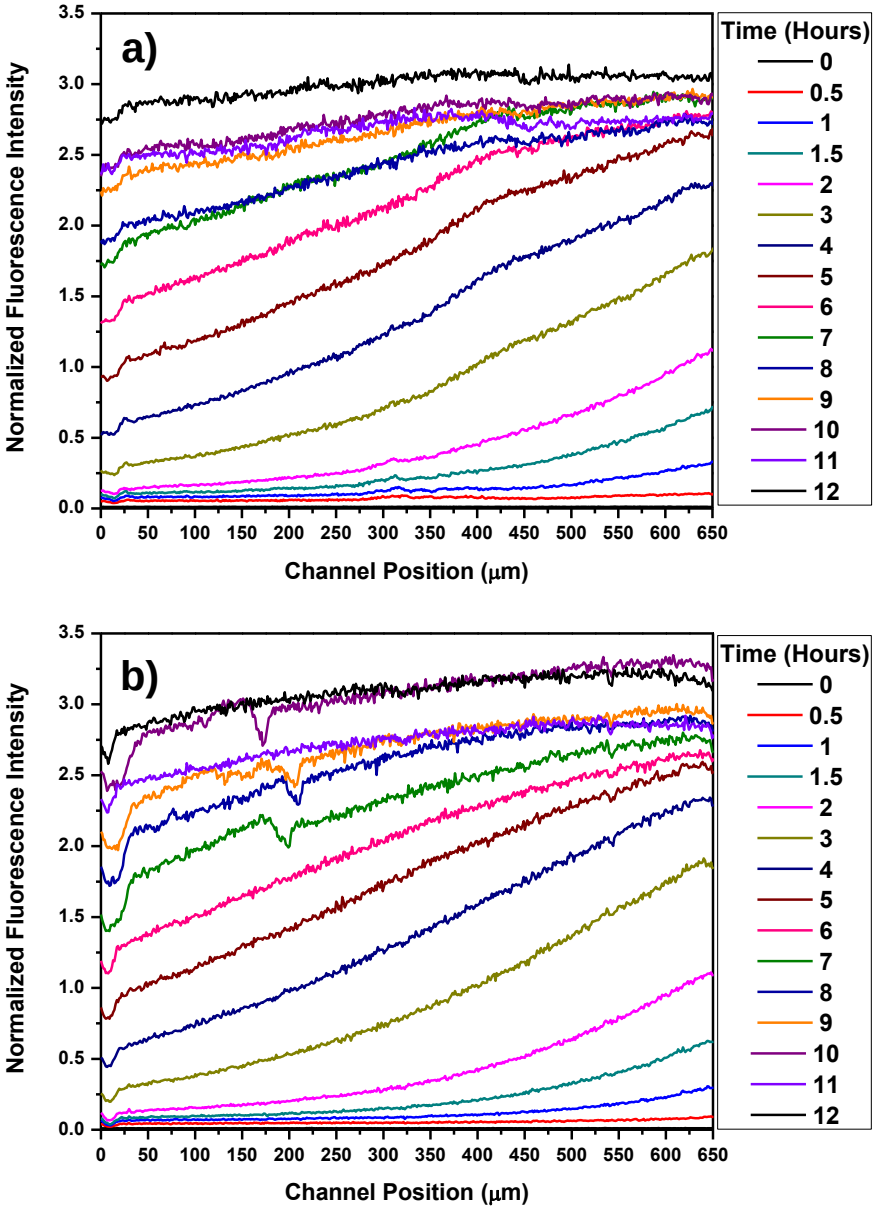

Figure 3.25 Concentration profiles in thiol-acrylate devices with 15% 50% 912 hydrogels at a thickness of a) ~4mm and b) ~2 mm

Unfortunately, in each of 15% gels, the gradient nearly levels off 8-10 hours into the experiment. This could be due to accumulation of the fluorophore in the gel caused by interactions between the rhodamine and polymer structure. Figure 3.26 shows the

gradient profile obtained using 1% agarose as the hydrogel layer. The gradient develops quickly and stays a uniform shape throughout the experiment, which is due to the extremely high water content in the agarose gel, which essentially has the diffusion properties of water. While the TAMR hydrogel does not perform as well as agarose at this point, a linear gradient across the center channel of the device can be developed successfully for several hours.

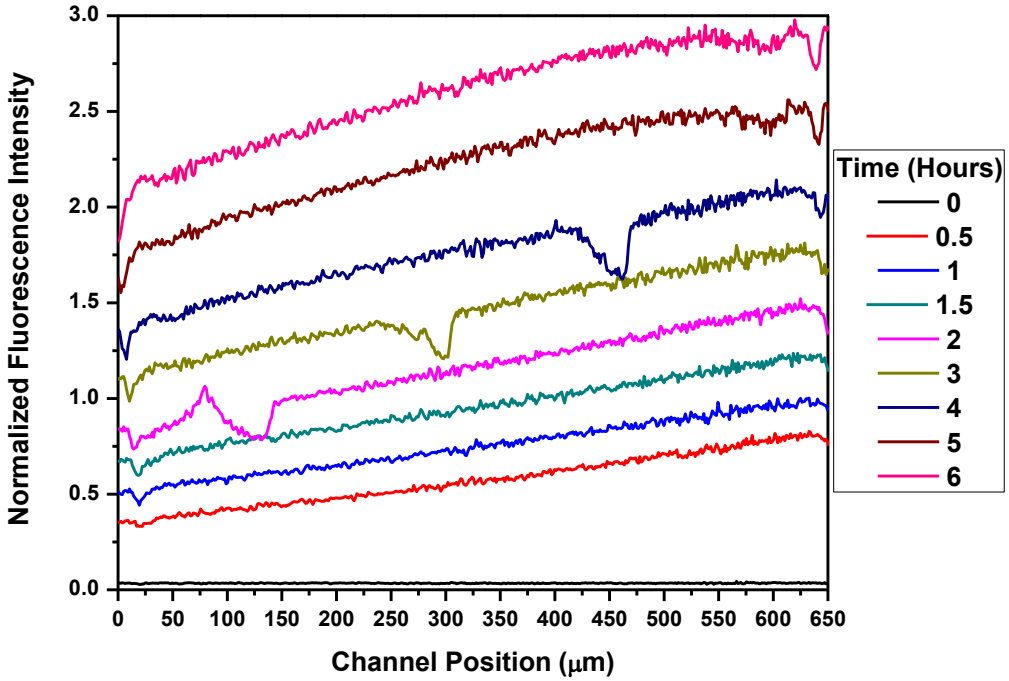

Figure 3.26 Concentration profile obtained in agarose

3.7.6 Algae Viability

In order to successfully study the chemotaxis of algae in the thiol-acrylate-based gradient generating device, the algae need to remain viable in the device for extended periods of time under flow-free conditions. Figure 3.27 shows the center channel of a thiol-acrylate gradient generator device with *Chlamydomonas reinhardtiidtii* algae present. The algae were injected into the channel, which was sealed at both ends by placing liquid agarose solution on the end ports and allowing it to solidify. The algae

were observed swimming around the channel without significant influence from flow through the channel. The algae were left in the device for 3 hours to determine if the TAMR or thiol-acrylate hydrogel had a negative impact on their viability. After 3 hours had elapsed, the algae were still swimming in the channel, which indicates the device is not dramatically harming the algae on this timescale. More detailed viability studies are ongoing where the algae will be incubated in the device for longer periods, and their viability will be quantified using a chemical staining approach.

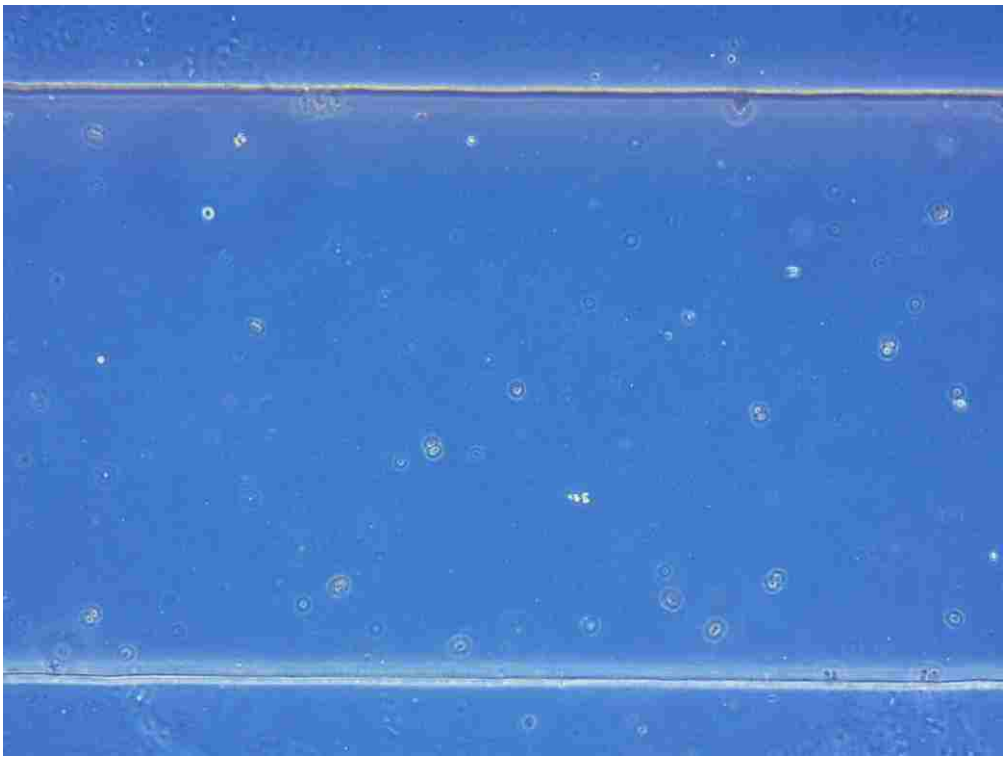

Figure 3.27 *Chlamydomonas reinhardtiidtii* in the center channel of a thiol-acrylate gradient-generating device (channel width 450 μm)

3.7.7 Conclusions

A gradient generating thiol-acrylate-based microfluidic device has been developed successfully. Using traditional materials such as agarose and PDMS requires an external support structure to keep the two device layers in frim contact with

each other to ensure a liquid tight seal. The thiol-acrylate device uses TAMR instead of PDMS and a thiol-acrylate hydrogel instead of agarose to produce a device that does not require any additional structures to remain sealed. The TAMR half of the device bonds to the hydrogel after the two are placed in contact, and the bond is such that the hydrogel will fail cohesively before detaching from the TAMR. The swelling properties of the thiol-acrylate hydrogels were determined as well as the effect of changing crosslink density on this behavior. Chemical gradients were established in the thiol-acrylate device and characterized using fluorescence microscopy. Finally, algae were seeded into the device and successfully maintained under flow-free conditions.

CHAPTER 4. SUMMARY AND CONCLUSIONS

The kinetics and some microfluidic applications of thiol-acrylate Michael addition polymerizations using multifunctional monomers have been researched and discussed. While thiol-acrylate Michael addition polymerizations using monofunctional monomers have been extensively studied, the kinetics in multifunctional systems remains largely unexplored despite the growing usefulness of thiol-acrylate materials. The aim of this study was to explore a range of both thiol and acrylate monomers to discern what structural changes affected the polymerization rate to provide a starting point for more focused future studies.

It was observed that secondary functionalities affect the polymerization rate through intramolecular interactions, which is consistent with previous reports in monofunctional systems. The polymerization rate constant was found to increase with increasing thiol and acrylate functionality, which was attributed to the beneficial intramolecular effects stemming from adding more ester linkages into the monomer structure. The increase in rate observed with increasing thiol functionality could be, at least in part, affected by another factor since spacing out the thiol groups while maintaining the same functionality actually decreased the rate. More focused studies are needed to isolate this effect, but a preliminary hypothesis is that when the thiol groups are held in close proximity to one another, deprotonation of one thiol by the enolate produced from the addition of an adjacent thiol is more likely, which would increase the rate by shifting the thiolate-base equilibrium.

The effect of changing the reaction mechanism from base-catalyzed to the nucleophile-initiated thiol-acrylate Michael addition mechanism was studied in

trifunctional thiol-acrylate mixtures. As expected, there was a significant increase in the rate of polymerization with the nucleophile-initiated mechanism, but the magnitude of this increase was much less than what has been previously reported in monofunctional systems. This decreased reactivity is likely due to the increased steric hindrance associated with forming enolates on triacrylates using the corresponding trithiol in addition to a reduction in the diffusivity of the active polymerization species through gelling network.

Perhaps the most important practical observation of this study was the spontaneous initiation of radical polymerization during thiol-acrylate Michael addition reactions. This phenomenon appears to occur in systems where the rate of the thiol-Michael addition is slow, such as in base-catalyzed systems with low base concentrations, systems using lower functionality monomers which are less reactive, and towards the end of nucleophile-initiated reactions. The cause of this phenomenon has yet to be determined, but further investigation in this area is important since unexpected radical polymerization in thiol-acrylate systems will produce materials with vastly different properties compared to materials where the thiol-acrylate Michael addition reaction is the dominant mechanism.

A range of properties for a thiol-acrylate microfluidic resin (TAMR) were determined, and two microfluidic applications featuring TAMR were presented. The TAMR is a two-part system that uses a built-in amine catalyst to cure the system. The kinetics of the curing process were investigated for several TAMR formulations, which showed that full conversion could be reached in only 3 hours at 50 °C or 10 hours at room temperature for one system. The surface of TAMR is relatively hydrophilic and

was found to vary based on the resin formulation and the surface on which it was cured. This adaptive surface effect was attributed to the orientation of the polymer functional groups towards or away from the curing surface based on its polarity. Changes in contact angle of 30° were observed by changing the curing surface from poly(styrene) to glass.

The absorption of water by the TAMR was quantified for several different resin compositions. Short term exposure to water only swelled the resin by 1-2% but over long-term exposure, some formulations swell as much as ~28%. Eventually, all of the samples reached a maximum swelling point before starting to degrade due to hydrolysis of the esters in the polymer backbone, but this only occurred after the samples were submerged for at least one month. The absorption of other solvents by TAMR was also quantified, and overall, the observed swelling was minimal over 24 hours, especially in nonpolar organic solvents.

The elastic modulus of the TAMR was shown to vary with polymer cure time as well as resin composition. There was no observed difference in the modulus between samples cured at room temperature or at elevated temperature, which means the curing of TAMR can be accelerated without compromising resin performance. Bonding between two pieces of TAMR was achieved through interfacial thiol-acrylate coupling reactions by incorporating excess thiol and acrylate functional groups into each resin piece. The bond strength did not decrease when the resin was cured at elevated temperatures, and even at room temperature, the bond strength at 30 minutes was sufficient to cause the thiol-acrylate material to fail cohesively when the resin pieces were forced apart. TAMR formulations using a 1-1 ratio of functional groups could also

be bound together though these samples failed adhesively when forced apart. TAMR was used to successfully replicate 30 μm sized microfluidic features, but removing bubbles from the curing resin remains a challenge.

A microfluidic device capable of detecting the presence of *E. coli* using a fluorescence based assay was produced. Bacterial capture was preformed using an antibody which was attached to the TAMR surface. While there was no conclusive evidence as to whether the antibody was covalently bound to the surface or just strongly adsorbed, the device successfully detected fluorescently labeled *E. coli* at a concentration of 10^5 cfu/mL without extensive process optimization or data treatment. Components of the bacterial cell, such as LPSs, were also successfully detected in this device.

Another microfluidic device was developed using TAMR in conjunction with a thiol-acrylate hydrogel to produce a gradient-generating device for the study of algal chemotaxis. Bonding between the TAMR and hydrogel layers was achieved without any surface modification or external support structure. Chemical gradients were successfully developed in the device, and the effect of changing several hydrogel parameters on the gradient was investigated. Preliminary results suggest that algae remain viable in the device for several hours, but work on this project is on ongoing.

Overall, an investigation into the kinetics of thiol-acrylate polymerizations using multifunctional monomers has revealed that there are still many interesting and potentially impactful problems to study in these systems. Similarly, while examining the properties of a thiol-acrylate material, several phenomena worthy of continued investigation were uncovered. Two microfluidic devices were fabricated using thiol-

acrylate materials to demonstrate the advantages and versatility of this chemistry in an area of study where the range of materials properties required for different applications is extremely broad. Hopefully, this work has demonstrated that, while they are not a recent development, thiol-acrylate Michael addition polymerizations are worthy of future studies on the polymerization mechanism, the properties of materials produced using these reactions, and on the practical applications of this versatile and robust chemistry.

REFERENCES

1. Posner, T., Beiträge zur Kenntniss der ungesättigten Verbindungen. II. Ueber die Addition von Mercaptanen an ungesättigte Kohlenwasserstoffe. *Berichte der deutschen chemischen Gesellschaft* **1905,** *38* (1), 646-657.

2. Goodyear, C. Improvement in India-Rubber Fabrics. U.S. Patent 3,633, June 15 1844.

3. Marvel, C. S.; Chambers, R. R., Polyalkylene Sulfides from Diolefins and Dimercaptans. *Journal of the American Chemical Society* **1948,** *70* (3), 993-998.

4. Marvel, C. S.; Caesar, P. D., Polyarylene-alkylene Sulfides1. *Journal of the American Chemical Society* **1951,** *73* (3), 1097-1099.

5. Morgan, C. R.; Magnotta, F.; Ketley, A. D., Thiol/ene photocurable polymers. *Journal of Polymer Science: Polymer Chemistry Edition* **1977,** *15* (3), 627-645.

6. Morgan, C. R., The photopolymerization of allylic and acrylic monomers in the presence of polyfunctional thiols. *Journal of Radiation Curing* **1980,** *7* (2), 10.

7. Klemm, E.; Sensfuss, S.; Holfter, U.; Flammersheim, H. J., Free-Radical stabilizers for the thiol/ene-systems. *Angewandte Makromolekulare Chemie* **1993,** *212* (1), 121-127.

8. Rakas, M. A.; Jacobine, A. F., Mechanical and dynamic mechanical properties of photocrosslinked norbornene-thiol copolymer films. *Journal of Adhesion* **1992,** *36* (4), 247-263.

9. Jacobine, A. F., Thiol-Ene Photopolymers. In *Radiation Curing in Polymer Science and Technology*, Fouassier, J. P., Ed. Elsevier: New York, 1993; pp 219-268.

10. Hoyle, C. E.; Cole, M.; Bachemin, M.; Yoder, B.; Mguyen, C.; Jonsson, S., Photopolymerization of Systems Incorporating Thiol-Enes. *Polym. Preprints* **2001,** *42*, 697-698.

11. Cramer, N. B.; Reddy, S. K.; Cole, M.; Hoyle, C.; Bowman, C. N., Initiation and Kinetics of Thiol-ene Photopolymerizations without Photoinitiators. *J. Polym. Sci. Part A Polym. Chem.* **2004,** *42*, 5817-5826.

12. Hoyle, C. E.; Lee, T. Y.; Roper, T., Thiol–Enes: Chemistry of the Past with a Promise for the Future. *J. Poly. Sci. Part A. Polym. Chem.* **2004,** *52*, 5301-5338.

13. Chan, J. W.; Wei, H.; Zhou, H.; Hoyle, C. E., The effects of primary amine catalyzed thio-acrylate Michael reaction on the kinetics, mechanical and physical properties of thio-acrylate networks. *Eur. Polym. J.* **2009,** *45*, 2717–2725.

14. Hoyle, C. E.; Bowman, C. N., Thiol-Ene Click Chemistry. *Angewandte Chemie International Edition* **2009,** *49* (9), 1540-1573.

15. Cramer, N. B.; Davies, T.; O'Brien, A. K.; Bowman, C. N., Mechanism and Modeling of a Thiol−Ene Photopolymerization. *Macromolecules* **2003,** *36* (12), 4631-4636.

16. Okay, O.; Bowman, C. N., Kinetic Modeling of Thiol-Ene Reactions with Both Step and Chain Growth Aspects. *Macromol. Theory Simul.* **2005,** *14*, 267-277.

17. Khire, V. S.; Kloxin, A. M.; Couch, C. L.; Anseth, K. S.; Bowman, C. N., Synthesis, Characterization and Cleavage of Linear Polymers Attached to Silica Nanoparticles Formed Using Thiol-Acrylate Conjugate Addition Reactions. *J. Polym. Sci. Part A: Polym. Chem.* **2008,** *46* (20), 6896-6906.

18. Chan, J. W.; Hoyle, C. E.; Lowe, A. B.; Bowman, M., Nucleophile-Initiated Thiol-Michael Reactions: Effect of Organocatalyst, Thiol, and Ene. *Macromolecules* **2010,** *43*, 6381–6388.

19. Hoyle, C. E.; Lowe, A. B.; Bowman, C. N., Thiol-click chemistry: a multifaceted toolbox for small molecule and polymer synthesis. *Chemical Society Reviews* **2010,** *39* (4), 1355-1387.

20. Lowe, A. B., Thiol-ene “click” reactions and recent applications in polymer and materials synthesis. *Polymer Chemistry* **2010,** *1* (1), 17-36.

21. Kharasch, M. S.; Read, A. T.; Mayo, F. R., Peroxide effect in the addition of reagents to unsaturated compounds. XVI. Styrene and isobutylene. *Chemistry & Industry* **1938,** *57*, 752.

22. Cramer, N. B.; Reddy, S. K.; O'Brien, A. K.; Bowman, C. N., Thiol−Ene Photopolymerization Mechanism and Rate Limiting Step Changes for Various Vinyl Functional Group Chemistries. *Macromolecules* **2003,** *36* (21), 7964-7969.

23. Hoyle, C. E.; Bowman, C. N., Thiol-ene click chemistry. *Angewandte Chemie* **2010,** *49* (9), 1540-73.

24. Cramer, N. B.; Bowman, C. N., Kinetics of thiol–ene and thiol–acrylate photopolymerizations with real-time fourier transform infrared. *J. Polym. Sci. A Polym. Chem.* **2001,** *39* (19), 3311-3319.

25. O'Brien, A. K.; Cramer, N. B.; Bowman, C. N., Oxygen inhibition in thiol–acrylate photopolymerizations. *Journal of Polymer Science Part A: Polymer Chemistry* **2006,** *44* (6), 2007-2014.

26. Lee, T. Y.; Smith, Z.; Reddy, S. K.; Cramer, N. B.; Bowman, C. N., Thiol−Allyl Ether−Methacrylate Ternary Systems. Polymerization Mechanism. *Macromolecules* **2007,** *40* (5), 1466-1472.

27. Cramer, N. B.; Couch, C. L.; Schreck, K. M.; Carioscia, J. A.; Boulden, J. E.; Stansbury, J. W.; Bowman, C. N., Investigation of thiol-ene and thiol-ene–methacrylate based resins as dental restorative materials. *Dental Materials* **2010,** *26* (1), 21-28.

28. Kade, M. J.; Burke, D. J.; Hawker, C. J., The Power of Thiol-ene Chemistry. *J. Polym. Sci. Part A: Polym. Chem.* **2010,** *48*, 743-750.

29. Lee, T. Y.; Guymon, C. A.; Jönsson, E. S.; Hoyle, C. E., The effect of monomer structure on oxygen inhibition of (meth)acrylates photopolymerization. *Polymer* **2004,** *45* (18), 6155-6162.

30. Decker, C.; Jenkins, A. D., Kinetic approach of oxygen inhibition in ultraviolet- and laser-induced polymerizations. *Macromolecules* **1985,** *18* (6), 1241-1244.

31. Cramer, N. B.; Scott, J. P.; Bowman, C. N., Photopolymerization of Thiol-Ene Polymers without Photoinitiators. *Macromolecules* **2002,** *35*, 5361-5365.

32. Zhao, Y. H.; Vuluga, D.; Lecamp, L.; Burel, F., A rapid, eco- and environmental friendly alternative to oil oxidation for the preparation of fatty coatings using photoinitiated thiol-ene chemistry. *Progress in Organic Coatings* **2016,** *101*, 216-224.

33. Meissner, M.; Thompson, H., The photolysis of mercaptans. *Transactions of the Faraday Society* **1938,** *34*, 1238-1239.

34. Klemm, E.; Sensfuß, S.; Holfter, U.; Schütz, H., Untersuchungen zur linearen thiol-en-photopolymerisation. *Die Makromolekulare Chemie* **1990,** *191* (10), 2403-2411.

35. Klemm, E.; Sensfuß, S., Untersuchungen zum selbstinitiierungs-mechanismus der thiol/En-polymerisation. *Die Makromolekulare Chemie* **1991,** *192* (1), 159-164.

36. Klemm, E.; Sensfuß, S.; Holfter, U.; Flammersheim, H. J., Free-Radical stabilizers for the thiol/ene-systems. *Die Angewandte Makromolekulare Chemie* **1993,** *212* (1), 121-127.

37. Kühne, G.; Diesen, J. S.; Klemm, E., New results of the self-initiation mechanism of SH/En addition polymerization. *Die Angewandte Makromolekulare Chemie* **1996,** *242* (1), 139-145.

38. Pryor, W. A.; Coco, J. H.; Daly, W. H.; Houk, K. N., Radical generation from polymolecular reactions of closed shell molecules. Molecule-assisted homolysis (MAH). Hydrogen atom transfer from a Diels-Alder adduct to an alkene. *Journal of the American Chemical Society* **1974,** *96* (17), 5591-5593.

39. Morgan, C. R.; Magnotta, F.; Ketley, A. D., Thiol/ene photocurable polymers. *J. Poly. Sci. Part A. Polym. Chem.* **1977,** *15*, 627.

40. Morgan, C. R.; Ketley, A. D., The effect of phosphines on thiol/ene curing systems. *Journal of Polymer Science: Polymer Letters Edition* **1978,** *16* (2), 75-79.

41. Jacobine, A. F.; Glaser, D. M.; Grabek, P. J.; Mancini, D.; Masterson, M.; Nakos, S. T.; Rakas, M. A.; Woods, J. G., Photocrosslinked norbornene–thiol copolymers: Synthesis, mechanical properties, and cure studies. *Journal of Applied Polymer Science* **1992,** *45* (3), 471-485.

42. Black, M.; Rawlins, J. W., Thiol–ene UV-curable coatings using vegetable oil macromonomers. *European Polymer Journal* **2009,** *45* (5), 1433-1441.

43. Khire, V. S.; Harant, A. W.; Watkins, A. W.; Anseth, K. S.; Bowman, C. N., Ultrathin Patterned Polymer Films on Surfaces Using Thiol−Ene Polymerizations. *Macromolecules* **2006,** *39* (15), 5081-5086.

44. Woods, J. G., Radiation-Curable Adhesives. In *Radiation Curing : Science and Technology* Pappas, S. P., Ed. Springer US: 1992; pp 333-398.

45. Moszner, N.; Schöb, W.; Rheinberger, V., Synthesis, characterization and thiol-ene polymerization of hydrolyzed/condensed norbornenyl silic acid ester. *Polymer Bulletin* **1996,** *37* (3), 289-295.

46. Rakas, M. A.; Jacobine, A. F., Mechanical and Dynamic Mechanical Properties of Photocrosslinked Norbornene-Thiol Copolymer Films. *The Journal of Adhesion* **1992,** *36* (4), 247-263.

47. Toh, H. K.; Bateman, I. R.; Diggins, D. R.; Cieslinski, B. G. High index/high Abbe number composition. U.S. Patent 5,977,276, 1999.

48. Chen, F.; Toh, H. K. UV curable high index vinyl esters. U.S. Patent 6,153,663, 2000.

49. Toh, H. K.; Bateman, I. R.; Diggins, D. R.; Cieslinski, B. G. High index/high abbe number composition. U.S. Patent 6,313,251, 2001.

50. Toh, H. K.; Chen, F.; Kok, C. M. Acrylic thio monomers. U.S. Patent 6,172,140, 2001.

51. Bhargava, R.; Wang, S.-Q.; Koenig, J. L., FTIR Imaging Studies of a New Two-Step Process To Produce Polymer Dispersed Liquid Crystals. *Macromolecules* **1999,** *32* (8), 2748-2760.

52. Bhargava, R.; Wang, S.-Q.; Koenig, J. L., Studying Polymer-Dispersed Liquid-Crystal Formation by FTIR Spectroscopy. 1. Monitoring Curing Reactions. *Macromolecules* **1999,** *32* (26), 8982-8988.

53. Bhargava, R.; Levin, I. W., Noninvasive Imaging of Molecular Dynamics in Heterogeneous Materials. *Macromolecules* **2003,** *36* (1), 92-96.

54. Nwabunma, D.; Kyu, T., Phase behavior, photopolymerization, and morphology development in mixtures of eutectic nematic liquid crystal and photocurable monomer. *Polymer* **2001,** *42* (2), 801-806.

55. Natarajan, L. V.; Shepherd, C. K.; Brandelik, D. M.; Sutherland, R. L.; Chandra, S.; Tondiglia, V. P.; Tomlin, D.; Bunning, T. J., Switchable Holographic Polymer-Dispersed Liquid Crystal Reflection Gratings Based on Thiol−Ene Photopolymerization. *Chemistry of Materials* **2003,** *15* (12), 2477-2484.

56. McNair, O. D.; Janisse, A. P.; Krzeminski, D. E.; Brent, D. E.; Gould, T. E.; Rawlins, J. W.; Savin, D. A., Impact Properties of Thiol–Ene Networks. *ACS Applied Materials & Interfaces* **2013,** *5* (21), 11004-11013.

57. Senyurt, A. F.; Wei, H.; Hoyle, C. E.; Piland, S. G.; Gould, T. E., Ternary Thiol-Ene/Acrylate Photopolymers: Effect of Acrylate Structure on Mechanical Properties. *Macromolecules* **2007,** *40*, 4901-4909.

58. McNair, O. D.; Gould, T. E.; Piland, S. G.; Savin, D. A., Characterization of mouthguard materials: A comparison of a commercial material to a novel thiolene family. *Journal of Applied Polymer Science* **2014,** *131* (13).

59. Pojman, J. A.; Varisli, B.; Perryman, A.; Edwards, C.; Hoyle, C., Frontal Polymerization with Thiol-Ene Systems. *Macromolecules* **2004,** *37*, 691-693.

60. Nason, C.; Pojman, J. A.; Hoyle, C., The Effect of a Trithiol and Inorganic Fillers on the Photo- Induced Thermal Frontal Polymerization of a Triacrylate. *J. Polym. Sci. Part A Polym. Chem.* **2008,** *46*, 8091-8096.

61. Aimetti, A. A.; Machen, A. J.; Anseth, K. S., Poly(ethylene glycol) hydrogels formed by thiol-ene photopolymerization for enzyme-responsive protein delivery. *Biomaterials* **2009,** *30* (30), 6048-6054.

62. DeForest, C. A.; Polizzotti, B. D.; Anseth, K. S., Sequential click reactions for synthesizing and patterning three-dimensional cell microenvironments. *Nature Materials* **2009,** *8* (8), 659-664.

63. Polizzotti, B. D.; Fairbanks, B. D.; Anseth, K. S., Three-Dimensional Biochemical Patterning of Click-Based Composite Hydrogels via Thiolene Photopolymerization. *Biomacromolecules* **2008,** *9* (4), 1084-1087.

64. Fairbanks, B. D.; Schwartz, M. P.; Halevi, A. E.; Nuttelman, C. R.; Bowman, C. N.; Anseth, K. S., A Versatile Synthetic Extracellular Matrix Mimic via Thiol-Norbornene Photopolymerization. *Advanced Materials* **2009,** *21* (48), 5005-5010.

65. Michael, A., On the Addition of Sodium Acetacetic Ether and Analagous Sodium Compounds to Unsaturated Organic Ethers. *Am. Chem. J.* **1887,** *9*, 115.

66. Mather, B. D.; Viswanathan, K.; Miller, K. M.; Long, T. E., Michael addition reactions in macromolecular design for emerging technologies. *Prog. Polym. Sci.* **2006,** *31*, 487-531.

67. Nair, D. P.; Podgórski, M.; Chatani, S.; Gong, T.; Xi, W.; Fenoli, C. R.; Bowman, C. N., The Thiol-Michael Addition Click Reaction: A Powerful and Widely Used Tool in Materials Chemistry. *Chem. Mater.* **2014,** *26* (1), 724-744.

68. Allen, C. F. H.; Fournier, J. O.; Humphlett, W. J., THE THERMAL REVERSIBILITY OF THE MICHAEL REACTION: IV. THIOL ADDUCTS. *Canadian Journal of Chemistry* **1964,** *42* (11), 2616-2620.

69. Gershbein, L. L.; Hurd, C. D., The Reaction of Hydrogen Sulfide with Acrylonitrile, Acrylic Ester and Crotonaldehyde. *Journal of the American Chemical Society* **1947,** *69* (2), 241-242.

70. Hurd, C. D.; Gershbein, L. L., Reactions of Mercaptans with Acrylic and Methacrylic Derivatives. *Journal of the American Chemical Society* **1947,** *69* (10), 2328-2335.

71. Ferruti, P.; Ranucci, E.; Sartore, L.; Bignotti, F.; Marchisio, M. A.; Bianciardi, P.; Veronese, F. M., Recent results on functional polymers and macromonomers of interest as biomaterials or for biomaterial modification. *Biomaterials* **1994,** *15* (15), 1235-1241.

72. Bounds, C. O.; Goetter, R.; Pojman, J. A.; Vandersall, M., Preparation and Application of Microparticles Prepared Via the Primary Amine-catalyzed Michael Addition of a Trithiol to a Triacrylate. *J. Polym. Sci. Part A: Polym. Chem.* **2012,** *50*, 409–422.

73. Vernon, B.; Tirelli, N.; Bächi, T.; Haldimann, D.; Hubbell, J. A., Water-borne, in situ crosslinked biomaterials from phase-segregated precursors. *J. Biomed. Mater. Res. Part A* **2003,** *64A* (3), 447-456.

74. Garber, L.; Chen, C.; Kilchrist, K. V.; Bounds, C.; Pojman, J.; Hayes, D., Thiol-acrylate nanocomposite foams for critical size bone defect repair: A novel biomaterial. *J. Biomed. Mater. Res. Part A* **2013,** *101A*, 3531-3541.

75. Smoak, M.; Garber, L.; Chen, C.; Hayes, D.; Pojman, J. A., Antimicrobial Cytocompatible Pentaerythritol Triacrylate-co-Trimethylolpropane Composite Scaffolds for Orthopaedic Implants. *J. Appl. Poly. Sci.* **2014,** *131* (22), 41099.

76. Bounds, C. O.; Upadhyay, J.; Totaro, N.; Thakuri, S.; Garber, L.; Vincent, M.; Huang, Z.; Pojman, J. A., Fabrication and characterization of stable hydrophilic microfluidic devices prepared via the in situ tertiary-amine catalyzed Michael addition of multifunctional thiols to multifunctional acrylates. *ACS Appl. Mater. Interfaces* **2013,** *5*, 1643–1655.

77. Zhang, W.; Tullier, M. P.; Patel, K.; Carranza, A.; Pojman, J. A.; Radadia, A. D., Microfluidics using a thiol-acrylate resin for fluorescence-based pathogen detection assays. *Lab Chip* **2015,** *15*, 4227-4231.

78. Pritchard, C. D.; O'Shea, T. M.; Siegwart, D. J.; Calo, E.; Anderson, D. G.; Reynolds, F. M.; Thomas, J. A.; Slotkin, J. R.; Woodard, E. J.; Langer, R., An injectable thiol-acrylate poly(ethylene glycol) hydrogel for sustained release of methylprednisolone sodium succinate. *Biomaterials* **2011,** *32* (2), 587-597.

79. Lutolf, M. P.; Hubbell, J. A., Synthesis and Physicochemical Characterization of End-Linked Poly(ethylene glycol)-co-peptide Hydrogels Formed by Michael-Type Addition. *Biomacromolecules* **2003,** *4* (3), 713-722.

80. Koehler, K. C.; Anseth, K. S.; Bowman, C. N., Diels–Alder Mediated Controlled Release from a Poly(ethylene glycol) Based Hydrogel. *Biomacromolecules* **2013,** *14* (2), 538-547.

81. Li, M.; De, P.; Gondi, S. R.; Sumerlin, B. S., End group transformations of RAFT-generated polymers with bismaleimides: Functional telechelics and modular block copolymers. *Journal of Polymer Science Part A: Polymer Chemistry* **2008,** *46* (15), 5093-5100.

82. Napoli, A.; Tirelli, N.; Kilcher, G.; Hubbell, A., New Synthetic Methodologies for Amphiphilic Multiblock Copolymers of Ethylene Glycol and Propylene Sulfide. *Macromolecules* **2001,** *34* (26), 8913-8917.

83. Rieger, J.; Van Butsele, K.; Lecomte, P.; Detrembleur, C.; Jerome, R.; Jerome, C., Versatile functionalization and grafting of poly(?-caprolactone) by Michael-type addition. *Chemical Communications* **2005,** (2), 274-276.

84. Tedja, R.; Soeriyadi, A. H.; Whittaker, M. R.; Lim, M.; Marquis, C.; Boyer, C.; Davis, T. P.; Amal, R., Effect of TiO2 nanoparticle surface functionalization on protein adsorption, cellular uptake and cytotoxicity: the attachment of PEG comb polymers using catalytic chain transfer and thiol-ene chemistry. *Polymer Chemistry* **2012,** *3* (10), 2743-2751.

85. Rim, C.; Son, D. Y., Facile and efficient synthesis of star-shaped oligomers from a triazine core. *Tetrahedron Letters* **2009,** *50* (28), 4161-4163.

86. Chan, J. W.; Yu, B.; Hoyle, C. E.; Lowe, A. B., Convergent synthesis of 3-arm star polymers from RAFT-prepared poly(N,N-diethylacrylamide) via a thiol-ene click reaction. *Chemical Communications* **2008,** (40), 4959-4961.

87. Zhang, Q.; Li, G.-Z.; Becer, C. R.; Haddleton, D. M., Cyclodextrin-centred star polymers synthesized via a combination of thiol-ene click and ring opening polymerization. *Chemical Communications* **2012,** *48* (65), 8063-8065.

88. Chatani, S.; Podgórski, M.; Wang, C.; Bowman, C. N., Facile and Efficient Synthesis of Dendrimers and One-Pot Preparation of Dendritic–Linear Polymer Conjugates via a Single Chemistry: Utilization of Kinetically Selective Thiol–Michael Addition Reactions. *Macromolecules* **2014,** *47* (15), 4894-4900.

89. Auty, S. E. R.; Andren, O.; Malkoch, M.; Rannard, S. P., The first peripherally masked thiol dendrimers: a facile and highly efficient functionalization strategy of polyester dendrimers via one-pot xanthate deprotection/thiol-acrylate Michael addition reactions. *Chemical Communications* **2014,** *50* (50), 6574-6577.

90. Jones, M. W.; Mantovani, G.; Ryan, S. M.; Wang, X.; Brayden, D. J.; Haddleton, D. M., Phosphine-mediated one-pot thiol-ene "click" approach to polymer-protein conjugates. *Chemical Communications* **2009,** (35), 5272-5274.

91. Boyer, C.; Davis, T. P., One- pot synthesis and biofunctionalization of glycopolymersviaRAFT polymerization and thiol-ene reactions. *Chemical Communications* **2009,** (40), 6029-6031.

92. Lutolf, M. P.; Tirelli, N.; Cerritelli, S.; Cavalli, L.; Hubbell, J. A., Systematic Modulation of Michael-Type Reactivity of Thiols through the Use of Charged Amino Acids. *Bioconjugate Chemistry* **2001,** *12* (6), 1051-1056.

93. Vandenbergh, J.; Ranieri, K.; Junkers, T., Synthesis of (Bio)-Degradable Poly(β-thioester)s via Amine Catalyzed Thiol−Ene Click Polymerization. *Macromolecular Chemistry and Physics* **2012,** *213* (24), 2611-2617.

94. Kilambi, H.; Reddy, S. K.; Beckel, E. R.; Stansbury, J. W.; Bowman, C. N., Influence of Secondary Functionalities on the Reaction Behavior of Monovinyl (Meth)Acrylates. *Chemistry of Materials* **2007,** *19* (4), 641-643.

95. Kilambi, H.; Stansbury, J. W.; Bowman, C. N., Enhanced reactivity of monovinyl acrylates characterized by secondary functionalities toward photopolymerization and Michael addition: Contribution of intramolecular effects. *Journal of Polymer Science Part A: Polymer Chemistry* **2008,** *46* (10), 3452-3458.

96. Odian, G., *Principles of Polymerization, 4th Ed.* 3rd ed. ed.; Wiley: New York, 2004.

97. Dmuchovsky, B.; Vineyard, B. D.; Zienty, F. B., The Mechanism of the Base-Catalyzed Addition of Thiols to Maleic Anhydride. *Journal of the American Chemical Society* **1964,** *86* (14), 2874-2877.

98. Wang, C.; Qi, C., Mechanistic insights into N- or P-centered nucleophile promoted thiol–vinylsulfone Michael addition. *Tetrahedron* **2013,** *69* (26), 5348-5354.

99. Espenson, J. H., *Chemical Kinetics and Reaction Mechanisms*. 2nd ed. ed.; McGraw-Hill: New York, 1995.

100. Newmark, R. A.; Palazzotto, J., Carbon-13 NMR Analysis of Pentaerythritol Triacrylate. *Appl. Spectrosc.* **1990,** *44* (5), 804-807.

101. Kilambi, H.; Reddy, S. K.; Schneidewind, L.; Stansbury, J. W.; Bowman, C. N., Influence of the secondary functionality on the radical-vinyl chemistry of highly reactive monoacrylates. *Journal of Polymer Science Part A: Polymer Chemistry* **2009,** *47* (19), 4859-4870.

102. Shin, J.; Matsushima, H.; Comer, C. M.; Bowman, C. N.; Hoyle, C. E., Thiol−Isocyanate−Ene Ternary Networks by Sequential and Simultaneous Thiol Click Reactions. *Chemistry of Materials* **2010,** *22* (8), 2616-2625.

103. Chatani, S.; Sheridan, R. J.; Podgórski, M.; Nair, D. P.; Bowman, C. N., Temporal Control of Thiol-Click Chemistry. *Chem. Mater.* **2013,** *25*, 3897−3901.

104. Chatani, S.; Nair, D. P.; Bowman, C. N., Relative reactivity and selectivity of vinyl sulfones and acrylates towards the thiol-Michael addition reaction and polymerization. *Polymer Chemistry* **2013,** *4* (4), 1048-1055.

105. Esfandiari, P.; Ligon, S. C.; Lagref, J. J.; Frantz, R.; Cherkaoui, Z.; Liska, R., Efficient stabilization of thiol-ene formulations in radical photopolymerization. *Journal of Polymer Science Part A: Polymer Chemistry* **2013,** *51* (20), 4261-4266.

106. McDonald, J. C.; Duffy, D. C.; Anderson, J. R.; Chiu, D. T.; Wu, H.; Schueller, O. J. A.; Whitesides, G. M., Fabrication of microfluidic systems in poly(dimethylsiloxane). *ELECTROPHORESIS* **2000,** *21* (1), 27-40.

107. Whitesides, G. M., The origins and the future of microfluidics. *Nature* **2006,** *442* (7101), 368-373.

108. Manz, A.; Graber, N.; Widmer, H. M., Miniaturized total chemical analysis systems: A novel concept for chemical sensing. *Sensors and Actuators B: Chemical* **1990,** *1* (1), 244-248.

109. Sackmann, E. K.; Fulton, A. L.; Beebe, D. J., The present and future role of microfluidics in biomedical research. *Nature* **2014,** *507* (7491), 181-189.

110. Gravesen, P.; Branebjerg, J.; Jensen, O. S., Microfluidics-a review. *Journal of Micromechanics and Microengineering* **1993,** *3* (4), 168.

111. David J. Beebe; Glennys A. Mensing, a.; Walker, G. M., Physics and Applications of Microfluidics in Biology. *Annual Review of Biomedical Engineering* **2002,** *4* (1), 261-286.

112. Squires, T. M.; Quake, S. R., Microfluidics: Fluid physics at the nanoliter scale. *Reviews of Modern Physics* **2005,** *77* (3), 977-1026.

113. Madou, M. J., *Fundamentals of Microfabrication: The Science of Miniaturization*. 2 ed.; CRC Press: 2002.

114. Terry, S. C.; Jerman, J. H.; Angell, J. B., A gas chromatographic air analyzer fabricated on a silicon wafer. *IEEE Transactions on Electron Devices* **1979,** *26* (12), 1880-1886.

115. Bassous, E.; Taub, H. H.; Kuhn, L., Ink jet printing nozzle arrays etched in silicon. *Applied Physics Letters* **1977,** *31* (2), 135-137.

116. Liang, Z.; Chiem, N.; Ocvirk, G.; Tang, T.; Fluri, K.; Harrison, D. J., Microfabrication of a Planar Absorbance and Fluorescence Cell for Integrated Capillary Electrophoresis Devices. *Analytical Chemistry* **1996,** *68* (6), 1040-1046.

117. Manz, A.; Miyahara, Y.; Miura, J.; Watanabe, Y.; Miyagi, H.; Sato, K., Design of an open-tubular column liquid chromatograph using silicon chip technology. *Sensors and Actuators B: Chemical* **1990,** *1* (1), 249-255.

118. Woolley, A. T.; Mathies, R. A., Ultra-High-Speed DNA Sequencing Using Capillary Electrophoresis Chips. *Analytical Chemistry* **1995,** *67* (20), 3676-3680.

119. Hadd, A. G.; Raymond, D. E.; Halliwell, J. W.; Jacobson, S. C.; Ramsey, J. M., Microchip Device for Performing Enzyme Assays. *Analytical Chemistry* **1997,** *69* (17), 3407-3412.

120. Woolley, A. T.; Hadley, D.; Landre, P.; deMello, A. J.; Mathies, R. A.; Northrup, M. A., Functional Integration of PCR Amplification and Capillary Electrophoresis in a Microfabricated DNA Analysis Device. *Analytical Chemistry* **1996,** *68* (23), 4081-4086.

121. Waters, L. C.; Jacobson, S. C.; Kroutchinina, N.; Khandurina, J.; Foote, R. S.; Ramsey, J. M., Microchip Device for Cell Lysis, Multiplex PCR Amplification, and Electrophoretic Sizing. *Analytical Chemistry* **1998,** *70* (1), 158-162.

122. Sollier, E.; Murray, C.; Maoddi, P.; Di Carlo, D., Rapid prototyping polymers for microfluidic devices and high pressure injections. *Lab on a Chip* **2011,** *11* (22), 3752-3765.

123. Becker, H.; Locascio, L. E., Polymer microfluidic devices. *Talanta* **2002,** *56* (2), 267-287.

124. Shoji, S.; Esashi, M.; Matsuo, T., Prototype miniature blood gas analyser fabricated on a silicon wafer. *Sensors and Actuators* **1988,** *14* (2), 101-107.

125. Lintel, H. T. G. v.; Pol, F. C. M. v. d.; Bouwstra, S., A piezoelectric micropump based on micromachining of silicon. *Sensors and Actuators* **1988,** *15* (2), 153-167.

126. Zengerle, R.; Ulrich, J.; Kluge, S.; Richter, M.; Richter, A., A bidirectional silicon micropump. *Sensors and Actuators A: Physical* **1995,** *50* (1), 81-86.

127. Queste, S.; Salut, R.; Clatot, S.; Rauch, J.-Y.; Khan Malek, C. G., Manufacture of microfluidic glass chips by deep plasma etching, femtosecond laser ablation, and anodic bonding. *Microsystem Technologies* **2010,** *16* (8), 1485-1493.

128. Giridhar, M. S.; Seong, K.; Schülzgen, A.; Khulbe, P.; Peyghambarian, N.; Mansuripur, M., Femtosecond pulsed laser micromachining of glass substrates with application to microfluidic devices. *Applied Optics* **2004,** *43* (23), 4584-4589.

129. An, R.; Li, Y.; Dou, Y.; Liu, D.; Yang, H.; Gong, Q., Water-assisted drilling of microfluidic chambers inside silica glass with femtosecond laser pulses. *Applied Physics A* **2006,** *83* (1), 27-29.

130. Schafer, D. N.; Gibson, E. A.; Salim, E. A.; Palmer, A. E.; Jimenez, R.; Squier, J. In *An Optically Integrated Microfluidic Cell Counter Fabricated by Femtosecond Laser Ablation and Anodic Bonding*, Conference on Lasers and Electro-Optics/International Quantum Electronics Conference, Baltimore, Maryland, 2009/05/31; Optical Society of America: Baltimore, Maryland, 2009; p CMMM1.

131. Ceriotti, L.; Weible, K.; de Rooij, N. F.; Verpoorte, E., Rectangular channels for lab-on-a-chip applications. *Microelectronic Engineering* **2003,** *67–68*, 865-871.

132. Adi, B.; Matan, N., Dry etching of deep cavities in Pyrex for MEMS applications using standard lithography. *Journal of Micromechanics and Microengineering* **2006,** *16* (11), 2287.

133. Kai, K.; Ville, S.; Sami, F., Deep plasma etching of glass for fluidic devices with different mask materials. *Journal of Micromechanics and Microengineering* **2008,** *18* (6), 064010.

134. Roberts, M. A.; Rossier, J. S.; Bercier, P.; Girault, H., UV Laser Machined Polymer Substrates for the Development of Microdiagnostic Systems. *Analytical Chemistry* **1997,** *69* (11), 2035-2042.

135. Srinivasan, R., Controlled degradation and ablation of polymer surfaces by ultraviolet laser radiation. *Polymer Degradation and Stability* **1987,** *17* (3), 193-203.

136. Becker, H.; Gartner, C., Polymer microfabrication technologies for microfluidic systems. *Analytical and Bioanalytical Chemistry* **2008,** *390* (1), 89-111.

137. Hupert, M. L.; Guy, W. J.; Llopis, S. D.; Shadpour, H.; Rani, S.; Nikitopoulos, D. E.; Soper, S. A., Evaluation of micromilled metal mold masters for the replication of microchip electrophoresis devices. *Microfluid. Nanofluid.* **2007,** *3* (1), 1-11.

138. Guber, A. E.; Heckele, M.; Herrmann, D.; Muslija, A.; Saile, V.; Eichhorn, L.; Gietzelt, T.; Hoffmann, W.; Hauser, P. C.; Tanyanyiwa, J.; Gerlach, A.; Gottschlich, N.; Knebel, G., Microfluidic lab-on-a-chip systems based on polymers—fabrication and application. *Chemical Engineering Journal* **2004,** *101* (1–3), 447-453.

139. Shiu, P.-P.; Knopf, G. K.; Ostojic, M., Fabrication of metallic micromolds by laser and electro-discharge micromachining. *Microsystem Technologies* **2009,** *16* (3), 477-485.

140. Huang, M.-S.; Chiang, Y.-C.; Lin, S.-C.; Cheng, H.-C.; Huang, C.-F.; Shen, Y.-K.; Lin, Y., Fabrication of microfluidic chip using micro-hot embossing with micro electrical discharge machining mold. *Polymers for Advanced Technologies* **2012,** *23* (1), 57-64.

141. Soper, S. A.; Ford, S. M.; Qi, S.; McCarley, R. L.; Kelly, K.; Murphy, M. C., Peer Reviewed: Polymeric Microelectromechanical Systems. *Analytical Chemistry* **2000,** *72* (19), 642 A-651 A.

142. Qi, S.; Liu, X.; Ford, S.; Barrows, J.; Thomas, G.; Kelly, K.; McCandless, A.; Lian, K.; Goettert, J.; Soper, S. A., Microfluidic devices fabricated in poly(methyl methacrylate) using hot-embossing with integrated sampling capillary and fiber optics for fluorescence detection. *Lab on a Chip* **2002,** *2* (2), 88-95.

143. Becker, H.; Heim, U., *Polymer hot embossing with silicon master structures*. Myu: Tokyo, Japan, 1999; Vol. 11.

144. Steigert, J.; Haeberle, S.; Brenner, T.; Müller, C.; Steinert, C. P.; Koltay, P.; Gottschlich, N.; Reinecke, H.; Rühe, J.; Zengerle, R.; Ducrée, J., Rapid prototyping of microfluidic chips in COC. *Journal of Micromechanics and Microengineering* **2007,** *17* (2), 333.

145. Jagannathan, N.; Ian, P., Polymer embossing tools for rapid prototyping of plastic microfluidic devices. *Journal of Micromechanics and Microengineering* **2004,** *14* (1), 96.

146. Effenhauser, C. S.; Bruin, G. J. M.; Paulus, A.; Ehrat, M., Integrated Capillary Electrophoresis on Flexible Silicone Microdevices: Analysis of DNA Restriction Fragments and Detection of Single DNA Molecules on Microchips. *Analytical Chemistry* **1997,** *69* (17), 3451-3457.

147. Qin, D.; Xia, Y.; Whitesides, G. M., Rapid prototyping of complex structures with feature sizes larger than 20 μm. *Advanced Materials* **1996,** *8* (11), 917-919.

148. Duffy, D. C.; McDonald, J. C.; Schueller, O. J. A.; Whitesides, G. M., Rapid Prototyping of Microfluidic Systems in Poly(dimethylsiloxane). *Analytical Chemistry* **1998,** *70* (23), 4974-4984.

149. Yang, Y.; Li, C.; Kameoka, J.; Lee, K. H.; Craighead, H. G., A polymeric microchip with integrated tips and in situ polymerized monolith for electrospray mass spectrometry. *Lab on a Chip* **2005,** *5* (8), 869-876.

150. Kim, D. S.; Lee, S. H.; Ahn, C. H.; Lee, J. Y.; Kwon, T. H., Disposable integrated microfluidic biochip for blood typing by plastic microinjection moulding. *Lab on a Chip* **2006,** *6* (6), 794-802.

151. Do, J.; Lee, S.; Han, J.; Kai, J.; Hong, C.-C.; Gao, C.; Nevin, J. H.; Beaucage, G.; Ahn, C. H., Development of functional lab-on-a-chip on polymer for point-of-care testing of metabolic parameters. *Lab on a Chip* **2008,** *8* (12), 2113-2120.

152. Tsao, C.-W.; DeVoe, D. L., Bonding of thermoplastic polymer microfluidics. *Microfluid. Nanofluid.* **2009,** *6* (1), 1-16.

153. Mair, D. A.; Geiger, E.; Pisano, A. P.; Frechet, J. M. J.; Svec, F., Injection molded microfluidic chips featuring integrated interconnects. *Lab on a Chip* **2006,** *6* (10), 1346-1354.

154. Chin, C. D.; Laksanasopin, T.; Cheung, Y. K.; Steinmiller, D.; Linder, V.; Parsa, H.; Wang, J.; Moore, H.; Rouse, R.; Umviligihozo, G.; Karita, E.; Mwambarangwe, L.; Braunstein, S. L.; van de Wijgert, J.; Sahabo, R.; Justman, J. E.; El-Sadr, W.; Sia, S. K., Microfluidics-based diagnostics of infectious diseases in the developing world. *Nat Med* **2011,** *17* (8), 1015-1019.

155. Swickrath, M. J.; Shenoy, S.; Mann, J. A.; Belcher, J.; Kovar, R.; Wnek, G. E., The design and fabrication of autonomous polymer-based surface tension-confined microfluidic platforms. *Microfluid. Nanofluid.* **2008,** *4* (6), 601-611.

156. Fang, X.; Wei, S.; Kong, J., Paper-based microfluidics with high resolution, cut on a glass fiber membrane for bioassays. *Lab on a Chip* **2014,** *14* (5), 911-915.

157. Pugmire, D. L.; Waddell, E. A.; Haasch, R.; Tarlov, M. J.; Locascio, L. E., Surface Characterization of Laser-Ablated Polymers Used for Microfluidics. *Analytical Chemistry* **2002,** *74* (4), 871-878.

158. Khan Malek, C. G., Laser processing for bio-microfluidics applications (part I). *Analytical and Bioanalytical Chemistry* **2006,** *385* (8), 1351-1361.

159. Liu, Y.; Rauch, C. B., DNA probe attachment on plastic surfaces and microfluidic hybridization array channel devices with sample oscillation. *Analytical Biochemistry* **2003,** *317* (1), 76-84.

160. Chen, C.-S.; Breslauer, D. N.; Luna, J. I.; Grimes, A.; Chin, W.-c.; Lee, L. P.; Khine, M., Shrinky-Dink microfluidics: 3D polystyrene chips. *Lab on a Chip* **2008,** *8* (4), 622-624.

161. Young, E. W. K.; Berthier, E.; Guckenberger, D. J.; Sackmann, E.; Lamers, C.; Meyvantsson, I.; Huttenlocher, A.; Beebe, D. J., Rapid Prototyping of Arrayed Microfluidic Systems in Polystyrene for Cell-Based Assays. *Analytical Chemistry* **2011,** *83* (4), 1408-1417.

162. Becker, H.; Heim, U., Hot embossing as a method for the fabrication of polymer high aspect ratio structures. *Sensors and Actuators A: Physical* **2000,** *83* (1–3), 130-135.

163. Flachsbart, B. R.; Wong, K.; Iannacone, J. M.; Abante, E. N.; Vlach, R. L.; Rauchfuss, P. A.; Bohn, P. W.; Sweedler, J. V.; Shannon, M. A., Design and fabrication of a multilayered polymer microfluidic chip with nanofluidic interconnects via adhesive contact printing. *Lab on a Chip* **2006,** *6* (5), 667-674.

164. Lee, G.-B.; Chen, S.-H.; Huang, G.-R.; Sung, W.-C.; Lin, Y.-H., Microfabricated plastic chips by hot embossing methods and their applications for DNA separation and detection. *Sensors and Actuators B: Chemical* **2001,** *75* (1–2), 142-148.

165. Klank, H.; Kutter, J. P.; Geschke, O., CO2-laser micromachining and back-end processing for rapid production of PMMA-based microfluidic systems. *Lab on a Chip* **2002,** *2* (4), 242-246.

166. Brown, L.; Koerner, T.; Horton, J. H.; Oleschuk, R. D., Fabrication and characterization of poly(methylmethacrylate) microfluidic devices bonded using surface modifications and solvents. *Lab on a Chip* **2006,** *6* (1), 66-73.

167. Chen, Y.; Zhang, L.; Chen, G., Fabrication, modification, and application of poly(methyl methacrylate) microfluidic chips. *ELECTROPHORESIS* **2008,** *29* (9), 1801-1814.

168. Kuo, J. S.; Ng, L.; Yen, G. S.; Lorenz, R. M.; Schiro, P. G.; Edgar, J. S.; Zhao, Y.; Lim, D. S. W.; Allen, P. B.; Jeffries, G. D. M.; Chiu, D. T., A new USP Class VI-compliant substrate for manufacturing disposable microfluidic devices. *Lab on a Chip* **2009,** *9* (7), 870-876.

169. Kuo, J. S.; Zhao, Y.; Ng, L.; Yen, G. S.; Lorenz, R. M.; Lim, D. S. W.; Chiu, D. T., Microfabricating high-aspect-ratio structures in polyurethane-methacrylate (PUMA) disposable microfluidic devices. *Lab on a Chip* **2009,** *9* (13), 1951-1956.

170. Kuo, J. S.; Chiu, D. T., Disposable microfluidic substrates: Transitioning from the research laboratory into the clinic. *Lab on a Chip* **2011,** *11* (16), 2656-2665.

171. Fiorini, G. S.; Jeffries, G. D. M.; Lim, D. S. W.; Kuyper, C. L.; Chiu, D. T., Fabrication of thermoset polyester microfluidic devices and embossing masters using rapid prototyped polydimethylsiloxane molds. *Lab on a Chip* **2003,** *3* (3), 158-163.

172. Fiorini, G. S.; Lorenz, R. M.; Kuo, J. S.; Chiu, D. T., Rapid Prototyping of Thermoset Polyester Microfluidic Devices. *Analytical Chemistry* **2004,** *76* (16), 4697-4704.

173. Fiorini, G. S.; Yim, M.; Jeffries, G. D. M.; Schiro, P. G.; Mutch, S. A.; Lorenz, R. M.; Chiu, D. T., Fabrication improvements for thermoset polyester (TPE) microfluidic devices. *Lab on a Chip* **2007,** *7* (7), 923-926.

174. Bartolo, D.; Degre, G.; Nghe, P.; Studer, V., Microfluidic stickers. *Lab on a Chip* **2008,** *8* (2), 274-279.

175. Hung, L.-H.; Lin, R.; Lee, A. P., Rapid microfabrication of solvent-resistant biocompatible microfluidic devices. *Lab on a Chip* **2008,** *8* (6), 983-987.

176. Wägli, P.; Guélat, B.; Homsy, A.; de Rooij, N. In *Microfluidic devices made of UV-curable glue (NOA81) for fluorescence detection based applications*, Proc. Micro Total Analysis Systems, 2010; pp 1937-1939.

177. Wägli, P.; Homsy, A.; de Rooij, N. F., Norland optical adhesive (NOA81) microchannels with adjustable wetting behavior and high chemical resistance against a range of mid-infrared-transparent organic solvents. *Sensors and Actuators B: Chemical* **2011,** *156* (2), 994-1001.

178. Lee, J. N.; Park, C.; Whitesides, G. M., Solvent Compatibility of Poly(dimethylsiloxane)-Based Microfluidic Devices. *Analytical Chemistry* **2003,** *75* (23), 6544-6554.

179. Delamarche, E.; Bernard, A.; Schmid, H.; Michel, B.; Biebuyck, H., Patterned Delivery of Immunoglobulins to Surfaces Using Microfluidic Networks. *Science* **1997,** *276* (5313), 779-781.

180. Martynova, L.; Locascio, L. E.; Gaitan, M.; Kramer, G. W.; Christensen, R. G.; MacCrehan, W. A., Fabrication of Plastic Microfluid Channels by Imprinting Methods. *Analytical Chemistry* **1997,** *69* (23), 4783-4789.

181. Giselbrecht, S.; Gietzelt, T.; Gottwald, E.; Trautmann, C.; Truckenmüller, R.; Weibezahn, K. F.; Welle, A., 3D tissue culture substrates produced by microthermoforming of pre-processed polymer films. *Biomed. Microdevices* **2006,** *8* (3), 191-199.

182. Truckenmuller, R.; Giselbrecht, S.; van Blitterswijk, C.; Dambrowsky, N.; Gottwald, E.; Mappes, T.; Rolletschek, A.; Saile, V.; Trautmann, C.; Weibezahn, K. F.; Welle, A., Flexible fluidic microchips based on thermoformed and locally modified thin polymer films. *Lab on a Chip* **2008,** *8* (9), 1570-1579.

183. Julien, G.; Thierry, C.; Patrice, M., Microinjection molding of thermoplastic polymers: a review. *Journal of Micromechanics and Microengineering* **2007,** *17* (6), R96.

184. McCormick, R. M.; Nelson, R. J.; Alonso-Amigo, M. G.; Benvegnu, D. J.; Hooper, H. H., Microchannel Electrophoretic Separations of DNA in Injection-Molded Plastic Substrates. *Analytical Chemistry* **1997,** *69* (14), 2626-2630.

185. Attia, U. M.; Marson, S.; Alcock, J. R., Micro-injection moulding of polymer microfluidic devices. *Microfluid. Nanofluid.* **2009,** *7* (1), 1-28.

186. and, Y. X.; Whitesides, G. M., SOFT LITHOGRAPHY. *Annual Review of Materials Science* **1998,** *28* (1), 153-184.

187. Zhao, X.-M.; Xia, Y.; Whitesides, G. M., Soft lithographic methods for nano-fabrication. *Journal of Materials Chemistry* **1997,** *7* (7), 1069-1074.

188. Aumiller, G. D.; Chandross, E. A.; Tomlinson, W. J.; Weber, H. P., Submicrometer resolution replication of relief patterns for integrated optics. *Journal of Applied Physics* **1974,** *45* (10), 4557-4562.

189. Friedel, C.; Crafts, J. M., Ueber einige neue organische Verbindungen des Siliciums und das Atomgewicht dieses Elementes. *Justus Liebigs Annalen der Chemie* **1863,** *127* (1), 28-32.

190. Muller, R., One hundred years of organosilicon chemistry. *Journal of Chemical Education* **1965,** *42* (1), 41.

191. Effenhauser, C. S.; Paulus, A.; Manz, A.; Widmer, H. M., High-Speed Separation of Antisense Oligonucleotides on a Micromachined Capillary Electrophoresis Device. *Analytical Chemistry* **1994,** *66* (18), 2949-2953.

192. Delamarche, E.; Bernard, A.; Schmid, H.; Bietsch, A.; Michel, B.; Biebuyck, H., Microfluidic Networks for Chemical Patterning of Substrates: Design and Application to Bioassays. *Journal of the American Chemical Society* **1998,** *120* (3), 500-508.

193. Jackman, R. J.; Duffy, D. C.; Ostuni, E.; Willmore, N. D.; Whitesides, G. M., Fabricating Large Arrays of Microwells with Arbitrary Dimensions and Filling Them Using Discontinuous Dewetting. *Analytical Chemistry* **1998,** *70* (11), 2280-2287.

194. Schueller, O. J. A.; Duffy, D. C.; Rogers, J. A.; Brittain, S. T.; Whitesides, G. M., Reconfigurable diffraction gratings based on elastomeric microfluidic devices. *Sensors and Actuators A: Physical* **1999,** *78* (2–3), 149-159.

195. Berthier, E.; Young, E. W. K.; Beebe, D., Engineers are from PDMS-land, Biologists are from Polystyrenia. *Lab on a Chip* **2012,** *12* (7), 1224-1237.

196. Yoon, J.-Y.; Garrell, R. L., Preventing Biomolecular Adsorption in Electrowetting-Based Biofluidic Chips. *Analytical Chemistry* **2003,** *75* (19), 5097-5102.

197. Bi, H.; Meng, S.; Li, Y.; Guo, K.; Chen, Y.; Kong, J.; Yang, P.; Zhong, W.; Liu, B., Deposition of PEG onto PMMA microchannel surface to minimize nonspecific adsorption. *Lab on a Chip* **2006,** *6* (6), 769-775.

198. Liu, H.; Zhang, Y., Droplet formation in a T-shaped microfluidic junction. *Journal of Applied Physics* **2009,** *106* (3), 034906.

199. Xu, J. H.; Li, S. W.; Tan, J.; Wang, Y. J.; Luo, G. S., Preparation of highly monodisperse droplet in a T-junction microfluidic device. *AIChE Journal* **2006,** *52* (9), 3005-3010.

200. Li, W.; Nie, Z.; Zhang, H.; Paquet, C.; Seo, M.; Garstecki, P.; Kumacheva, E., Screening of the Effect of Surface Energy of Microchannels on Microfluidic Emulsification. *Langmuir* **2007,** *23* (15), 8010-8014.

201. Morra, M.; Occhiello, E.; Marola, R.; Garbassi, F.; Humphrey, P.; Johnson, D., On the aging of oxygen plasma-treated polydimethylsiloxane surfaces. *Journal of Colloid and Interface Science* **1990,** *137* (1), 11-24.

202. Eddington, D. T.; Puccinelli, J. P.; Beebe, D. J., Thermal aging and reduced hydrophobic recovery of polydimethylsiloxane. *Sensors and Actuators B: Chemical* **2006,** *114* (1), 170-172.

203. Bodas, D.; Khan-Malek, C., Formation of more stable hydrophilic surfaces of PDMS by plasma and chemical treatments. *Microelectronic Engineering* **2006,** *83* (4–9), 1277-1279.

204. Lawton, R. A.; Price, C. R.; Runge, A. F.; Doherty Iii, W. J.; Saavedra, S. S., Air plasma treatment of submicron thick PDMS polymer films: effect of oxidation time and storage conditions. *Colloids and Surfaces A: Physicochemical and Engineering Aspects* **2005,** *253* (1–3), 213-215.

205. Hillborg, H.; Gedde, U. W., Hydrophobicity recovery of polydimethylsiloxane after exposure to corona discharges. *Polymer* **1998,** *39* (10), 1991-1998.

206. Hillborg, H.; Tomczak, N.; Olàh, A.; Schönherr, H.; Vancso, G. J., Nanoscale Hydrophobic Recovery: A Chemical Force Microscopy Study of UV/Ozone-Treated Cross-Linked Poly(dimethylsiloxane). *Langmuir* **2004,** *20* (3), 785-794.

207. Farrar, N. R.; Ashbee, K. H. G., Destruction of epoxy resins and of glass-fibre-reinforced epoxy resins by diffused water. *Journal of Physics D: Applied Physics* **1978,** *11* (6), 1009.

208. Nicholas, J.; Ashbee, K. H. G., Further destruction of composite materials by the freezing or boiling of phase-separated water. *Journal of Physics D: Applied Physics* **1978,** *11* (6), 1015.

209. Narkis, M.; Nicolais, L.; Apicella, A.; Bell, J. P., Hot water aging of polycarbonate. *Polymer Engineering & Science* **1984,** *24* (3), 211-217.

210. Senden, D.; Engels, T.; Söntjens, S.; Govaert, L., The effect of physical aging on the embrittlement of steam-sterilized polycarbonate. *Journal of Materials Science* **2012,** *47* (16), 6043-6046.

211. Fedors, R. F., Osmotic effects in water absorption by polymers. *Polymer* **1980,** *21* (2), 207-212.

212. Robeson, L. M.; Crisafulli, S. T., Microcavity formation in engineering polymers exposed to hot water. *Journal of Applied Polymer Science* **1983,** *28* (9), 2925-2936.

213. Lassila, L. V. J.; Nohrström, T.; Vallittu, P. K., The influence of short-term water storage on the flexural properties of unidirectional glass fiber-reinforced composites. *Biomaterials* **2002,** *23* (10), 2221-2229.

214. Pizzi, A.; Mittal, K. L., *Handbook of Adhesive Technology, Revised and Expanded*. Taylor & Francis: 2003.

215. Bell, J. P.; Reffner, J. A.; Petrie, S., Amine-cured epoxy resins: Adhesion loss due to reaction with air. *Journal of Applied Polymer Science* **1977,** *21* (4), 1095-1102.

216. Mabey, D.; Peeling, R. W.; Ustianowski, A.; Perkins, M. D., Tropical infectious diseases: Diagnostics for the developing world. *Nat Rev Micro* **2004,** *2* (3), 231-240.

217. Niemz, A.; Ferguson, T. M.; Boyle, D. S., Point-of-care nucleic acid testing for infectious diseases. *Trends in Biotechnology 29* (5), 240-250.

218. Yager, P.; Domingo, G. J.; Gerdes, J., Point-of-Care Diagnostics for Global Health. *Annual Review of Biomedical Engineering* **2008,** *10* (1), 107-144.

219. Hsieh, K.; Patterson, A. S.; Ferguson, B. S.; Plaxco, K. W.; Soh, H. T., Rapid, Sensitive, and Quantitative Detection of Pathogenic DNA at the Point of Care through Microfluidic Electrochemical Quantitative Loop-Mediated Isothermal Amplification. *Angewandte Chemie* **2012,** *124* (20), 4980-4984.

220. Myers, F. B.; Lee, L. P., Innovations in optical microfluidic technologies for point-of-care diagnostics. *Lab on a Chip* **2008,** *8* (12), 2015-2031.

221. Ferguson, B. S.; Buchsbaum, S. F.; Wu, T.-T.; Hsieh, K.; Xiao, Y.; Sun, R.; Soh, H. T., Genetic Analysis of H1N1 Influenza Virus from Throat Swab Samples in a Microfluidic System for Point-of-Care Diagnostics. *Journal of the American Chemical Society* **2011,** *133* (23), 9129-9135.

222. Cho, I.-H.; Radadia, A. D.; Farrokhzad, K.; Ximenes, E.; Bae, E.; Singh, A. K.; Oliver, H.; Ladisch, M.; Bhunia, A.; Applegate, B.; Mauer, L.; Bashir, R.; Irudayaraj, J., Nano/Micro and Spectroscopic Approaches to Food Pathogen Detection. *Annual Review of Analytical Chemistry* **2014,** *7* (1), 65-88.

223. Gubala, V.; Harris, L. F.; Ricco, A. J.; Tan, M. X.; Williams, D. E., Point of Care Diagnostics: Status and Future. *Analytical Chemistry* **2012,** *84* (2), 487-515.

224. Sin, M. L. Y.; Mach, K. E.; Wong, P. K.; Liao, J. C., Advances and challenges in biosensor-based diagnosis of infectious diseases. *Expert Review of Molecular Diagnostics* **2014,** *14* (2), 225-244.

225. Foudeh, A. M.; Fatanat Didar, T.; Veres, T.; Tabrizian, M., Microfluidic designs and techniques using lab-on-a-chip devices for pathogen detection for point-of-care diagnostics. *Lab on a Chip* **2012,** *12* (18), 3249-3266.

226. Gervais, L.; de Rooij, N.; Delamarche, E., Microfluidic Chips for Point-of-Care Immunodiagnostics. *Advanced Materials* **2011,** *23* (24), H151-H176.

227. Choi, S.; Goryll, M.; Sin, L. Y. M.; Wong, P. K.; Chae, J., Microfluidic-based biosensors toward point-of-care detection of nucleic acids and proteins. *Microfluid. Nanofluid.* **2011,** *10* (2), 231-247.

228. Perna, N. T.; Plunkett Iii, G.; Burland, V.; Mau, B.; Glasner, J. D.; Rose, D. J.; Mayhew, G. F.; Evans, P. S.; Gregor, J.; Kirkpatrick, H. A.; Posfai, G.; Hackett, J.; Klink, S.; Boutin, A.; Ying, S.; Miller, L.; Grotbeck, E. J.; Davis, N. W.; Lim, A.; Dimalanta, E. T., Genome sequence of enterohaemorrhagic Escherichia coli O157:H7. *Nature* **2001,** *409* (6819), 529.

229. Fratamico, P. M.; DebRoy, C.; Liu, Y.; Needleman, D. S.; Baranzoni, G. M.; Feng, P., Advances in Molecular Serotyping and Subtyping of Escherichia coli. *Frontiers in Microbiology* **2016,** *7*, 644.

230. Morrison, D. C.; Jacobs, D. M., Binding of polymyxin B to the lipid A portion of bacterial lipopolysaccharides. *Immunochemistry* **1976,** *13* (10), 813-818.

231. Schindler, M.; Osborn, M. J., Interaction of divalent cations and polymyxin B with lipopolysaccharide. *Biochemistry* **1979,** *18* (20), 4425-4430.

232. Moore, R. A.; Bates, N. C.; Hancock, R. E., Interaction of polycationic antibiotics with Pseudomonas aeruginosa lipopolysaccharide and lipid A studied by using dansyl-polymyxin. *Antimicrobial Agents and Chemotherapy* **1986,** *29* (3), 496-500.

233. Mares, J.; Kumaran, S.; Gobbo, M.; Zerbe, O., Interactions of Lipopolysaccharide and Polymyxin Studied by NMR Spectroscopy. *Journal of Biological Chemistry* **2009,** *284* (17), 11498-11506.

234. Folch, A.; Ayon, A.; Hurtado, O.; Schmidt, M. A.; Toner, M., Molding of Deep Polydimethylsiloxane Microstructures for Microfluidics and Biological Applications. *Journal of Biomechanical Engineering* **1999,** *121* (1), 28-34.

235. Beebe, D. J.; Moore, J. S.; Yu, Q.; Liu, R. H.; Kraft, M. L.; Jo, B.-H.; Devadoss, C., Microfluidic tectonics: A comprehensive construction platform for microfluidic systems. *Proceedings of the National Academy of Sciences* **2000,** *97* (25), 13488-13493.

236. Wertz, C. F.; Santore, M. M., Effect of Surface Hydrophobicity on Adsorption and Relaxation Kinetics of Albumin and Fibrinogen: Single-Species and Competitive Behavior. *Langmuir* **2001,** *17* (10), 3006-3016.

237. Malmsten, M., Ellipsometry Studies of Protein Layers Adsorbed at Hydrophobic Surfaces. *Journal of Colloid and Interface Science* **1994,** *166* (2), 333-342.

238. Fritz, J. L.; Owen, M. J., Hydrophobic Recovery of Plasma-Treated Polydimethylsiloxane. *The Journal of Adhesion* **1995,** *54* (1-4), 33-45.

239. Owen, M. J.; Smith, P. J., Plasma treatment of polydimethylsiloxane. *Journal of Adhesion Science and Technology* **1994,** *8* (10), 1063-1075.

240. Zhou, J.; Ellis, A. V.; Voelcker, N. H., Recent developments in PDMS surface modification for microfluidic devices. *ELECTROPHORESIS* **2010,** *31* (1), 2-16.

241. Yu, L.; Li, C. M.; Liu, Y.; Gao, J.; Wang, W.; Gan, Y., Flow-through functionalized PDMS microfluidic channels with dextran derivative for ELISAs. *Lab on a Chip* **2009,** *9* (9), 1243-1247.

242. Huang, B.; Wu, H.; Kim, S.; Kobilka, B. K.; Zare, R. N., Phospholipid biotinylation of polydimethylsiloxane (PDMS) for protein immobilization. *Lab on a Chip* **2006,** *6* (3), 369-373.

243. Heyries, K. A.; Blum, L. J.; Marquette, C. A., Direct Poly(dimethylsiloxane) Surface Functionalization with Vinyl Modified DNA. *Chemistry of Materials* **2008,** *20* (4), 1251-1253.

244. Eteshola, E.; Leckband, D., Development and characterization of an ELISA assay in PDMS microfluidic channels. *Sensors and Actuators B: Chemical* **2001,** *72* (2), 129-133.

245. Sui, G.; Wang, J.; Lee, C.-C.; Lu, W.; Lee, S. P.; Leyton, J. V.; Wu, A. M.; Tseng, H.-R., Solution-Phase Surface Modification in Intact Poly(dimethylsiloxane) Microfluidic Channels. *Analytical Chemistry* **2006,** *78* (15), 5543-5551.

246. Boxshall, K.; Wu, M.-H.; Cui, Z.; Cui, Z.; Watts, J. F.; Baker, M. A., Simple surface treatments to modify protein adsorption and cell attachment properties within a poly(dimethylsiloxane) micro-bioreactor. *Surf. Interface Anal.* **2006,** *38* (4), 198-201.

247. Wu, D.; Zhao, B.; Dai, Z.; Qin, J.; Lin, B., Grafting epoxy-modified hydrophilic polymers onto poly(dimethylsiloxane) microfluidic chip to resist nonspecific protein adsorption. *Lab on a Chip* **2006,** *6* (7), 942-947.

248. Backer, L.; McGillicuddy, D., Harmful algal blooms. *Oceanography* **2006,** *19* (2), 94-106.

249. Landsberg, J. H., The Effects of Harmful Algal Blooms on Aquatic Organisms. *Reviews in Fisheries Science* **2002,** *10* (2), 113-390.

250. Glibert, P. M.; Anderson, D. M.; Gentien, P.; Granéli, E.; Sellner, K. G., The global, complex phenomena of harmful algal blooms. **2005**.

251. Heisler, J.; Glibert, P. M.; Burkholder, J. M.; Anderson, D. M.; Cochlan, W.; Dennison, W. C.; Dortch, Q.; Gobler, C. J.; Heil, C. A.; Humphries, E.; Lewitus, A.; Magnien, R.; Marshall, H. G.; Sellner, K.; Stockwell, D. A.; Stoecker, D. K.; Suddleson, M., Eutrophication and harmful algal blooms: A scientific consensus. *Harmful Algae* **2008,** *8* (1), 3-13.

252. Anderson, D. M.; Glibert, P. M.; Burkholder, J. M., Harmful algal blooms and eutrophication: Nutrient sources, composition, and consequences. *Estuaries* **2002,** *25* (4), 704-726.

253. Hallegraeff, G. M., A review of harmful algal blooms and their apparent global increase. *Phycologia* **1993,** *32* (2), 79-99.

254. Dewan, A.; Kim, J.; McLean, R. H.; Vanapalli, S. A.; Karim, M. N., Growth kinetics of microalgae in microfluidic static droplet arrays. *Biotechnology and Bioengineering* **2012,** *109* (12), 2987-2996.

255. Kim, H. S.; Weiss, T. L.; Thapa, H. R.; Devarenne, T. P.; Han, A., A microfluidic photobioreactor array demonstrating high-throughput screening for microalgal oil production. *Lab on a Chip* **2014,** *14* (8), 1415-1425.

256. Wu, J.; Wu, X.; Lin, F., Recent developments in microfluidics-based chemotaxis studies. *Lab on a Chip* **2013,** *13* (13), 2484-2499.

257. Cheng, S.-Y.; Heilman, S.; Wasserman, M.; Archer, S.; Shuler, M. L.; Wu, M., A hydrogel-based microfluidic device for the studies of directed cell migration. *Lab on a Chip* **2007,** *7* (6), 763-769.

258. Ahmed, T.; Shimizu, T. S.; Stocker, R., Bacterial Chemotaxis in Linear and Nonlinear Steady Microfluidic Gradients. *Nano Letters* **2010,** *10* (9), 3379-3385.

259. Hoffman, A. S., Hydrogels for biomedical applications. *Adv. Drug Deliv. Rev.* **2012,** *64, Supplement*, 18-23.

260. Divoux, T.; Mao, B.; Snabre, P., Syneresis and delayed detachment in agar plates. *Soft Matter* **2015,** *11* (18), 3677-3685.

261. Baker, J. P.; Hong, L. H.; Blanch, H. W.; Prausnitz, J. M., Effect of Initial Total Monomer Concentration on the Swelling Behavior of Cationic Acrylamide-Based Hydrogels. *Macromolecules* **1994,** *27* (6), 1446-1454.

APPENDIX. PERMISSION FOR SECTION 3.6

Microfluidics using a thiol–acrylate resin for fluorescence-based pathogen detection assays

W. Zhang, M. P. Tullier, K. Patel, A. Carranza, J. A. Pojman and A. D. Radadia, Lab Chip, 2015, 15, 4227
DOI: 10.1039/C5LC00971E

VITA

Michael Perrin Tullier was born in Baton Rouge, Louisiana in May of 1990 where he has lived for his entire life. He attended Our Lady of Mercy Catholic School for elementary and middle school before graduating with honors from Catholic High School in 2008. Michael then attended Louisiana State University, where he was a member of the LSU Tiger Marching Band, and graduated magna cum laude with a Bachelor of Science degree in Chemistry and a history minor in May 2012. After graduation, he remained at Louisiana State University to continue working in the lab of Dr. John A Pojman and pursue a Doctorate of Philosophy in Chemistry, which he anticipates receiving in 2017.